STUDY OF COMPLETE AND INCOMPLETE FUSION OF WEAKLY BOUND NUCLEI AT NEAR BARRIER ENERGIES

A THESIS

SUBMITTED TO THE FACULTY OF SCIENCE KURUKSHETRA UNIVERSITY, KURUKSHETRA FOR THE DEGREE

OF

DOCTOR OF PHILOSOPHY IN PHYSICS

BY **RAJIV CHAHAL**

UNDER THE SUPERVFISION OF **Dr. RAJESH KHARAB**

DEPARTMENT OF PHYSICS
KURUKSHETRA UNIVERSITY
KURUKSHETRA- 136119

SEPTEMBER, 2017

DECLARATION

I, Rajiv Chahal, hereby declare that the matter embodied in the thesis entitled "STUDY OF COMPLETE AND INCOMPLETE FUSION OF WEAKLY BOUND NUCLEI AT NEAR BARRIER ENERGIES" submitted to the Faculty of Science, Kurukshetra University, Kurukshetra is the result of my own work carried out under the supervision and guidance of Dr. Rajesh Kharab, Associate Professor, Department of Physics, Kurukshetra University, Kurukshetra. I further declare that the matter presented in this thesis has not been submitted previously for the award of any other degree

(Rajiv Chahal)
Department of Physics
Kurukshetra University
Kurukshetra-136119

September , 2017

KURUKSHETRA UNIVERSITY KURUKSHETRA

(Established by State Legislative Act XII of 1956)

Dr. RAJESH KHARAB ASSOCIATE PROFESSOR DEPARMENT OF PHYSICS KURUKSHETRA UNIERSITY KURUKSHETRA-136119

Phone: (++91) -01744-238196/238410 Ext.: 2130, 2482 Mob. No.: 9416262306

Fax: (++91)-01744-238277

E-mail: kharabrajesh@rediffmail.com

CERTIFICATE

This is to certify that the matter presented in this thesis entitled, "STUDY OF COMPLETE AND INCOMPLETE FUSION OF WEAKLY BOUND NUCLEI AT NEAR BARRIER ENERGIES" submitted by Mr. Rajiv Chahal for the award of Doctor of Philosophy in Physics to the Kurukshetra University, Kurukshetra is an original piece of work carried out by him under my supervision. The work presented in the thesis has not been submitted for the award of any other degree.

(Dr. Rajesh Kharab) Supervisor

CONTENTS

		Page. No.		
ACKNOWLEDGEMENTS				
LIS	LIST OF PUBLICATIONS			
СН	IAPTER-1 INTRODUCTION	1-22		
1.1	Introduction	1		
	References	20		
CH	CHAPTER-2 BARRIER PENETRATION MODEL			
2.1	Barrier Penetration Model	23		
2.2	The Interaction Potential	37		
	References	40		
CH	CHAPTER-3 CLASSICAL DYNAMICAL MODEL			
3.1	Classical Dynamical Model	41		
3.2	WKB Approximation and Tunneling Factor	47		
	References	54		
CH	CHAPTER-4 RESULTS AND DISCUSSION			
4.1	Results and Discussion	55		
4.2	Contribution of ICF in ⁹ Be+ ¹⁶⁹ Tm, ¹⁸¹ Ta and ¹⁸⁷ Re Fusion Reaction	ns 56		
4.3	The Tunneling Effect	64		
4.4	Energy Dependent Woods-Saxon Potential and Fusion	70		
4.5	Optimum Barrier Radius for Deformed Targets	83		
	References	86		
CH	IAPTER-5 CONCLUSIONS	87-90		
5.1	Conclusions	87		
	References	90		

ACKNOWLEDGEMENTS

"At this ecstatic time of presenting my Ph.D. thesis I bow to almighty God"

Ph.D. is a long haul full of obstacles and barriers, but the support and encouragement of some people simply made this journey considerably pleased and easier. Here I want to give my acknowledgements to those who were always with me during this tenure.

In the first place, I would like to express my deepest and sincere gratitude to my worthy and respected supervisor, Dr. Rajesh Kharab, Associate Professor, Department of Physics, Kurukshetra University, Kurukshetra for his genial inspiration and enthusiastic encouragement throughout the course of my work. His wide knowledge, logical way of thinking and positive attitude towards research and also towards life have been of great value for me and for all associated with him. I always remember the tireless efforts that my supervisor has made over day and night in giving a good shape to this thesis. He is truly hardworking researcher and it's an honor for me to be one of his Ph.D. students.

I am sincerely grateful to Dr. R. K. Moudgil, Chairman and Prof., Dr. M. S. Yadav, Prof. and Ex-Chairman, Department of Physics, Kurukshetra University, Kurukshetra for their valuable help and support throughout my work.

I would like to acknowledge Prof. Shyam Kumar, Prof. Sanjeev Aggarwal, Prof. Fakir Chand, Dr. Annu Sharma, Dr. Manish Kumar, Dr. Suman Mahendia and Dr. Hardev Singh, faculty members of the department for their invaluable advice and encouragement during my Ph.D.

I am thankful to my research colleagues Dr. Rajiv kumar, Dr. Manjeet Singh, Dr. Sukhvinder, Dr. Pardeep Singh, Dr. Ravinder Kumar, Dr. Anju Kumari and Dr. Rishipal Chahal for the philosophical discussions and all time helping hands at various stages in the progress of this work.

My special thanks are due to my friends Dr. Jitender, Rajender, Deepak, Amandeep, Devender and all the research scholars of the Department of Physics for their kind support and enjoyable company during the present work.

I am also grateful to all the non-teaching staff of the Department of Physics, for their cooperation and help during this work. The Tagore hostel's staff and all the mess workers are acknowledged for their kind behavior due to which the hostel becomes another home for me.

Last but not the least, I have a deep sense of gratitude to my family without their support it would be impossible for me to complete this work. The blessings of my father, Shri. Satpal Chahal helps me to face all the difficulties of life and motivated me in every phase of my life. The unconditional love, which I got from my mother, Smt. Saraswati Devi, is my greatest strength. I wish that my deeds will always make her proud. The affection, fun and crazy ideas which I shared with my wife Ritu, my daughter Vrinda, my son Viren, my sister, my brother-in-law and maternal nephews, my father-in-law, mother-in-law and brother-in-law giving my best in every situation.

I would like to thank everybody who remained helpful during the successful realization of this thesis and express my apology to those whom I could not mention inadvertently.

(Rajiv Chahal)

LIST OF PUBLICATIONS

INTERNATIONAL JOURNALS

- 1. Rajesh Kharab, **Rajiv Chahal** and Rajiv Kumar, Nucl. Phys. A **960** (2017) 11–21.
- 2. Rajesh Kharab, **Rajiv Chahal** and Rajiv Kumar, Nucl. Phys. A **946** (2016) 1–10.
- 3. Rajesh Kharab, **Rajiv Chahal** and Rajiv Kumar, Mod. Phys. Lett. A **31** (2016) 1650201.
- 4. **Rajiv Chahal**, Anju Kumari and Rajesh Kharab, Appl. Sci. Lett. **2** (2016) 64 -67.

INTERNATIONAL/NATIONAL SYMPOSIUM

- 1. Rajesh Kharab, **Rajiv Chahal** and Rajiv Kumar, Proc. DAE-BRNS Symp. on Nucl. Phys. **60** (2015) 422-423.
- 2. Rajesh Kharab, **Rajiv Chahal** and Rajiv Kumar, Proc. DAE-BRNS Symp. on Nucl. Phys. **61** (2016) 428-429.

INTRODUCTION

Nuclear physics deals primarily with the studies carried out to understand exact nature of short ranged strong nuclear interaction and hence the structural and behavioral aspects of various nuclei under different physical conditions. The major tools of nuclear physics studies are various decay processes occurring in radioactive nuclei and nuclear reactions induced by impinging energetic beams of nuclei on stable targets [1-4]. Depending on experimental conditions during nucleus-nucleus collision wide variety of nuclear phenomena like elastic scattering, inelastic scattering and nuclear reactions occur. The elastic scattering is the process in which projectile interacts with target and deviates from its path without transfer of energy that is projectile and target stays in their ground states. While in case of inelastic scattering there is a transfer of energy during collision and hence either both projectile and target or target is left in excited state. Besides these, there may occur processes in which the charge number and/or mass number of the target changes after interaction and are referred to as nuclear reactions. The nuclear reactions are broadly classified into following three categories.

1. Compound Reactions: - These are two step processes which occur through the formation of a compound nucleus. Infect during this process the interacting nuclei coalesce to form highly excited compound nucleus (CN) that lives for relatively long time. Since the time required by a nucleon to complete an orbit inside the nucleus is typically of the order of ~ 10⁻²² sec, the reaction time for compound nucleus formation must be much larger than 10⁻²² sec. Owing to long lifetime of compound nucleus, excitation energy is shared by all nucleons. If sufficient energy is localized on one or more nucleons then CN decays through nucleon(s) emission. Since the CN lives long enough it loses memory of its formation. Consequently the probability of various decay modes is independent of entrance channel. Usually these reactions take place at small impact parameter and at low energy. Fusion, Fusion-fission and Fusion evaporation etc. are some typical examples of compound nuclear reactions. The process of formation of compound nucleus through fusion of two nuclei is shown in Fig. 1.1.

- **2. Direct reactions**: These reactions occur at a very short time scale in comparison to CN reactions. When two nuclei make 'glancing' contact and separate immediately, then the process is termed as direct reactions (DR). These reactions usually occur near the surface of the target nucleus and at large impact parameters. These reactions occur within 10⁻²²sec time scale or less, and hence there is no time for projectile to distribute its energy with target. Transfer reactions, Deep inelastic collision and breakup etc. are some examples of direct reactions. The breakup of projectile into two fragments is shown schematically in Fig. 1.2
- **3. Resonance Reactions:** The reactions in which the incoming projectile forms a quasi bound state before the outgoing particle is ejected are termed as resonance reactions. In these reactions, there are sharp peaks in the reaction excitation function which are termed as resonances and represent quasi bound quantum state of compound nucleus being formed. The resonances occur at some particular value of energies for which there is a smooth matching between wave function inside and outside the potential as shown in Fig. 1.3.

Among various reaction channels discussed above, the nuclear fusion reactions have attracted a great deal of attention in connection with the energy production in stars, nucleo-synthesis of chemical elements in stellar environment and production of super heavy elements. Classically the fusion can occur only when the interacting nuclei have sufficient kinetic energy to overcome the repulsive Coulomb barrier between them and get trapped inside the potential pocket of compound nucleus. But quantum mechanically, fusion may occur even at energies smaller then the barrier energies through the so called quantum mechanical tunneling [5]. Infect, the kinetic energy determines whether the process is going over the barrier or quantum tunneling through the barrier. Thus, the fusion of two nuclei around the Coulomb barrier provides a fascinating testing ground for theories of quantum tunneling. Initially, the studies of nuclear fusion reactions were limited to reactions induced by stable nuclei.

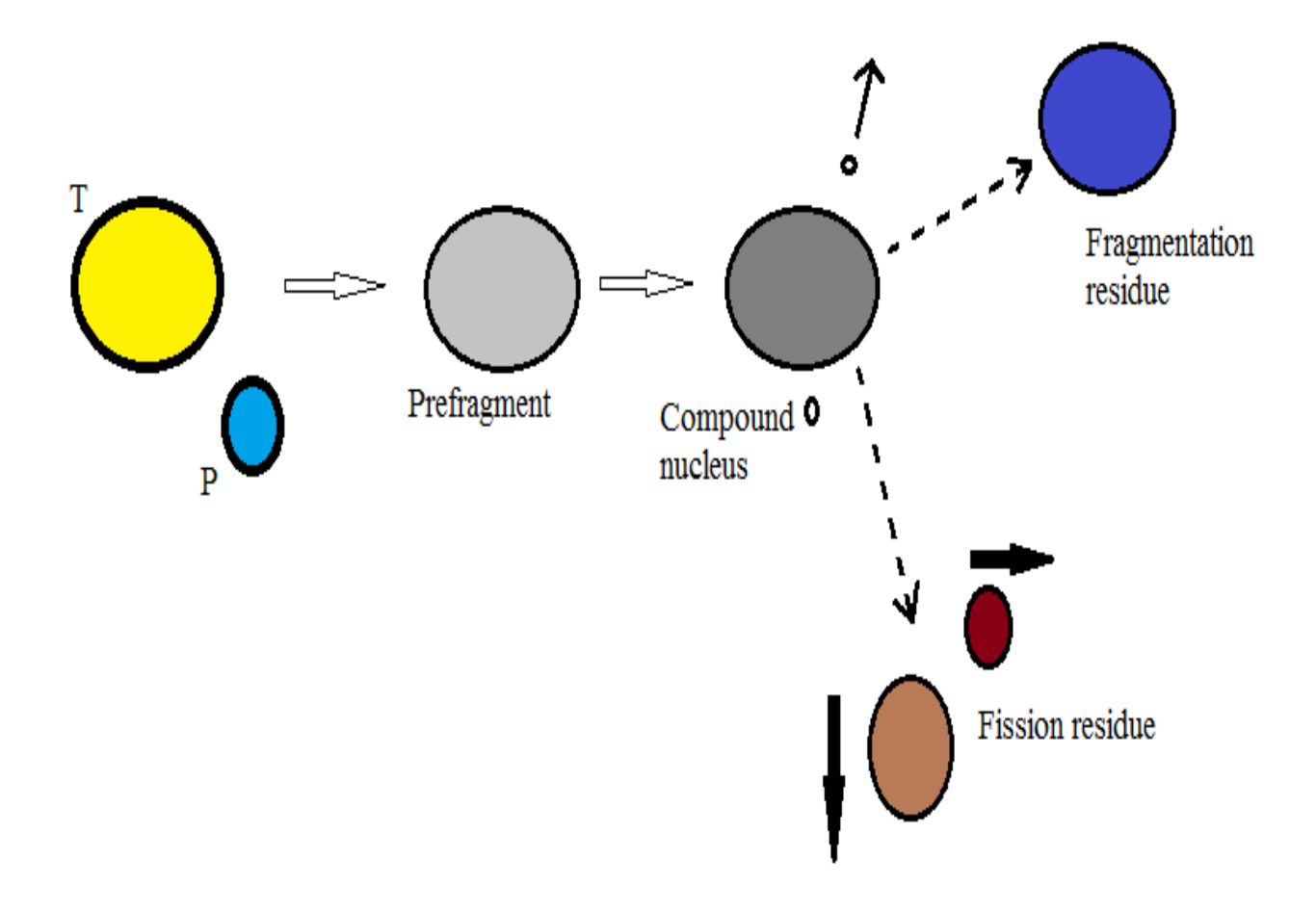


Fig.1.1 Pictorial view of the two step compound nuclear reaction. In first stage, excited prefragment is formed, after the thermal equilibrium is established a compound nucleus is formed, which then decay via particle evaporation or fission.

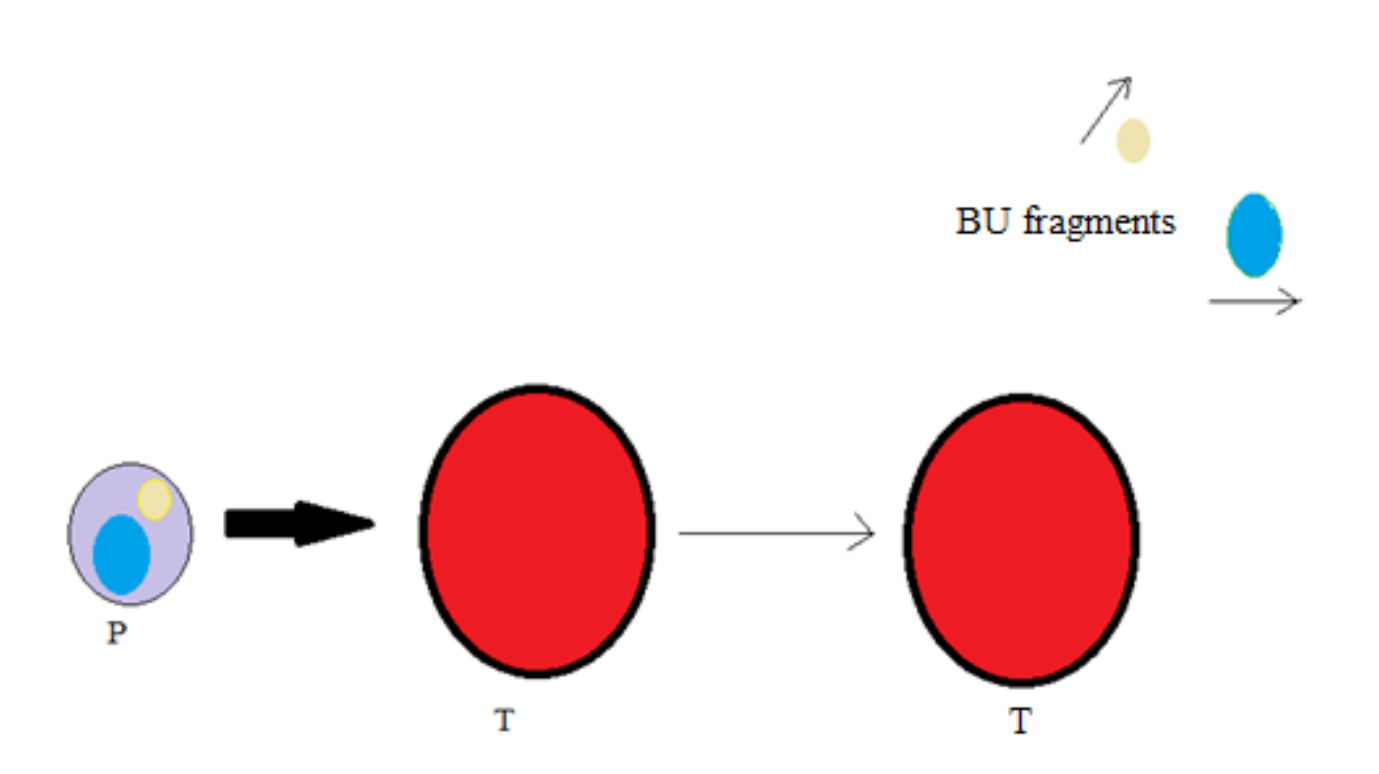


Fig.1.2 Mechanism of breakup (a direct reaction) of projectile.

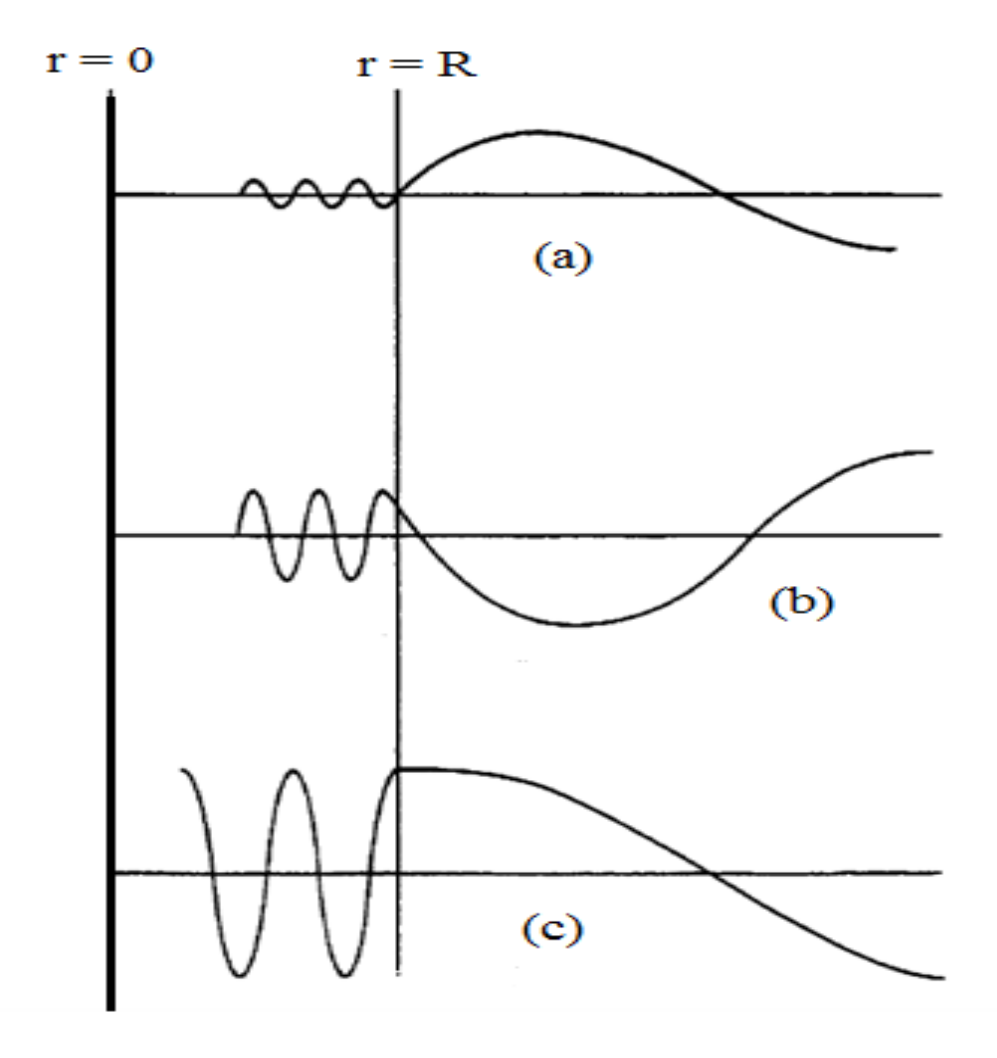


Fig1.3 (a) Far from resonance, the exterior and interior wave functions match badly and probability of penetration of the nucleus is negligible small. (b) As the match improves, there is a higher probability to penetrate. (c) At resonance the amplitudes match exactly, the incident particle penetrates easily, and the cross section rise to a maximum.

However in mid nineties with the advancement in high energy Radioactive Ion Beams (RIB's) [6-9] facilities it has become possible to induce various nuclear reactions by using beam of nuclei lying in the vicinity of drip lines. The positions of proton and neutron drip lines on N-Z graph have been shown schematically in Fig. 1.4. The drip lines represent the limits of nuclear stability where the binding energy of additional nucleon(s) becomes zero and the excessive neutron or proton can no longer be kept in the nucleus they literally drip out. The initial experiments carried out by I. Tanihata et al [6-7, 10] using beams of ¹¹Li have indicated the existence of a novel neutron halo structure. Subsequently, various experiments carried out by using beams of many neutron rich and proton rich nuclei have confirmed the existence of one neutron halo, two neutrons halo, one proton halo and two protons halo among some of these neutron and proton rich nuclei as depicted in Fig. 1.5 [11]. Generally a halo state consists of loosely bound nucleon(s) mostly in s-state extremely far away from the core of normal nuclear density and hence leads to root mean square (r.m.s) radius much larger than that is expected from the $r_0A^{1/3}$ systematic $(r_0 \sim 1.2 \text{fm})$ for stable nuclei as shown schematically in Fig. 1.6. Since the binding energy of halo nucleon(s) is quite low, about 50% of the time these remains outside the range of the core potential that is in the classically forbidden region. Besides very small binding energy the formation of halo can occur in nuclei having valance nucleon(s) in low orbital angular momentum state that is s- or p- states because of low centrifugal barrier. However in case of proton-halo nuclei the Coulomb barrier suppresses halo formation in elements with Z > 10. Jensen and Riisager [12] proposed that the necessary and sufficient condition for the occurrence of halo states in nuclei having valence nucleon in s-state is that the binding energy should be $B < \frac{2}{(A)^{2/3}}$

MeV while in case of valence nucleons in p-state there is an additional limitation that the charge number should be $Z < 0.44 A^{4/3}$.

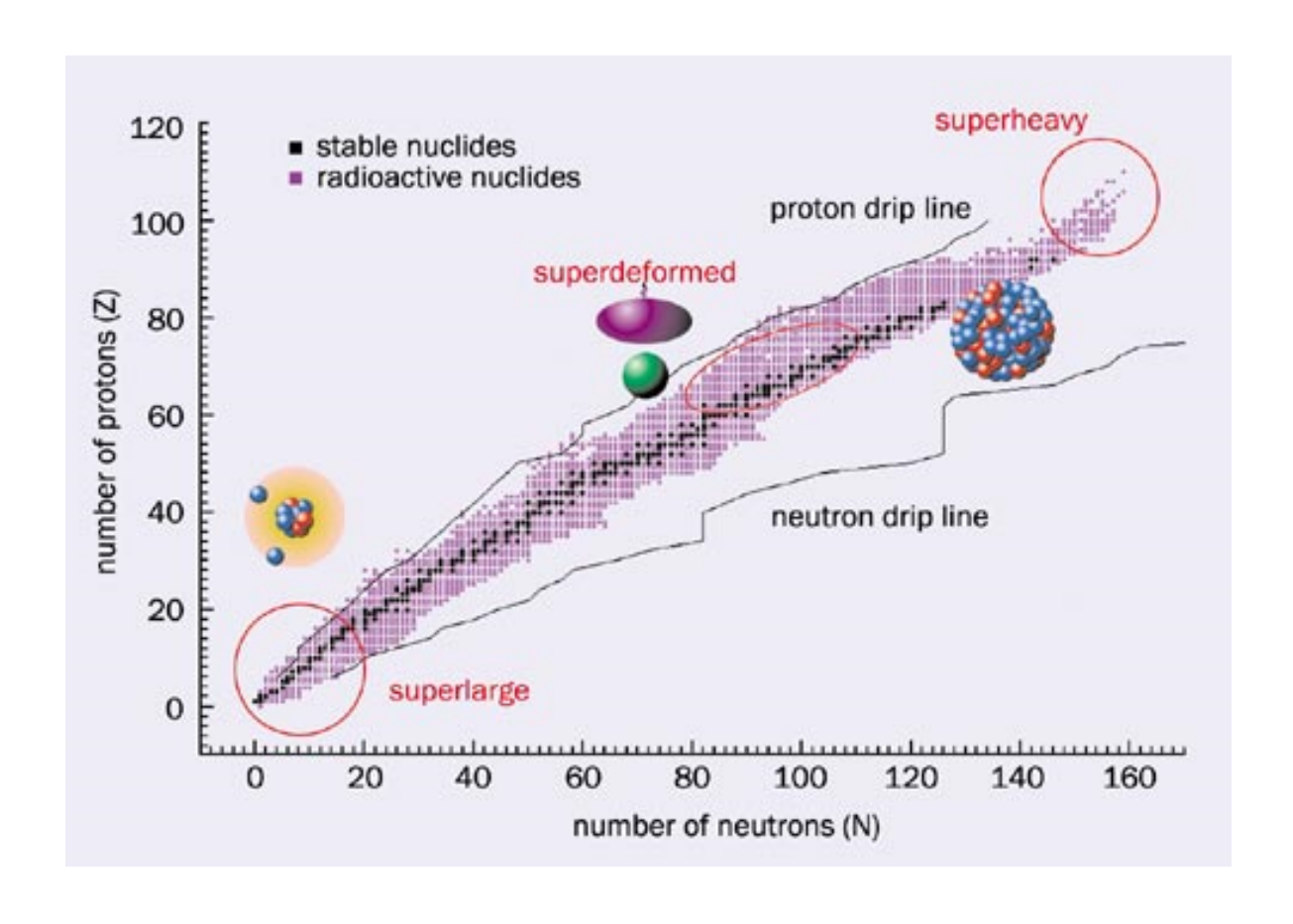


Fig.1.4 Nuclear landscape showing the stable and unstable nuclei lying in between the neutron and the proton drip lines.

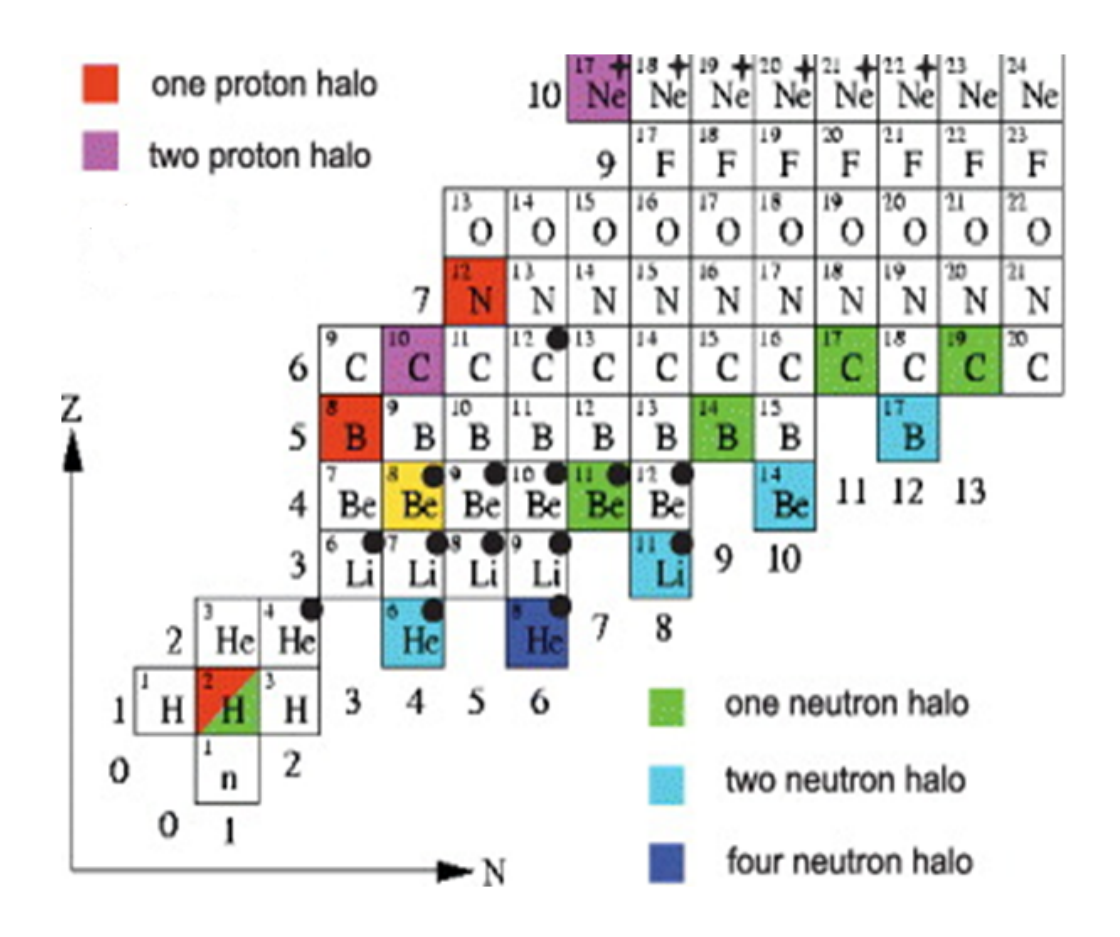


Fig.1.5 The portion of nuclear chart consisting of well known halo nuclei.

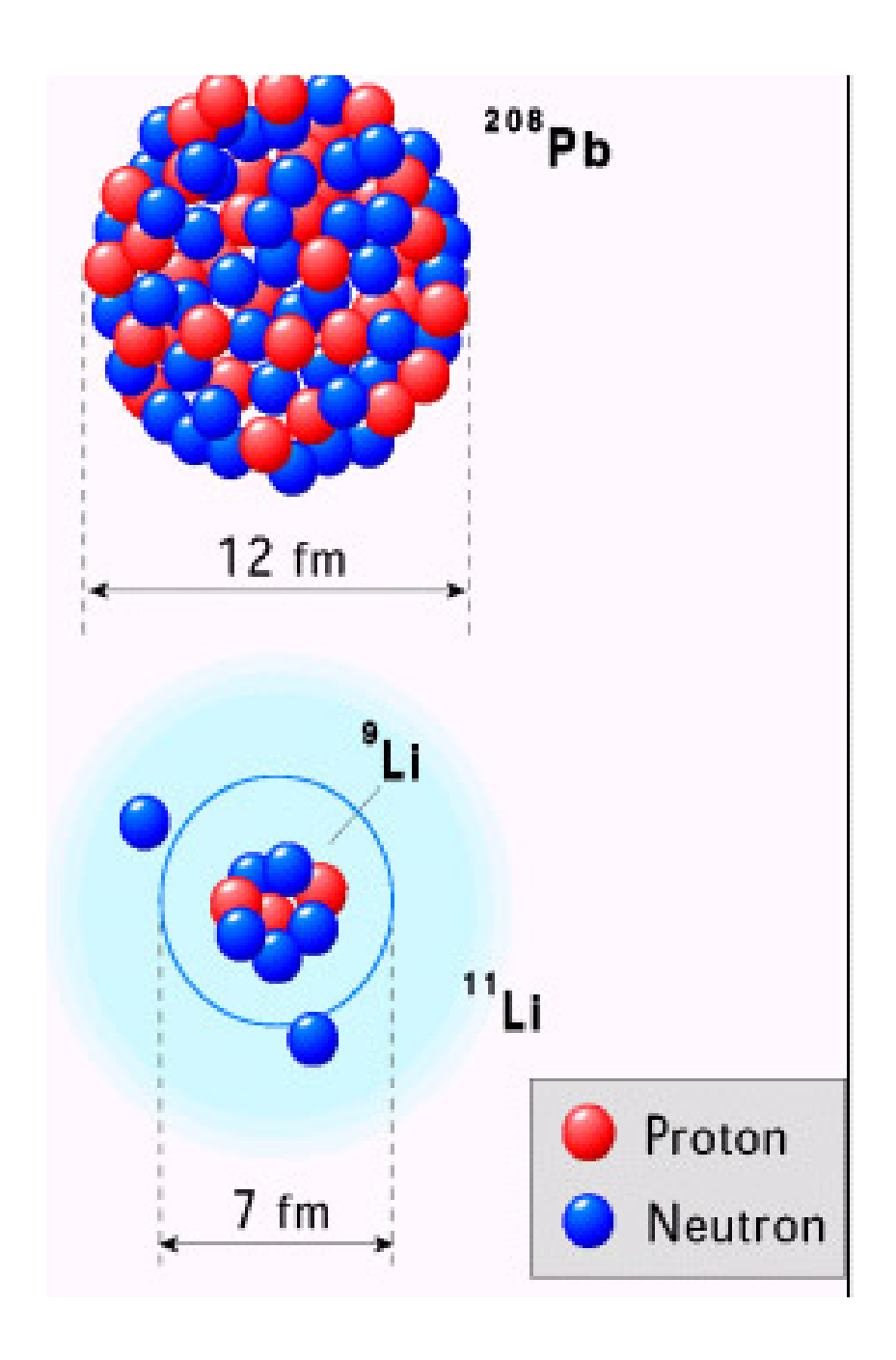


Fig.1.6 The neutron halo in ¹¹Li extends to fill the volume equivalent to ²⁰⁸Pb, with very dilute, pure neutron matter.

The unique characteristic features of halo nuclei such as small binding energy, large values of isospin, extended wave functions of the valence nucleon(s), narrow momentum distributions, large spatial extension, existence of soft dipole (Pygmy) resonances and large breakup probabilities are expected to strongly affect all the possible reaction channels.

Now a day, besides the halo nuclei, the beams of various stable but weakly bound nuclei are also available with reasonable intensities which have created a renewed interest in fusion involving weakly bound stable and unstable nuclei. Infect owing to very low binding energy of projectiles, the reactions involving these nuclei differ in a fundamental way from those involving tightly bound nuclei as shown in Figs. 1.7 and 1.8 [13-20]. For well bound projectile and target the breakup probability is quite low and hence the breakup effects are negligibly small. Usually in this case the direct complete fusion (DCF), nucleon(s) transfer and inelastic excitation etc. are few dominant reaction channels which are of great importance in different contexts. In direct complete fusion the projectile moves towards target with an appreciable amount of energy such that it over come the barrier between the two nuclei or tunnels through it and gets fused with the target without undergoing breakup. The resulting nucleus may be formed in its ground state or in bound or unbound (resonant) excited states. In case of the compound nucleus formed in an excited state it decays via the emission of γ -rays or neutrons, protons or other charged particles, or fission fragments. The transfer reaction is a rearrangement process wherein one or more nucleons are transferred from the projectile to the target nucleus or vice versa. It is important to note that transfer process should be distinguished from the mass transfer occurring in quasi-fission processes [21] in which exchange of nucleons leads to a deformed composite system which subsequently decays into fission-like fragments. In the inelastic excitation the projectile interacts with the target and loses some of its energy and results in the excitation of the target nucleus.

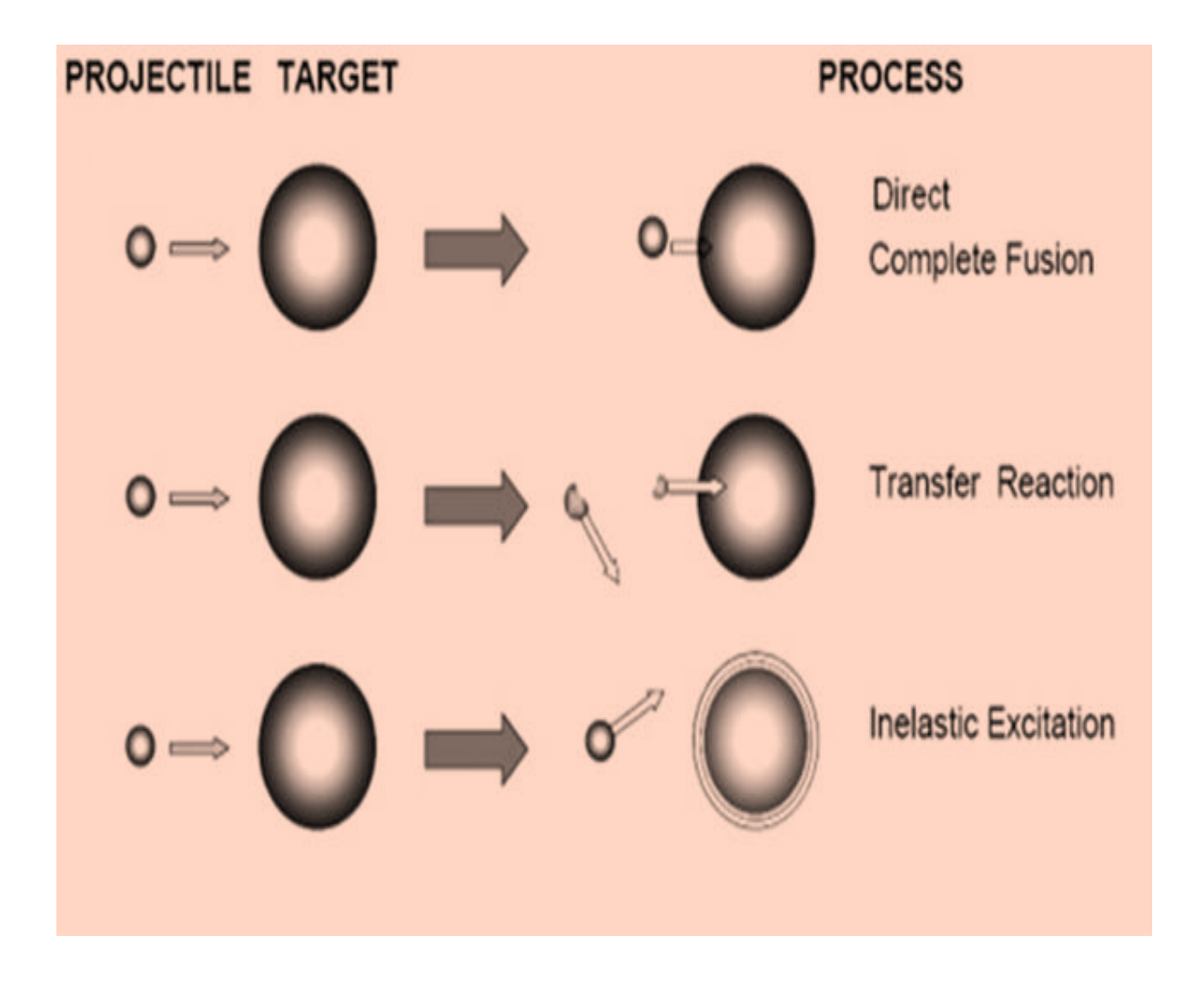


Fig.1.7 Possible reaction mechanisms for a tightly bound projectile.

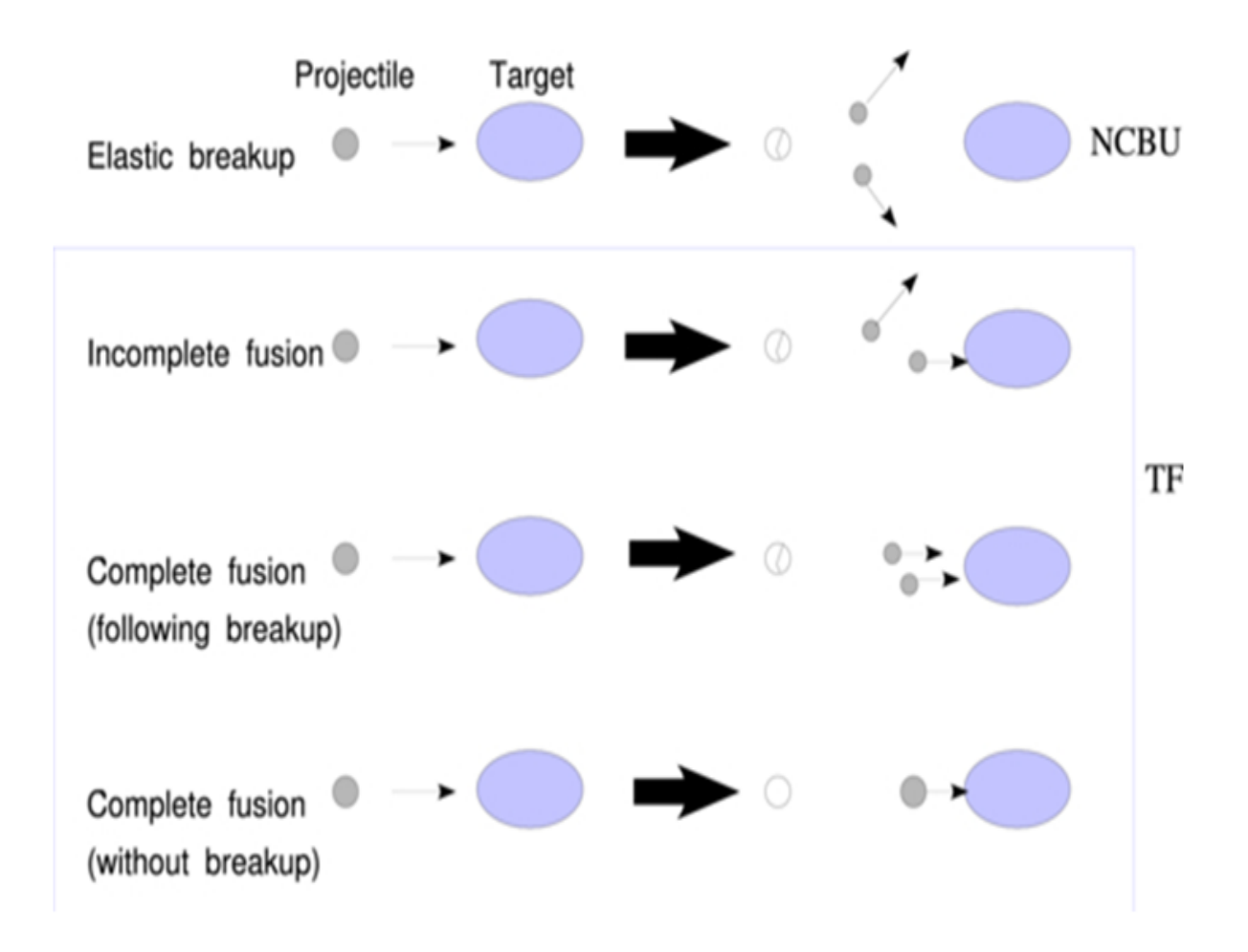


Fig.1.8 Schematic representation of the fusion and breakup processes that can take place in the collision of a weakly bound projectile.

The reactions involving weakly bound projectiles are strongly influenced mainly by two factors namely static effects of large spatial extension and dynamic effects of large breakup probabilities. Some weakly bound nuclei have a long tail in density distribution which gives rise to lowering of fusion barriers and hence enhances the fusion cross section. Secondly because of low breakup threshold, as listed in Table 1.1 for some light weakly bound nuclei, the couplings with the breakup channel are of immense importance.

Table 1.1 Breakup thresholds of some typical weakly bound nuclei.

Stable weakly bound nuclei	Breakup threshold	Unstable weakly bound nuclei (halo)	Breakup threshold
9 Be	1.67MeV	¹¹ Be	0.5MeV
⁶ Li	1.48MeV	Li	0.3MeV
⁷ Li	2.45MeV	⁶ He	0.97MeV

One of the immediate consequences of this coupling is to induce unusual fusion channels in the reactions induced by weakly bound nuclei as shown in Fig. 1.8. However, in order to study the influence of breakup, it is necessary to distinguish between prompt breakup and delayed breakup. In the former, the breakup process occurs when the weakly bound projectile is approaching the target. The latter takes place in two steps. First, the projectile is excited to a long-lived resonance above the breakup threshold, as it traverses the interaction region. Then, the resonance decays into the breakup channel, when the projectile is following the outgoing branch of the trajectory. Only prompt breakup, which occurs on a time scale of 10^{-22} s, may affect fusion. In delayed breakup the resonance life-time is much longer than the collision time. Thus, the projectile breaks up when the collision is over and hence it does not affect the fusion cross section [22-24]. The breakup removes flux from the elastic scattering and takes place either in the long-range Coulomb field (Coulomb breakup) or in the short range nuclear field (nuclear breakup) [25]. Coulomb breakup dominates for heavy targets and at impact parameters larger than the sum of the radii of interacting nuclei where the short-range nuclear interaction is negligible. For lighter targets and at impact parameters smaller or comparable to sum of radii of interacting nuclei the Coulomb interaction becomes less important and the breakup is predominantly the nuclear breakup process.

Thus in case of reactions induced by weakly bound nuclei, in addition to these reactions the incomplete fusion (ICF), sequential complete fusion (SCF) and elastic breakup reactions are equally probable reaction channels. In an incomplete fusion a large parts but not the whole of the projectile fuses with the target nucleus. For light nuclei, wherein only few nucleons are involved, incomplete fusion and transfer reactions remain conceptually different mechanisms but may lead to the formation of the same final nucleus in the same excitation state as the two processes are indistinguishable. Also the angular momenta involved in the two processes are similar, since the (semi classical) value of the critical angular momentum is small. The incomplete fusion has been described as a two-step process of fusion following breakup in which the projectile is first broken into two or more fragments by Coulomb and/or nuclear forces and some of the fragments penetrate the barrier and fuse with the target. Strictly speaking, events where all fragments fuse with the target nucleus after breakup are also possible and are referred to as sequential complete fusion which is experimentally indistinguishable from direct complete fusion. The direct complete fusion (DCF), which may occur for both tightly as well as loosely bound projectiles, corresponds to the complete capture of the projectile by the target without explicitly going through the breakup channel. The sum of complete fusion (CF=DCF+SCF) and incomplete fusion (ICF) is termed as total fusion (TF). The quantitative estimation of separate contribution of CF and ICF in TF is an important aspect to understand the reaction dynamics of fusion induced by weakly bound nuclei. Another important issue is to investigate the role of breakup in the enhancement or suppression of the fusion cross section. The words enhancement and suppression are based on a comparison with some standard cross section. Thus, the choice of the standard should be very clear. A lot of theoretical and

experimental studies have already been carried out to address these issues [13, 26-60].

Sinha et al. [26, 27] measured TF for the ⁷Li+²⁸Si system, at energies below and above the barrier and have compared the data with coupled channel calculations. They found a slight enhancement at sub-barrier energies and no effect at energies just above the barrier. Kumawat et al. [28] measured the CF cross section for the 6Li+90Zr system at energies above the Coulomb barrier and observed that the data was suppressed by 34% compared to coupled channel predictions. However, Hu et al. [29] measured the CF cross section for ⁶Li+⁹⁶Zr, a similar system, at above-barrier energies and found a suppression of only 25% compared to coupled channel calculations. Rath et al. [30-32] measured CF and TF of 6,7Li + 144,152Sm systems, at energies below and above the Coulomb barrier and have compared their experimental CF cross sections with predictions of coupled channel calculations involving inelastic channels, using the CCFULL code [33]. They also performed calculations involving both inelastic and transfer channels, using the FRESCO code [34]. Their results have indicated a suppression of the experimental CF cross section of the order of 30% for all systems especially at above barrier energy region. They further observed that the suppression is more important for fusion induced by ⁶Li than by ⁷Li. Pradhan et al. [35] measured the CF and ICF cross sections for ⁶Li + ¹⁵⁹Tb systems, at energies above the Coulomb barrier. Comparing their CF data with results of coupled channel calculations, they found that the experimental CF cross section for $^{6}\text{Li} + ^{159}\text{Tb}$ is suppressed by more than 30%. Mukherjee et al. [36] performed a similar experiment for ⁷Li + ¹⁵⁹Tb system and found a suppression of 26% in CF cross section data in comparison to coupled channel calculations. Palshetkar et al. [37] measured CF, ICF and transfer cross sections for ^{6,7}Li + ¹⁹⁷Au systems, at energies below and above the barrier. The comparison between experiments and CC calculations indicated that the CF data for the ⁶Li and ⁷Li projectiles were suppressed by 35% and 15% respectively. Shrivastava et al. [38] measured the CF cross section for ⁶Li + ¹⁹⁸Pt system and have found that the data well below the barrier is very well described by the CC calculation. Thus, there is no hindrance of fusion at deep sub-barrier energies for this system. At energies above the barrier, there is

some suppression of the CF cross section. C.L. Gua et al. [61] observed that contribution of ICF in TF for system ⁶Li + ¹⁵⁴Sm is around 28% in above barrier energy region while M. Dasgupta et al. [48] have observed ratio of ICF to TF for ^{6,7}Li+ ²⁰⁹Bi systems goes from 90% to 30% as energy goes from sub barrier region to far above barrier region.

Besides ^{6,7}Li, good quality beams of ⁹Be with high intensities are also available at various accelerator facilities worldwide [7, 8]. The beams of ⁹Be have attracted significant attention as it can be generated with high intensity in the energy range between 10MeV and 60MeV with lesser efforts. The 9Be is a weakly bound nucleus having one neutron separation energy of nearly1.67MeV and it easily breaks up into n +8Be two body channel with 8Be either in ground state or in excited state. The so formed ⁸Be is then dissociated into two alphas through delayed (life time $\sim 10^{-16}$ s) and prompt (life time $\sim 10^{-22}$ s) breakup processes. This breakup channel strongly affects the fusion cross section in near barrier energy region. Many authors have measured CF cross sections for reactions induced by ⁹Be beams on ⁸⁹Y, ¹²⁴Sn, ¹⁴⁴Sm, ¹⁶⁹Tm, ¹⁸¹Ta, ¹⁸⁷Re and ¹⁸⁶W targets [39-45]. The measured CF cross sections were compared with predictions of CC calculations using CCFULL or FRESCO codes. In all cases, data showed some enhancement below the Coulomb barrier and suppression in above barrier region. The suppressions found for ⁸⁹Y, ¹²⁴Sn, ¹⁴⁴Sm, ¹⁶⁹Tm, ¹⁸¹Ta, ¹⁸⁷Re and ¹⁸⁶W targets were 20%, 28%, 10% (later corrected to 16% [46]), 34%, 34%, 30% and 40% respectively. For reactions induced by 9Be on 169Tm, 181Ta and 187Re ratio of ICF to TF is found to be 30% in above barrier energy region while it increases to 90% as incident energy goes from above barrier to deep sub barrier region. This conclusive remark was found to be in clear contradiction with the observation of P.R.S Gomes et al. [58] for ⁹Be+¹⁴⁴Sm system that ICF to TF ratio was found to be 15% throughout the energy range. Clearly the range of suppression or enhancement is quite wide and involves substantial ambiguity and hence needs further investigations.

It is well known that the simplest theoretical way to understand the fusion of two nuclei is the Barrier Penetration Model (BPM) [14, 62-63] wherein the projectile is assumed to penetrate through potential barrier between two interacting nuclei and form a composite nucleus. At low energies, the barrier penetration occurs via quantum tunneling phenomenon which is a slow quantum leak through the classical barrier due to the wave nature of nuclei. In fact, the behavior of sub-barrier fusion cross-section strongly depends upon the nature of the reactant nuclei as a result there are unexpected variations in sub-barrier fusion cross-sections even for different isotopes of a given element. At energies below the Coulomb barrier, a large enhancement in the fusion cross-section by several orders of magnitude in comparison to the predictions of one dimensional barrier penetration model was observed. This enhancement in the sub-barrier fusion cross-section was found to have a link with the intrinsic structure of colliding nuclei. Indeed, the coupling of the relative motion of projectile and target to the internal degrees of freedom such as static deformation, vibration of nuclear surface, rotations, neck formation, nucleon transfer reactions etc. enhances the sub-barrier fusion cross-section.

So far different approaches have been proposed to analyze fusion cross section data which takes in to account these effects. The coupled channel method is a standard theoretical approach to study the effects of nuclear intrinsic degrees of freedom on the fusion cross section which consists in solving numerically the coupled channels equations that determine the wave functions of the relative motion. Since weakly bound nuclei may get dissociated very easily, it becomes necessary to include the coupling with the continuum. This is achieved through the Continuum Discreatized Coupled Channel (CDCC) [64-68] method devised by the Surrey group to study breakup and fusion reactions induced by weakly bound projectiles [67, 69-70]. The CC approach, however, becomes quite cumbersome when more and more number of channels are needed to be included in the analysis. Hence another approach based on Dynamic Polarization Potential (DPP) is found to be more appropriate in such cases. In the dynamic polarization potential approach the coupling between different excited states does not pose any problem as it can be considered as additive, so that the polarization potential induced by the coupling to two states is approximately the sum of the potentials corresponding to the coupling to each one independently. Thus dynamic polarization potential approach becomes more useful to include the coupling to large sets of states, like the continuum of breakup states, for which standard coupled channels calculations become very difficult [71-72].

An alternative formulation based on multidimensional quantum tunneling is given by the path integral approach. This approach is very convenient when the internal structure is represented by an algebraic model such as the interacting boson model. Also the effects of coupling between the nuclear structure and translational motion can be discussed in two limiting cases namely sudden and adiabatic approximation. These approximations are very useful for obtaining analytical results which provide a conceptual framework for understanding the fusion process. For deformed nuclei, in which the excitation energies are very low, sudden approximation provides a reasonably good description of the data. In rotation-vibration coupling, sudden approximation can be utilized to reduce the size of the channel coupling. While in case of large excitation energy of first excited states the adiabatic approximation works very well. In the intermediate cases between sudden and adiabatic tunneling, the effects of the environment are not straightforward to illustrate in simple physical terms.

Besides the channel coupling effects, it is very crucial to calculate separately the contribution of ICF and CF in TF for reactions induced by weakly bound nuclei. The first calculations of separate cross sections for CF and ICF processes were performed by Hagino, Dasgupta and Hinde [52-53], treating the reaction as a three-body problem in two dimensions and using classical physics. Subsequently, a three body Classical Trajectory Monte-Carlo (CTMC) model developed by K. Hagino and others [53] was a great step forward in this direction. This method follows the classical trajectories of breakup fragments after the breakup and thus provides an unambiguous separation between complete and incomplete fusion cross sections but this model does not fill a gap in the sense of assessing the importance of ICF and SCF.

Further a three-dimensional classical dynamical model that treats breakup stochastically is proposed by A. Diaz-Torres for low energy reactions of weakly bound nuclei [54-56, 73]. It allows a consistent calculation of breakup, incomplete and complete fusion cross sections. In addition, the classical dynamical model (CDM) is advantageous in the sense that besides separate CF and ICF calculations one can calculate the no-capture breakup (NCBU) cross

section, angular and relative energy distribution of fragments also. It is important to mention that various channel coupling effects may be mocked up by introducing the energy dependence in the nucleus—nucleus potential. The energy dependent potential in conjunction with one dimensional Wong's formula represent a very simple method to analyze, though qualitatively, excitation functions of various projectile—target combinations having different channel coupling effects.

In the present work we have studied the relative contribution of ICF and CF in TF for reactions induced by ⁹Be on various targets using CDM and Wong's formula in conjugation with energy dependent Woods–Saxon potential (EDWSP). After giving a brief introduction in chapter 1, the main steps involved in the derivation of Wong's formula and the details of EDWSP are presented in chapter 2. The conceptual development of the CDM is outlined in chapter 3. The detailed discussion of our results regarding the complete, incomplete and total fusion cross section in near barrier energy region is given in chapter 4. Finally in chapter 5 we present the important conclusions and possible future extension of the present work.

References

- [1]. C. H. Dasso et al., Nucl. Phys. A 405 (1983) 381.
- [2]. C. H. Dasso et al., Phys. Lett. B 183 (1987) 141.
- [3]. P. E. Hodgson, E. Gadioli and E. Gadioli-Erba, Introductory Nuclear Physics, Clarendon press Oxford (1997).
- [4]. L. F. Canto, P. R. S. Gomes, R. Donangelo and M. S. Hussein, Phys. Rep. 424 (2006) 1-111.
- [5]. L. I. Schiff, Quantum Mechanics, Tata McGraw-Hill, New Delhi, 2010.
- [6]. I. Tanihata et al., Phys. Rev. Lett. 55 (1985) 2676.
- [7]. I. Tanihata et al., Phys. Lett. B 206 (1988) 592.
- [8]. J.F. Liang and C. Signorini, Int. J. Mod. Phys. E 14 (2005) 1121.
- [9]. Y. Blumenfeld, T. Nilsson and P. Van Duppen, Phys. Scr. T152 (2013) 014023, and references therein.
- [10]. I. Tanihata et al., Phys. Lett. B 160 (1985) 380.
- [11]. P. G. Hansen and B. Jonson, Europhys. Lett. 4 (1987) 409.
- [12]. A. S. Jensen and K. Riisager, Phys. Lett. B 480 (2000) 39.
- [13]. L.F. Canto, P.R.S. Gomes, R. Donangelo, J. Lubian and M.S. Hussein Phys. Rep. 596 (2015) 1.
- [14]. P. Banerjee et al., Pramana journal of physics 61 (2003) 529.
- [15]. K. Rusek, N. Keeley, K.W. Kemper and R. Raabe, Phys. Rev. C 67 (2003) 041604(R).
- [16]. K. Rusek, N. Alamanos, N. Keeley, V. Lapoux and A. Pakou, Phys. Rev. C 70 (2004) 014603.
- [17]. P.R.S Gomes et al., Phys. Lett. B 695 (2011) 320.
- [18]. P.R.S. Gomes et al., Phys. Rev. C 71 (2005) 034608.
- [19]. N. Keeley et al., Nucl. Phys. A 582 (1995) 314.
- [20]. V.V. Sargsyan et al., Phys. Rev. C 86 (2012) 014602 and the references there in.
- [21]. W. J. Swiatecki, Phys. Scr. 24 (1981) 113.
- [22]. A. Di Pietro et al., Phys. Rev. C 69 (2004) 044601.
- [23]. E.F. Aguilera et al., Phys. Rev. C 79 (2009) 021601(R).
- [24]. C. Beck et al., Nucl. Phys. A 834 (2010) 440c

- [25]. S.Hussein, R.Lichtenthäler, F.M.Nunes and I.J.Thompson, Phys. Lett. B 91 (2006) 640.
- [26]. M. Sinha et al., Phys. Rev. C 78 (2008) 027601.
- [27]. M. Sinha et al., Phys. Rev. C 76 (2007) 027603.
- [28]. H. Kumawat et.al., Phys. Rev. C 86 (2012) 024607.
- [29]. S.P. Hu et al., Phys. Rev. C 91 (2015) 044619.
- [30]. P.K. Rath et al., Phys.Rev. C 79 (2009) 051601(R).
- [31]. P.K. Rath et al., Phys. Rev. C 88 (2013) 044617.
- [32]. P.K. Rath et al., Nucl. Phys. A 874 (2012) 14.
- [33]. K. Hagino, N. Rowley and A.T. Kruppa, Comput. Phys. Comm. 123 (1999) 143.
- [34]. I.J. Thompson, Comput. Phys. Rep. 7 (1988) 167.
- [35]. M.K. Pradhan et al., Phys. Rev. C 83 (2011) 064606.
- [36]. A. Mukherjee et al., Phys. Lett. B 636 (2006) 91.
- [37]. C.S. Palshetkar et al., Phys. Rev. C 89 (2014) 024607.
- [38]. A. Shrivastava et al., Phys. Rev. Lett. 103 (2009) 232702.
- [39]. C.S. Palshetkar et al., Phys. Rev. C 82 (2010) 044608.
- [40]. V.V. Parkar et al., Phys. Rev. C 82 (2010) 054601.
- [41]. P.R.S. Gomes et al., Phys. Rev. C 73 (2006) 064606.
- [42]. Y.D. Fang et al., Phys. Rev. C 91 (2015) 014608.
- [43]. N.T. Zhang et al., Phys. Rev. C 90 (2014) 024621.
- [44]. Y.D. Fang et al., Phys. Rev. C 87 (2013) 024604.
- [45]. P.R.S. Gomes et al., Phys. Lett. B 634 (2006) 356.
- [46]. P.R.S. Gomes et al., Phys. Rev. C 84 (2011) 014615.
- [47]. M. Dasgupta et al., Phys. Rev. Lett. 82 (1999) 1395.
- [48]. M. Dasgupta et al., Phys. Rev. C 70 (2004) 024606.
- [49]. S.B. Moraes et al., Phys. Rev. C 61 (2000) 064608.
- [50]. P.R.S. Gomes et al., Phys. Lett. B 601 (2004) 20.
- [51]. G.V. Martí et al., Phys. Rev. C 71 (2005) 027602.
- [52]. M. Dasgupta et al., Phys. Rev. C 66 (2002) 041602(R).
- [53]. K. Hagino, M. Dasgupta and D.J. Hinde, Nucl. Phys. A 738 (2004) 475.
- [54]. A. Diaz-Torres et al., Phys. Rev. Lett. 98 (2007) 152701.
- [55]. A. Diaz-Torres, Comput. Phys. Comm. 182 (2011) 1100.
- [56]. A. Diaz-Torres, J. Phys. G: Nucl. Part. Phys. 37 (2010) 075109.

- [57]. H.D. Marta, L.F. Canto and R. Donangelo, Phys. Rev. C 89 (2014) 034625.
- [58]. P.R.S. Gomes et al., Phys. Rev. C 73 (2006) 064606.
- [59]. M. dasgupta et al., Phys. Rev. C 81 (2010) 024608.
- [60]. H. Kumawat et al., Phys. Rev. C 86 (2012) 024607.
- [61]. C.L. Gua et al., Phys. Rev. C 92 (2015) 014615.
- [62]. C. Beck, Nucl. Phys. A 787 (2007) 251c.
- [63]. E.F. Aguilera et al., Phys. Rev. C 79 (2009) 021601(R).
- [64]. K. Hagino, A. Vitturi, C.H. Dasso and S.M. Lenzi, Phys. Rev. C 61 (2000) 037602.
- [65]. A. Diaz-Torres and I.J. Thompson, Phys. Rev. C 65 (2002) 024606.
- [66]. A. Diaz-Torres, I.J. Thompson and C. Beck, Phys. Rev. C 68 (2003) 044607.
- [67]. J.A. Tostevin, F.M. Nunes and I.J. Thompson, Phys. Rev. C 63 (2001) 024617.
- [68]. C. Beck and N. Keeley, A. Diaz-Torres, Phys. Rev. C 75 (2007) 054605
- [69]. F. M. Nunes and I. J. Thompson, Phys. Rev. C 59 (1999) 2652.
- [70]. F. M. Nunes and I. J. Thompson, Phys. Rev. C 57 (1998) R2818.
- [71]. N. Keeley, K. W. Kemper and K. Rusek, Phys. Rev. C 66 (2002) 044605: N. Keeley and K. Rusek, Phys. Lett. B 427 (1998) 1
- [72]. H. Feshbach, Ann. Phys. 19 (1962) 287; Ann. Phys. 5 (1958) 357.
- [73]. R. Rafiei et al., Phys. Rev. C 81 (2010) 024601.

BARRIER PENETRATION MODEL

2.1 Barrier Penetration Model

The barrier penetration model (BPM) is the simplest quantum mechanical way to analyze the fusion excitation functions. In general fusion excitation function of reactions involving heavy-ions depends strongly on the intrinsic degrees of freedom of the nuclei involved in collision. Nevertheless, the gross features of the elastic and the total reaction cross sections can be described by a simple Schrödinger equation in the space of the projectile—target separation degree of freedom by generalizing the potential to be complex energy dependent potential given as [1-4]

$$U^{opt}(r) = V^{opt}(r) - iW^{opt}(r)$$
(2.1.1)

The explicit energy dependence in the potential is omitted for the sake of simplicity. The real part of the interaction, $V^{opt}(r)$ consisting of Columbic and nuclear terms, can be written in the form

$$V^{opt}(r) = V_C(r) + V_N(r)$$
 (2.1.2)

where V_C is pure Coulomb term which arises because of the positive charge possessed by the interacting nuclei and is a long-ranged repulsive term while V_N which is associated with strong nuclear forces is a short ranged attractive term. The imaginary part, $W^{opt}(r)$, is a short-ranged function accounting for the incident flux lost to excited channels. Within this approach, the reaction dynamics is governed by the following Schrödinger equation

$$[T + V^{opt}(r) - iW^{opt}(r)]\Psi^{(+)}(\vec{r}) = E\Psi^{(+)}(\vec{r})$$
(2.1.3)

Here T is the kinetic energy operator for the projectile–target relative motion and E is its total energy. The wave function $\Psi^{(+)}(\vec{r})$ can be written as sum of the wave functions corresponding to pure Coulomb scattering $\Phi^{sc}_{C}(\vec{k},\vec{r})$ and the scattering wave $\Psi^{sc}_{N}(\vec{k},\vec{r})$ arising from nuclear part of the scattering potential that is

$$\Psi^{(+)}(\vec{r}) = \Phi_C^{sc}(\vec{k}, \vec{r}) + \Psi_N^{sc}(\vec{k}, \vec{r})$$
(2.1.4)

where \vec{k} is the incident wave vector. The wave function $\Phi_C^{sc}(\vec{k}, \vec{r})$ is obtained by solving Eq. (2.1.3) by switching off potentials V_N and W^{opt} under the scattering boundary condition given by

$$\Phi_{C}(\vec{k}, \vec{r}, z)\Big|_{|r-z| \to \infty} \to \frac{1}{(2\pi)^{3/2}} \left[\exp(ikz + i\eta \ln k(r-z)) + \frac{\exp(ikr - i\eta \ln(2kr))}{r} f_{C}(\theta) \right] (2.1.5)$$

Above, $f_C(\theta)$ is the scattering amplitude associated with the long ranged Coulomb interaction and is given by the following expression

$$f_C(\theta) = \frac{z_P z_T e^2}{2mv^2} \frac{\exp[-i\eta(\ln(1-\cos\theta)/2) + i\pi + 2i\delta_0]}{\sin^2(\theta/2)}$$
(2.1.6)

with
$$\exp(2i\delta_0) = \frac{\Gamma(1+i\eta)}{\Gamma(1-i\eta)}$$

and $\eta = \frac{z_1 z_2 e^2}{hv}$ is called Sommerfeld parameter.

Here δ_0 is the phase shift in s-partial wave, $\Gamma(n)$ is gamma function, $z_P e$ and $z_T e$ are the charges on the projectile and target respectively, V is the relative velocity of projectile-target system and θ is scattering angle.

The scattering wave function $\Psi_N^{sc}(\vec{k},\vec{r})$ corresponds to pure nuclear interaction and is obtained by solving Eq. (2.1.3) by switching off V_C term and retaining V_N and W^{opt} terms under boundary condition

$$\Psi^{sc}(\vec{k}, \vec{r})_{r \to \infty} \to \frac{1}{(2\pi)^{3/2}} \frac{[f_N(\theta) \exp i(kr - \eta \ln(2kr))]}{r}$$
 (2.1.7)

Here $f_N(\theta)$ is the scattering amplitude, associated with the short ranged nuclear interaction, which is usually expanded in partial waves

$$f_N(\theta) = \frac{1}{2ik} \sum_{l} (2l+1) P_l(\cos \theta) e^{2i\sigma_l} (S_{N,\ell} - 1)$$
 (2.1.8)

with P_l as the Legendre polynomial, σ_ℓ as the Coulomb phase shift and $S_{N,\ell}$ as the nuclear S-matrix. The elastic differential scattering cross-section is given by the modulus square of the sum of scattering amplitudes through the expression

$$\frac{d\sigma(\theta)}{d\Omega} = \left| f_C(\theta) + f_N(\theta) \right|^2 \tag{2.1.9}$$

It is pertinent to mention here that because of the presence of the imaginary part in the potential, the usual continuity equation is not satisfied. But the modified continuity equation can be derived by using the following Schrödinger equation

$$\left[-\frac{\hbar^2}{2\mu} \nabla^2 + U^{opt}(r,t) \right] \Psi^{(+)} = i\hbar \frac{\partial \Psi^{(+)}}{\partial t}$$
 (2.1.10)

Here μ is the reduced mass of projectile-target system i.e. $\mu = \frac{m_P m_T}{m_P + m_T}$

where m_P and m_T are the masses of projectile and target respectively.

Taking complex conjugate of Eq. (2.1.10), we get

$$\left[-\frac{\hbar^2}{2\mu}\nabla^2 + \left(U^{opt}(r,t)\right)^*\right]\Psi^{(+)^*} = -i\hbar\frac{\partial\Psi^{(+)^*}}{\partial t}$$
(2.1.11)

Now, pre multiply Eq. (2.1.10) by $\Psi^{(+)^*}$ and Eq.(2.1.11) by $\Psi^{(+)}$ and then subtracting the resulting equations, we have

$$i\hbar\Psi^{(+)^*}\frac{\partial\Psi^{(+)}}{\partial t} + i\hbar\Psi^{(+)}\frac{\partial\Psi^{(+)^*}}{\partial t} = -\frac{\hbar^2}{2\mu} \left[\Psi^{(+)^*}\nabla^2\Psi^{(+)} - \Psi^{(+)}\nabla^2\Psi^{(+)^*}\right] + \left[\Psi^{(+)^*}U^{opt}(r,t)\Psi^{(+)} - \Psi^{(+)}\left(U^{opt}(r,t)\right)^*\Psi^{(+)^*}\right]$$
(2.1.12)

or

$$i\hbar \frac{\partial}{\partial t} \left[\Psi^{(+)^*} \Psi^{(+)} \right] = -\frac{\hbar^2}{2\mu} \nabla \left[\Psi^{(+)^*} \nabla \Psi^{(+)} - \Psi^{(+)} \nabla \Psi^{(+)^*} \right] - 2iW^{opt} \Psi^{(+)^*} \Psi^{(+)} \quad (2.1.13)$$

Further simplification leads to

$$\frac{\partial}{\partial t} \left[\Psi^{(+)^*} \Psi^{(+)} \right] = -\frac{\hbar}{2 \, \mu i} \nabla \left[\Psi^{(+)^*} \nabla \Psi^{(+)} - \Psi^{(+)} \nabla \Psi^{(+)^*} \right] - \frac{2}{\hbar} W^{opt} \Psi^{(+)^*} \Psi^{(+)} \quad (2.1.14)$$

٥r

$$\frac{\partial \rho}{\partial t} = -\nabla \cdot \vec{j} - \frac{2}{\hbar} W^{opt} \Psi^{(+)^*} \Psi^{(+)}$$
(2.1.15)

where

$$\vec{j} = \frac{\hbar}{2\mu i} \left[\Psi^{(+)^*} \nabla \Psi^{(+)} - \Psi^{(+)} \nabla \Psi^{(+)^*} \right]$$
 (2.1.16)

is called current density and

$$\rho = \Psi^{(+)^*} \Psi^{(+)} \tag{2.1.17}$$

is called position probability density.

For stationary energy states that is for constant value of $\rho(r,t)$ Eq. (2.1.15) becomes

$$\nabla . \vec{j} = -\frac{2}{\hbar} W^{opt} \Psi^{(+)^*} \Psi^{(+)}$$

or

$$\vec{\nabla}.\vec{j} = -\frac{2}{\hbar}W^{opt}|\Psi^{(+)}|^2 \tag{2.1.18}$$

In order to interpret the modified continuity equation, let us consider the case of non stationary states

$$\frac{\partial \rho}{\partial t} + \nabla \cdot \vec{j} = -\frac{2}{\hbar} W^{opt} \Psi^{(+)^*} \Psi^{(+)} \tag{2.1.19}$$

Since $\rho(r,t) = \Psi^{(+)^*} \Psi^{(+)}$ is always a positive quantity, so right hand side of Eq. (2.1.18) acts as a source of probability for negative value of W^{opt} and acts as a sink for positive value of W^{opt} . But for physical reasons W^{opt} is either zero or positive and hence the particles are being absorbed. The absorption cross-section σ_{abs} is defined as the total number of particles absorbed in complete configurational space in unit time provided a unit incident particles flux. For plane incident wave, wave density is unity and current density is $\frac{\hbar k}{\mu}$, the absorption cross section can be obtained by integrating Eq. (2.1.18) over a sphere of radius $R \rightarrow \infty$

$$\int_{V} \vec{\nabla} \cdot \vec{j} dV = \frac{8\pi}{\hbar \left(\frac{\hbar k}{\mu}\right)^{0}} W^{opt} \left|\Psi^{(+)}\right|^{2} dr$$
(2.1.20)

Using Gauss-divergence theorem

$$\int_{V} \vec{\nabla} \cdot \vec{j} dV = \int_{S} \hat{r} \cdot \vec{j} dS \tag{2.1.21}$$

Eq. (2.1.20) becomes

$$\sigma_{abs} = \frac{(2\pi)^3 k}{E} < \Psi^{(+)} | W^{opt} | \Psi^{(+)} >$$
 (2.1.22)

Here we have divided right hand side by incident current as absorption cross section is defined for unit incident particle flux.

In general the imaginary part of potential is given by the sum of separate contributions from fusion absorption W^F and absorption through direct reaction channels W^D i.e.

$$W^{opt}(r) = W^{F}(r) + W^{D}(r)$$
(2.1.23)

Above, $W^F(r)$ is a volumetric term and $W^D(r)$ is generally a surface term, which is relevant at $r \approx R_P + R_T$ so that the fusion cross section and the total cross section for direct reactions are given by the expressions

$$\sigma_F = \frac{(2\pi)^3 k}{E} < \Psi^{(+)} | W^F | \Psi^{(+)} > \tag{2.1.24}$$

$$\sigma_D = \frac{(2\pi)^3 k}{E} < \Psi^{(+)} | W^D | \Psi^{(+)} >$$
 (2.1.25)

For practical purposes, one carries out the partial-waves expansion [5]

$$\Psi^{(+)}(\vec{k};\vec{r}) = \frac{1}{(2\pi)^{3/2}} \sum_{l} (2l+1) P_l(\cos\theta) i^l e^{i\delta_l} \frac{u_l(k,r)}{kr}$$
(2.1.26)

here δ_l is the phase shift for l^{th} partial wave and $P_l(\cos\theta)$ is the Legendre polynomial. Here $<\Psi^{(+)}|W^F|\Psi^{(+)}>$ implies volume integration over complete configurational space $d\tau$ i.e.

$$<\Psi^{(+)}|W^F|\Psi^{(+)}>=\int_V (\Psi^{(+)}(\vec{k};\vec{r}))^*W^F\Psi^{(+)}(\vec{k};\vec{r})d\tau$$
. Neglecting spins we

have

$$<\Psi^{(+)}|W^F|\Psi^{(+)}> = \frac{4\pi}{k^2(2\pi)^3} \sum_{l} (2l+1) \int dr W^F(r) |u_l(k;r)|^2$$
 (2.1.27)

Eq. (2.1.24) becomes

$$\sigma_F = \frac{\pi}{k^2} \sum_{l} (2l+1)T_l^F$$
 (2.1.28)

with

$$T_{l}^{F} = \frac{4k}{E} \int dr W^{F}(r) |u_{l}(k;r)|^{2}$$
 (2.1.29)

as fusion probability. Similarly

$$\sigma_D = \frac{\pi}{k^2} \sum_{l} (2l+1) T_l^D$$
 (2.1.30)

with

$$T_{l}^{D} = \frac{4k}{E} \int dr W^{D}(r) |u_{l}(k;r)|^{2}$$
 (2.1.31)

Here $u_l(k;r)$ is the wave function corresponding to l^{th} partial wave having angular momentum $l\hbar$ and is obtained by numerical integration of the following radial equation from the origin, where one sets $u_l(k;0)=0$ as boundary condition.

$$-\frac{\hbar^2}{2\mu} \frac{d^2 u_l(k,r)}{dr^2} + \left[E - V_{eff}^l + iW^{OPT}\right] u_l(k,r) = 0$$
 (2.1.32)

here $V_{\it eff}^{\it l}$ is given by

$$V_{eff}^{l} = V_{C} + V_{N} + \frac{l(l+1)\hbar^{2}}{2\mu r^{2}}$$
 (2.1.33)

The initial value of derivative can be chosen arbitrarily, since it only affects the overall normalization. The Eq. (2.1.32) can be rewritten as

$$\frac{d^2 u_l(k,r)}{dr^2} = k_l^2 u_l(k,r)$$
 (2.1.34)

with

$$k_{l} = \sqrt{\frac{2\mu}{\hbar^{2}} \left(E - V_{eff}^{l} + iW^{OPT} \right)}$$
 (2.1.35)

as the effective local wave number. Now if the effective local wave number varies sufficiently slowly with the distance so that

$$\left| \frac{dk_l}{d \, \mathbf{r}} \frac{1}{k_l^2} \right| << 1$$

as is frequently the case at sufficiently large distance from a turning point. Then using the JWKB approximation, the solution of Eq. (2.1.34) is

$$u_l(k,\mathbf{r}) = \frac{A_l}{\sqrt{k_l}} exp \left[i \int_{R_0}^{\mathbf{r}} k_l d\mathbf{r} \right] + \frac{B_l}{\sqrt{k_l}} exp \left[-i \int_{R_0}^{\mathbf{r}} k_l d\mathbf{r} \right]$$
(2.1.36)

The first term represents the outgoing wave and the second term ingoing wave. The ratio $\frac{A_l}{B_l}$ depends on the nature of the potential near R_0 (internal radius where the fusion starts and which is smaller than barrier radius R_B) and on the condition imposed on $u_l(k,r)$ at $r \ll R_0$. The ratio $R_l = \frac{A_l}{B_l} exp \left[-2 \int\limits_{R_0}^r Im \, k_l \, d \, r \right] \text{ decreases with } r \text{ for negative } W^{OPT} \text{. If } R_l$

becomes negligible beyond r_i (internal turning point), the outgoing branch may be neglected and $u_l(k,r)$ becomes [6]

$$u_{l}(k,\mathbf{r}) = \frac{B_{l}}{\sqrt{k_{l}}} \exp \left[-i \int_{R_{0}}^{\mathbf{r}} k_{l} d\mathbf{r}\right]$$
 (2.1.37)

Taking logarithm on both sides;

$$\log\left[u_{l}(k,r)\sqrt{k_{l}}(r)\right] = \log(B_{l}) + \left[-i\int_{R_{0}}^{r} k_{l}d r\right]$$

The logarithmic derivative of $u_l(\vec{k}, \mathbf{r})$ is obtained as

$$\frac{d}{dr}log\left[u_{l}(k,r)\sqrt{k_{l}}(r)\right] = -ik_{l}(r)$$

$$\left(\frac{1}{u_{l}(k,r)\sqrt{k_{l}}(r)}\right)\frac{d}{dr}\left[u_{l}(k,r)\sqrt{k_{l}}(r)\right] = -ik_{l}$$

$$\left(\frac{1}{u_{l}(k,r)\sqrt{k_{l}}(r)}\right)\left[\frac{du_{l}(k,r)}{dr}\sqrt{k_{l}}(r) + \frac{u_{l}(k,r)}{2\sqrt{k_{l}}(r)}\frac{dk_{l}}{dr}\right] = -ik_{l}(r)$$

$$\frac{1}{u_{l}(k,r)}\frac{du_{l}(k,r)}{dr} + \frac{1}{2(k_{l}(r))}\frac{dk_{l}}{dr} = -ik_{l}$$

$$\frac{1}{u_{l}(k,r)}\frac{du_{l}(k,r)}{dr} = -\frac{1}{2k_{l}(r)}\frac{dk_{l}}{dr} - ik_{l}$$
(2.1.38)

It is noted that $\frac{du_l}{d\mathbf{r}}\Big|_{\mathbf{r}\approx R_0}$ depends only on $k_l(\mathbf{r})$ and its derivative and does

not depend on the values of optical potential in $r < R_0$ region. Since the logarithmic derivative of wave function is given by Eq. (2.1.38), it is convenient to start the numerical integration at $r = R_0$ instead of at the origin [6-9].

Now in order to present the fusion cross-section in a way which is suitable for approximation we substitute the Eq. (2.1.18) into Eq. (2.1.24) and obtain

$$\sigma_F = \left(\frac{\hbar}{2}\right) \frac{(2\pi)^3 k}{E} \int \left(-\nabla \cdot \vec{j}\right) d^3 \mathbf{r}$$

or

$$\sigma_F = \frac{(2\pi)^3}{v} \int (-\nabla \cdot \vec{j}) d^3 \mathbf{r}$$
 (2.1.39)

Here $v = \frac{\hbar k}{\mu}$ is the asymptotic relative velocity.

Using Gauss-divergence theorem

$$\int \left(-\nabla . \vec{j}\right) d^3 \mathbf{r} = \int_{S} \left(-\stackrel{\wedge}{\mathbf{r}} . \vec{j}\right) ds$$

We may write

$$\sigma_F = \frac{(2\pi)^3}{v} \int_{s} \left(-\vec{r} \cdot \vec{j} \right) ds$$

The integration is carried out over the surface of a sphere of radius R_F , containing region where $W^F(\mathbf{r})$ is relevant that is $ds = R_F^2 d\Omega$ so that

$$\sigma_F = \frac{(2\pi)^3}{v} R_F^2 \int_{s} \left(-\vec{\mathbf{r}} \cdot \vec{j} \right) d\Omega$$
 (2.1.40)

Above \widehat{r} is the radial unit vector, which corresponds to the normal to the spherical surface at the direction determined by $\Omega(\equiv \theta, \phi)$. Since

 $\nabla = \hat{r}\partial/\partial r - i\vec{r} \times \vec{L}$ [10], and the dot product $\hat{r}.(\vec{r} \times \vec{L})$ vanish, we have

$$\widehat{r}.\overrightarrow{j} = \frac{\hbar}{2\mu i} \left[(\Psi^{(+)})^* \frac{\partial \Psi^{(+)}}{\partial r} - (\Psi^{(+)}) \frac{\partial (\Psi^{(+)})^*}{\partial r} \right]$$
(2.1.41)

Substituting Eq. (2.1.26) in to Eq. (2.1.41), integrating over the surface and using the orthogonality of Legendre polynomials we get

$$\sigma_F = -\frac{(2\pi)^3}{v} R_F^2 \times \frac{4\pi}{(2\pi)^3} \sum_{l} (2l+1) \frac{1}{k^2 r^2} \frac{\hbar}{2\mu i} \left[u_l^* \frac{du_l}{dr} - u_l \frac{du_l^*}{dr} \right]$$
(2.1.42)

or

$$\sigma_F = \frac{\pi}{k^2} \sum_{l} (2l+1) \frac{j_l^F}{-\frac{v}{4}}$$
 (2.1.43)

Above

$$j_{l}^{F} \equiv j_{l}(R_{F}) = \frac{\hbar}{2\mu i} \left[u_{l}^{*}(k;r) \frac{du_{l}(k;r)}{dr} - u_{l}(k;r) \frac{du_{l}^{*}(k;r)}{dr} \right]_{r=R_{F}} \text{ is the}$$

radial current evaluated at $r = R_F$.

Now comparing the Eq. (2.1.43) and Eq. (2.1.28) the fusion probability comes out to be

$$T_l^F = \frac{j_l^F}{-\frac{v}{4}} \tag{2.1.44}$$

The major disadvantage of this equation is that it depends on arbitrary normalization of the radial wave function. In order to get rid of this disadvantage it is convenient to write u_l as the sum

$$u_{l}(k;r) = u_{l}^{(-)}(k;r) + u_{l}^{(+)}(k;r)$$
(2.1.45)

where $u_l^{(-)}$ and $u_l^{(+)}$ are, respectively, solutions of the radial equation with incoming and outgoing boundary conditions at $r \to \infty$ and have the following asymptotic forms [11]

$$u_l^{(-)}(k; r \to \infty) = \frac{i}{2} \exp \left[-i(kr - \frac{l\pi}{2} - \eta \ln(2\rho) + \sigma_l) \right]$$
 (2.1.46)

$$u_l^{(+)}(k; r \to \infty) = -\frac{i}{2} \overline{S}_l \exp \left[i(kr - \frac{l\pi}{2} - \eta \ln(2\rho) + \sigma_l) \right]$$
 (2.1.47)

where \overline{S}_l is the S-matrix associated with the short-ranged potentials. The incident radial current is now expressed in terms of $(u_l^{(-)})$ as

$$j_l^{in} = \lim_{r \to \infty} j_l^{(-)}(r) = \frac{\hbar}{2\mu i} \lim_{r \to \infty} \left[(u_l^{(-)})^* \frac{du_l^{(-)}}{dr} - (u_l^{(-)}) \frac{d(u_l^{(-)})^*}{dr} \right]$$
(2.1.48)

Now

$$u_{l}^{(-)*} \frac{du_{l}^{(-)}}{dr} = \frac{-i}{2} exp \left[i \left(k \, r - \frac{l\pi}{2} - \eta \, ln(2k \, r) + \delta_{l} \right) \right] \times \left[\frac{i}{2} exp \left[-i \left(k \, r - \frac{l\pi}{2} - \eta \, ln(2k \, r) + \delta_{l} \right) \right] \right] \times \left[-ik + i\eta \, \frac{2k}{2kr} \right]$$

$$u_{l}^{(-)*} \frac{du_{l}^{(-)}}{dr} = \frac{-i^{2}}{4} \left[-ik + \frac{i\eta}{r} \right]$$

$$u_{l}^{(-)*} \frac{du_{l}^{(-)}}{dr} = \frac{1}{4} \left[-ik + \frac{i\eta}{r} \right]$$
(2.1.49)

Similarly

$$u_l^{(-)} \frac{du_l^{(-)^*}}{dr} = \frac{1}{4} \left[ik - \frac{i\eta}{r} \right]$$
 (2.1.50)

and

$$u_{l}^{(-)*} \frac{du_{l}^{(-)}}{dr} - u_{l}^{(-)} \frac{du_{l}^{(-)*}}{dr} = \frac{1}{4} \left[-ik + \frac{i\eta}{r} \right] + \frac{1}{4} \left[-ik + \frac{i\eta}{r} \right] = \frac{1}{4} \left[-2ik + \frac{2i\eta}{r} \right]$$

Taking $\lim r \to \infty$

$$\lim_{r \to \infty} \left[u_l^{(-)*} \frac{du_l^{(-)}}{d \, r} - u_l^{(-)} \frac{du_l^{(-)*}}{d \, r} \right] = \frac{-ik}{2}$$
 (2.1.51)

Now putting Eq. (2.1.51) into Eq. (2.1.48) we get

$$j_l^{in}(\mathbf{r}) = \lim_{r \to \infty} j_l^{(-)} = \frac{\hbar}{2\mu i} \left[\frac{-ik}{2} \right] = \frac{-\hbar k}{4\mu} = \frac{-p}{4\mu}$$

$$j_l^{in}(\mathbf{r}) = \lim_{r \to \infty} j_l^{(-)} = \frac{-\nu}{4}$$
 (2.1.52)

Using this result, Eq. (2.1.44) takes the form

$$T_l^F = -\frac{j_l^F}{j_l^{in}} \tag{2.1.53}$$

If, the imaginary potential associated with fusion absorption is taken as Woods–Saxon function of small radius R_F , diffusivity and incoming wave boundary conditions are assumed to be applicable at $R_F \approx R_0$ then a very simple expression for T_l^F can be obtained within the WKB approximation,

$$(T_l^F)_{WKB} = \exp[-2\Phi^{WKB}]$$
 (2.1.54)

with

$$\Phi^{WKB} = \int_{R_E}^{\infty} \operatorname{Im}\{k_l(r)\}dr \tag{2.1.55}$$

Here, since the imaginary potential vanishes from R_F to ∞ , $k_l(r)$ is real in the classically allowed region and at sub-barrier energies the integral can be evaluated between the internal and the external classical turning points r_i and

 r_e . That is,

$$\Phi^{WKB} = \int_{r}^{r_e} k_l(r)dr \tag{2.1.56}$$

where $k_l(r) = ik(r)$. One of the important limitation of WKB approximation for the fusion probability is that it is accurate at collision energies well below the potential barrier, V_B , but leads to wrong results around the barrier. At $E = V_B$, $(T_l^F)_{WKB} = 1$ while the quantum mechanical value is $T_l^F = 1/2$. This difficulty is removed in an improved Kemble's version of WKB approximation [12]. In this modified version, the transmission of progressive matter wave through an approximately parabolic potential barrier was considered. In case when incident projectile energy is lower than the top of the parabolic hill and the projectile are incident from the left of potential hill then the constancy of current density leads to the following transmission co-efficient

$$T = \frac{1}{1 + \exp[2\Phi_{WKB}]}$$
 (2.1.57a)

Further if the energy of incident particles is more than the maximum of potential hill then the integrand will be imaginary and the transmission coefficient becomes

$$T = \frac{1}{1 + \exp[-2\Phi'_{WKB}]}$$
 (2.1.57b)

with Φ_{WKB} and Φ'_{WKB} denotes the integral $\left(\frac{2\pi}{h}\right)^{z^2}_{z_1}|p|d\xi$ and

$$\left(\frac{2\pi}{h}\right)\int_{z_1}^{z_2} |p||d\xi|$$
 respectively, z_1 , z_2 are the classical turning points and

 $p = \sqrt{2\mu(E - V_B)}$. This problem was also discussed in the work of Hill and Wheeler [13] under the following parabolic approximation for potential

$$V_{l}(r) \cong B_{l} - \frac{1}{2}u\omega_{l}^{2}(r - R_{l})^{2}$$
(2.1.58)

they actually evaluated the integral in closed form and obtains

$$T_l^{HW} = \frac{1}{1 + \exp[2\pi\Phi^{HW}]}$$
 (2.1.59)

with

$$\Phi^{HW} = \frac{(E - B_l)}{\hbar \omega_l} \tag{2.1.60}$$

here Φ^{HW} is the energy deficit relative to the top of the barrier, divided by characteristic quantum energy, E_{curv} , which is fixed by the curvature of the top of the barrier and by the effective mass associated with the fission mode of deformation. E_{curv} can be visualize by reversing the sign of potential so that barrier peak becomes a trough and the system will behave like a harmonic oscillator in the neighborhood of the critical point, with a natural circular frequency, ω_l and a characteristic quantum energy, $\hbar\omega_l$. Above E is the incident beam energy and B_l is the barrier height. The Hill–Wheeler approximation for the fusion cross sections was further modified by Wong [14] considering the following assumptions,

$$R_l = R_{l=0} \equiv R_B \tag{2.1.61}$$

$$\omega_l = \omega_{l=0} \equiv \omega \tag{2.1.62}$$

$$B_l = V_B + \frac{\hbar^2}{2\mu R_B^2} (l + 1/2)^2$$
 (2.1.63)

with $V_B=B_{l=0}$ and assuming that many partial-waves contribute to fusion cross section so that the summation over l may be replaced by integral over continuous variable $l+\frac{1}{2}$, the Hill-Wheeler formula for fusion cross section

is

$$\sigma_F = \frac{\pi}{k^2} \sum_{l} (2l+1) \frac{1}{1 + \exp(\frac{2\pi}{\hbar \omega} [V_l - E])}$$
 (2.1.64)

Since the centrifugal barrier V_l can be written as

$$V_{l} = V_{B} + \frac{\hbar^{2}}{2\mu R_{B}^{2}}l(l+1) = V_{B} + \frac{\hbar^{2}}{2\mu R_{B}^{2}}(l+1/2)^{2} - \frac{\hbar^{2}}{8\mu R_{B}^{2}}$$
(2.1.65)

we may write the fusion cross-section as

$$\sigma_{F} = \frac{\pi}{k^{2}} \sum_{l=0}^{\infty} (2l+1) \left[\frac{1}{1 + \exp(\frac{2\pi}{\hbar\omega} [V_{B} - \frac{\hbar^{2}}{2uR_{B}^{2}} - E]) \exp(\frac{2\pi}{\hbar\omega} [\frac{(l+1/2)^{2}\hbar^{2}}{2uR_{B}^{2}}])} \right] (2.1.66)$$

For further simplifications, let us assume that

$$b = \exp\frac{2\pi}{\hbar\omega} \left[V_B - \frac{\hbar^2}{2uR_B^2} - E \right]$$
 (2.1.67)

$$a = \frac{2\pi}{\hbar\omega} \frac{\hbar^2}{2uR_R^2} \tag{2.1.68}$$

So that

$$\sigma_F = \frac{\pi}{k^2} \sum_{l=0}^{\infty} \left[\frac{2(l+1/2)}{1 + b \exp(a(l+1/2)^2)} \right]$$
 (2.1.69)

As large number of the partial waves contribute to the fusion cross-section, the summation over l may be changed into the integration

$$\sigma_F = \frac{\pi}{k^2} \int_{l=0}^{\infty} \left[\frac{2(l+1/2)dl}{1 + b \exp(a(l+1/2)^2)} \right]$$
 (2.1.70)

In order to evaluate the integral, let us change the variable of the integration from l to x by assuming $x = [l+1/2]^2$ so that Eq. (2.1.70) becomes

$$\sigma_F = \frac{\pi}{k^2} \int_{l=\frac{1}{4}}^{\infty} \frac{dx}{(1 + b \exp(ax))}$$
 (2.1.71)

or

$$\sigma_F = \frac{\pi}{k^2} \int_{l=\frac{1}{4}}^{\infty} \frac{\exp(-ax)dx}{[\exp(-ax) + b]}$$
 (2.1.72)

Further, the substitution $\exp(-ax) = t$ leads to

$$\sigma_F = \frac{\pi}{k^2} \int_{\exp(-\frac{a}{4})}^{\infty} -\frac{dt}{a(b+t)}$$

Now by performing the integration with respect to 't', one obtains

$$\sigma_F = \frac{\pi}{ak^2} \ln \left[1 + \frac{\exp(-a/4)}{b} \right] \tag{2.1.73}$$

By putting the values of b and a from Eqs. (2.1.67) and (2.1.68) into Eq. (2.1.73) we get the following final expression of Wong's formula for the fusion cross-section

$$\sigma_F = \frac{\hbar \omega R_B^2}{2E} \ln \left[1 + \exp \left(\frac{2\pi}{\hbar \omega} (E - V_B) \right) \right]$$
 (2.1.74)

Here R_B , V_B and $\hbar\omega$ are barrier position, barrier height and barrier curvature respectively and play very crucial role in the determination of fusion cross section. It is important to mention that results of Wong's approximation are better than that of Hill-Wheeler approximation which may be ascribed to the fact that in Wong's formula the unrealistic transparency of the parabolic barrier is partially corrected.

The barrier position which strongly depends on sizes of colliding nuclei is parameterized as $R_B = r_b (A_P^{1/3} + A_T^{1/3}); r_b \approx 1.4 \, fm$ [15]. The barrier height, which is very sensitive barrier parameter, is the value of total interaction potential,

$$V_T(R,L) = V_{nucl}(R) + V_{Coul}(R) + V_{Rot}(R,L)$$
(2.2.1)

for two colliding nuclei at $R=R_B$. Here V_{nucl} , V_{Coul} and V_{Rot} stands for the nuclear, Coulomb and the centrifugal potentials respectively. The Coulomb potential may be conveniently taken as the potential due to uniformly charged spheres of radii R_P (projectile radius) and R_T (target radius) such that

$$V_{Coul}(R) = \begin{cases} \frac{Z_{P}Z_{T}e^{2}}{R} forR > R_{P} + R_{T} \\ \frac{Z_{P}Z_{T}e^{2}}{2(R_{P} + R_{T})} \left[3 - \frac{R^{2}}{(R_{P} + R_{T})^{2}} \right] forR < R_{P} + R_{T} \end{cases}$$
(2.2.2)

and the centrifugal term is given by

$$V_{Rot} = \frac{\hbar^2 L(L+1)}{2 \mu R^2}$$
 (2.2.3)

Above Z_P and Z_T are the atomic numbers of projectile and target. The R is the relative distance between the centers of the projectile and the target, μ is the reduced mass of the projectile–target system and L is the angular momentum quantum number. For the nuclear part of the potential V_{nucl} , we employ three parametric energy dependent Woods–Saxon potential

$$V_{nucl} = \frac{-V_0}{\left[1 + \exp\left(\frac{R - R_0}{a}\right)\right]}$$
 (2.2.4)

with V_0 , R_0 and 'a' as the depth, range and diffuseness parameters. The energy dependence in the potential is introduced through the diffuseness parameter, which defines slope of the nuclear potential in the tail region of Coulomb barrier where fusion starts to take place, by the following relation [16, 17]

$$a(E) = 0.85 \left[1 + \frac{r_0}{13.75 \left(A_p^{-\frac{1}{3}} + A_T^{-\frac{1}{3}} \right) \left(1 + \exp\left(\frac{E/V_{B0}}{0.03} - 0.96 \right) \right)} \right] fm$$
 (2.2.5)

The other two parameters of the potential are evaluated by using

$$R_0 = r_0 (A_P^{1/3} + A_T^{1/3})$$
 and

$$V_0 = -52.99 \left(\frac{R_P R_T}{R_P + R_T} \right)$$

with $r_0=1.2$ fm, $R_P=1.5A_P^{1/3}-0.77A_P^{-1/3}$ fm and

$$R_T = 1.5A_T^{1/3} - 0.77A_T^{-1/3} fm$$

Besides the barrier position and height the barrier curvature is also an important ingredient for the calculations and is related to the double derivative of the potential at barrier position through the following expression [18]

$$\hbar\omega = \sqrt{\frac{\hbar^2 \left| V_T^{"}(R_B) \right|}{\mu}} \tag{2.2.6}$$

An alternative determination of potential parameters may be used wherein

$$a(E) = 0.63 \left[1 + \frac{1}{13.75 \left(A_p^{-\frac{1}{3}} + A_T^{-\frac{1}{3}} \right) \left(1 + \exp\left(\frac{E/V_{B0}}{0.03} - 0.96 \right) \right)} \right] fm$$
 (2.2.7)

which is slightly modified form of expression given in Ref.[15, 3] such that the minimum diffuseness becomes 0.63fm with the range and depth parameters are obtained by using Broglia-Winther parameterization [19] as under

$$R_0 = R_P + R_T + 0.29$$

$$R_{P(T)} = 1.233 A_{P(T)}^{1/3} - 0.98 A_{P(T)}^{-1/3}$$

$$V_0 = 16\pi\gamma \check{R}a(E)$$

$$\check{R} = R_P R_T / (R_P + R_T)$$

$$\gamma = \gamma_0 \left[1 - 1.8 \frac{(N_P - Z_P)(N_T - Z_T)}{A_P A_T} \right]$$

with $\gamma_0 = 0.95$ MeVfm⁻².

To extract CF (or ICF) from TF, a phenomenological selection function given by

$$f\left(\frac{E}{V_{B}}\right) = \begin{cases} 0.08 & for \frac{E}{V_{B}} < 0.91\\ -13.34 \left(\frac{E}{V_{B}}\right)^{2} + 29.99 \left(\frac{E}{V_{B}}\right) - 16.16 \end{bmatrix} & for 0.91 \le \frac{E}{V_{B}} \le 1.13 \\ 0.70 & for \frac{E}{V_{B}} > 1.13 \end{cases}$$
 (2.2.8)

is used in such a way that we have

$$\sigma_{CF} = f \left(\frac{E}{V_B} \right) \sigma_{TF} \tag{2.2.9}$$

equivalently

$$\sigma_{ICF} = \left[1 - f\left(\frac{E}{V_B}\right)\right] \sigma_{TF} \tag{2.2.10}$$

References

- H. Feshbach, C.E. Porter and V.F. Weisskopft, Phys. Rev. 90 (1953) 166;
 Phys. Rev. 96 (1954) 448.
- [2]. H. Feshbach, Ann. Phys. (NY) 5 (1958) 357; Ann. Phys. (NY) 19 (1962)
- [3]. Manjeet Singh, Sukhvinder S. Duhan and Rajesh Kharab, Nucl. Phys. A 897 (2013) 198.
- [4]. L.F. Canto, P.R.S. Gomes, R. Donangelo and M.S. Hussein, Phys. Rep. 424 (2006) 1.
- [5]. C.J. Joachain, Quantum Collision Theory, North-Holland, Amsterdam, 1983.
- [6]. G.H. Rawitscher, Phys. Rev. 135 (1964) B605; Nucl. Phys. 85 (1966) 337.
- [7]. S. C. Miller, Jr and R. H. Good, Jr, Phys. Rev. 91 (1953) 174.
- [8]. N. H. Frank and L. A. Young, Phys. Rev. 38 (1931) 80.
- [9]. G. H. Rawitscher, Nucl. Phys. 85 (1963) 337.
- [10]. J.D. Jackson, Classical Electrodynamics, Wiley, New York, 1975.
- [11]. Abramowitz, I. Stegun, Handbook of Mathematical Functions, Dover, New York, 1972.
- [12]. E.C. Kemble, Phys. Rev. 48 (1935) 549.
- [13]. D.L. Hill and J.A. Wheeler, Phys. Rev. 89 (1953) 1102.
- [14]. C.Y. Wong, Phys. Rev. Lett. 31 (1973) 766.
- [15]. D. Glas and U. Mosel, Phys. Rev. C 10 (1974) 2620.
- [16]. Manjeet Singh, Sukhvinder S. Duhan and Rajesh Kharab, Mod. Phys. Lett. A 26 (2011) 2129.
- [17]. Sukhvinder S. Duhan, Manjeet Singh, Rajesh Kharab and H.C. Sharma, Mod. Phys. Lett. A 26 (2011) 1017.
- [18]. L.F. Canto, P.R.S. Gomes, J. Lubian, L.C. Chamon and E. Crema, J. Phys. G, Nucl. Part. Phys. 36 (2009) 015109.
- [19]. W. Reisdorf, J. Phys. G: Nucl. Part. Phys. 20 (1994) 1297.

CLASSICAL DYNAMICAL MODEL

3.1 Classical Dynamical Model

The classical dynamical model used to describe nuclear reactions involving loosely bound nuclei is based on the assumption that the projectile-target relative motion can be treated classically [1-2]. Within this approach, when a weakly bound projectile is incident on target T with energy E₀ and orbital angular momentum L₀, its motion is along a determinate path with definite distance of closest approach R_{min}(E₀, L₀). The path of the projectile is traced by solving the classical equation of motion under the influence of mutual Coulomb and nuclear forces between the projectile and target. This interaction generate a Coulomb barrier for head-on (L $_0$ =0) collisions of height $V_{\scriptscriptstyle B}^{\scriptscriptstyle PT}$ at a separation R_B^{PT} . Since projectile is weakly bound it is highly prone to dissociate and the process of breakup of projectile is assumed to be completely random process. Let $P_{BU}^{L}(R)$ be the density of local breakup probability such that the probability of breakup of projectile in the region R to R+dR is $P_{BU}^{L}(R)dR$, R being the projectile target relative separation. For such a breakup event to occur there must be a finite probability of surviving the projectile in the interval ∞ to R, let it be S(R). Now it is quite obvious that $S(R+dR) = S(R)[1 - P_{BU}^{L}(R)dR]$ represents the probability of survival of projectile at R+dR.

Rearranging terms, we have

$$\frac{S(R+dR) - S(R)}{dR} = -S(R)P_{BU}^{L}(R)$$

$$\frac{dS(R)}{dR} = -S(R)P_{BU}^{L}(R)$$
 (3.1.1)

At $R=\infty$, the projectile must survive that is $S(\infty)=1$. Under this boundary condition the above equation i.e.

$$\frac{dS(R)}{S(R)} = -P_{BU}^{L}(R)dR \tag{3.1.2}$$

can be easily integrated to give

$$S(R) = \exp[-\int_{R}^{R} P_{BU}^{L}(R) dR]$$
 (3.1.3)

If $\int_{-\infty}^{R} P_{BU}^{L}(R) dR \ll 1$ then S(R) may be approximated, by retaining only first

two terms of exponential expansion, as

$$S(R) \approx 1 - \int_{-\infty}^{R} P_{BU}^{L}(R) dR \tag{3.1.4}$$

and the breakup probability at R which is simply 1-S(R), is given by

$$P_{BU}(R) \approx \int_{-\infty}^{R} P_{BU}^{L}(R) dR. \qquad (3.1.5)$$

Since the breakup may occur either when the projectile is approaching to the target or when it is going away from the target after crossing, we may write

$$P_{BU}(R_{\min}) = 2 \int_{R_{\min}}^{\infty} P_{BU}^{L}(R) dR.$$
 (3.1.6)

On the empirical ground or on the basis of the CDCC calculations, it is found that the integral in above equation can be expressed as an exponential function of distance of closest approach that is [1-3]

$$P_{BU}(R_{\min}) = A \exp(-\alpha R_{\min}) \tag{3.1.7}$$

It immediately leads to the fact that the local breakup function at any arbitrary R has the same exponential form $P_{BU}(R) \propto \exp(-\alpha R)$.

The position of breakup of the projectile on its orbit is determined by sampling a breakup radius R_{BU} on the interval $[R_{min}(E_0, L_0), \infty]$ with the weighting $P_{BU}(R)$ which clearly place most R_{BU} in the vicinity of R_{min} . It is worth noting that if the chosen L_0 is less than the critical partial wave for projectile fusion, L_{cr} , then the associated trajectory would normally lead to CF, i.e., $R_{min} \leq R_B^{PT}$. For these L_0 , R_{min} is set to be R_B^{PT} , when sampling R_{BU} , and all breakup events are confined to the incoming branch of the projectile trajectory. On the other hand for $L_0 > L_{cr}$ breakup can take place on both the entrance and the exit branches of the classical orbit, which are sampled equally. Thus the function given by Eq. (3.1.7) is used as a sampling

function to determine the position on the trajectory at which the projectile gets dissociated instantaneously into constituent fragments F1 and F2.

For the sake of simplicity, it is assumed that the interaction of fragments with the target and with each other can be described by a two-body central potential. At the breakup position the dynamical variables like inter-fragment separation, relative angular momentum of fragments and the total internal energy of the excited projectile are all determined through Monte Carlo simulation. Initially the separation between two fragments in the projectile is calculated by using radial probability distribution which in turn is obtained by employing a Gaussian function for the radial part of ground state wave function of the projectile. This Gaussian approximation is well justified for 0⁺ ground state of the projectile.

The orientation of inter-fragment separation is isotropic that is it may be chosen randomly over 4π solid angle. The relative angular momentum of fragments is sampled uniformly on the interval $[0,\ell_{max}]$ and its orientation is chosen randomly among the directions orthogonal to the orientation of interfragment separation. Regarding total internal energy, on the basis of faster convergence and similar outcomes instead of a uniform function, an exponentially decreasing function is chosen to sample it between the top of the barrier and a chosen maximum \mathcal{E}_{max} . It is worth mentioning that both ℓ_{max}

and \mathcal{E}_{max} are increased until the convergence occurs. Now the instantaneous velocity of the fragments and the target in the centre of mass frame at the point of breakup is determined by employing energy, linear momentum and angular momentum conservation laws. After the breakup, the two body system becomes a three body system and the separation between the three bodies as well as that between projectile and target is known. The total energy of the three body system is given by $E_{tot} = \varepsilon_{12} + U_{1T}(r_{1T}) + U_{2T}(r_{2T}) + P_{PT}^2 / 2\mu_{PT}$

is conserved and is equal to the total energy $E_{total} = \frac{m_T}{m_T + m_P} E_0$ in the overall centre-of-mass (CM) system. Here ε_{12} is the relative energy of the fragments of the projectile, $U_{1(2)T}$ is interaction potential between fragment

1(2) and the target and P_{PT} is the relative linear momentum of the projectile and target. The energy conservation immediately provides the modulus of relative velocity between P and T ($V_{PT} = P_{PT} / \mu_{PT}$)

The knowledge of $\vec{\tilde{v}}_P$ and $\vec{\tilde{v}}_T$, velocities of P and T with respect to overall CM, is required for providing initial condition for subsequent propagation of three bodies in time. These velocities are related to each other through

$$\vec{\widetilde{v}}_T = -\frac{m_P}{m_T} \vec{\widetilde{v}}_P \tag{3.1.8}$$

$$\vec{V}_{PT} = \vec{\tilde{v}}_P - \vec{\tilde{v}}_T \tag{3.1.9}$$

The magnitude of velocity \vec{V}_{PT} is already known through energy conservation, its direction is determined by using conservation of angular momentum. The total angular momentum $\vec{L}_{tot} = \vec{\ell}_{12} + \vec{L}_{PT}$ in overall CM system is known as $\vec{L}_{total} = m_P b_0 (\vec{v} - \vec{V}_{CM})$. Here $\vec{\ell}_{12}, b_0, \vec{v}$ and \vec{V}_{CM} are the relative angular momentum of the fragments of projectile, impact parameter, velocity of projectile in laboratory system and the CM velocity respectively. The \vec{L}_{PT} , angular momentum associated with relative motion of P and T about CM, is known and is written as

$$\vec{L}_{PT} = m_P \vec{R}_{PT} \times \vec{\widetilde{v}}_P$$

Now splitting $\vec{\tilde{v}}_P$ in radial and transverse component, we may write

$$\vec{\widetilde{v}}_P = \widetilde{v}_P^{(r)} \vec{r} + \widetilde{v}_P^{(q)} \vec{q} \tag{3.1.10}$$

with $\vec{r} = \vec{R}_{PT} / R_{PT}$ and $\vec{q} = \vec{n} \times \vec{r}$ when $\vec{n} = \vec{L}_{PT} / L_{PT}$. The transverse component of the velocity of projectile and target are given by

$$\widetilde{v}_P^{(q)} = L_{PT} / (m_P R_{PT})$$
 and

$$\widetilde{v}_T^{(q)} = -L_{PT} / (m_T R_{PT})$$

respectively. Now using Eqs. (3.1.8) and (3.1.9), it is quite straight forward to obtain the following expression for radial velocity component

$$\widetilde{v}_{P}^{(r)} = \pm \frac{\left\{ V_{PT}^{2} - \left[\widetilde{v}_{P}^{(q)} \left(1 + \frac{m_{P}}{m_{T}} \right) \right]^{2} \right\}^{1/2}}{\left(1 + \frac{m_{P}}{m_{T}} \right)}$$
(3.1.11)

These velocity and position vectors of the fragments of the projectile and target are transformed to the laboratory system using Galilean transformation. The basic strategy to numerate the ICF, CF and NCBU events is to assume that a fragment is fused with the target if the trajectory takes it within the fragment target barrier radius. Let N be the number of breakup events sampled and N_0 , N_1 and N_2 be the number of events with 0,1and 2 captured fragments respectively, then the ratio \tilde{P}_i = N_i /N [i=0(NCBU), 1(ICF) or 2(CF)] provides the relative yields of these three processes with \tilde{P}_0 + \tilde{P}_1 + \tilde{P}_2 =1 and the absolute probabilities for these processes are [1-2]

$$P_0(E_0, L_0) = P_{BU}(R_{\min})\tilde{P}_0$$
(3.1.12)

$$P_1(E_0, L_0) = P_{BU}(R_{\min})\widetilde{P}_1$$
(3.1.13)

$$P_{2}(E_{0}, L_{0}) = [1 - P_{BU}(R_{\min})]H(L_{cr} - L_{0}) + P_{BU}(R_{\min})\widetilde{P}_{2}$$
(3.1.14)

with H(x) as the Heaviside step function and L_{cr} as the critical partial wave for fusion. The first term in the expression of $P_2(E_0, L_0)$ corresponds to direct complete fusion (DCF) while the second one to sequential complete fusion (SCF). The cross sections for these processes are calculated by using following standard prescription

$$\sigma_i(E_0) = \pi \lambda^2 \sum_{L_0} (2L_0 + 1) P_i(E_0, L_0)$$
(3.1.15)

where $\lambda^2 = \hbar^2/(2\mu E_0)$ is the de-Broglie wavelength and $\mu = m_p m_T/(m_p + m_T)$ is the reduced mass of the projectile-target system.

This model is implemented in the code PLATYPUS [4]. Although this method is quite successful in explaining the CF, ICF and TF data at above barrier energies but fails at around and sub barrier energies. The failure of the model at around and sub barrier energies may be attributed to the fact that at these

energies the quantum mechanical tunneling effect becomes significant and cannot be ignored. Here we have incorporated quantum mechanical tunneling correction based on WKB approximation [5] in this model.

3.2 WKB Approximation and Tunneling

Factor

The WKB method is based on the expansion of wave function in powers of \hbar and is quite useful for approximate solution of quantum mechanical problems in appropriate cases.

Consider the following basic Schrödinger wave equations in one dimension

$$\frac{d^2u}{dx^2} + k^2(x)u = 0 \quad \text{for } k^2 > 0$$
 (3.2.1)

$$\frac{d^2u}{dx^2} - \gamma^2(x)u = 0 \quad \text{for } \gamma^2 > 0$$
 (3.2.2)

such that

$$k(x) = \frac{1}{\hbar} \sqrt{2\mu(E - V(x))} \quad \text{when } V(x) < E$$
 (3.2.3)

and

$$\gamma(x) = \frac{1}{\hbar} \sqrt{2\mu(V(x) - E)} \text{ when } V(x) > E$$
(3.2.4)

are always real. For convenience, let us assume that

$$u(x) = A \exp(\frac{i}{\hbar}S(x)) \tag{3.2.5}$$

be the solution of Eq. (3.2.1) which on substitution results is

$$\left(\frac{dS}{dx}\right)^2 - i\hbar \frac{d^2S}{dx^2} - k^2\hbar^2 = 0 \tag{3.2.6}$$

Now expanding S(x) in powers of \hbar

$$S(x) = S_0(x) + S_1(x)\hbar + S_2(x)\frac{\hbar^2}{2} + \dots$$
 (3.2.7)

substituting the expansion in Eq. (3.2.6) and equating the coefficients of terms having \hbar raised to power one, we get

$$-S_0^{"2} + 2\mu(E - V) = 0 \tag{3.2.8}$$

and

$$iS_0'' - 2S_0'S_1' = 0$$
 (3.2.9)

These Eqs. may be rewritten as

$$S_0^{'2} - k^2 \hbar^2 = 0 (3.2.10)$$

and

$$S_{1}^{'} = \frac{ik^{'}}{2k} \tag{3.2.11}$$

Integration of (3.2.10) immediately gives

$$S_0(x) = \pm \hbar \int_0^x k(x') dx'$$
 (3.2.12)

and that of (3.2.11) gives

$$S_1 = \frac{i}{2} \ln k(x) \tag{3.2.13}$$

here the arbitrary constants of integration are omitted because these may be absorbed in A.

Now if only first two terms in the expansion of S are retained, then

$$u = A \exp(\frac{i}{\hbar} S_0) \exp(iS_1)$$
(3.2.14)

Using Eqs. (3.2.12) and (3.2.13) we get

$$u(x) = \frac{A}{k^{1/2}} \exp(\pm i \int_{-\infty}^{x} k dx)$$
 for $V < E$ (3.2.15)

Similarly the approximate solution of Eq. (3.2.2) is

$$u(x) = \frac{B}{\gamma^{1/2}} \exp(\pm \int_{-\infty}^{x} \gamma dx)$$
 for $V > E$ (3.2.16)

These solutions may be treated accurate in that part of the domain of x where

$$\left|\frac{k'}{2k^2}\right| << 1$$
 that is when the potential energy changes so slowly that the

momentum of particle is always constant over many wavelengths. But this condition does not hold good near turning point and hence these approximate solutions are asymptotically valid.

Since wave Eqs. (3.2.1) and (3.2.2) are regular at a turning point there are analytic solutions at these points which have above asymptotic form. In order to find exact solution having desired asymptotic form consider that the origin

of x lies at a turning point, V(x) < E to the right of the turning point (positive x) and that

$$\xi(x) \equiv \int_{0}^{x} k dx$$

Now if $k^2(x) = Cx^n$, C being positive constant, Eq. (3.2.1) have solutions

$$u(x) = A\sqrt{\frac{\xi}{k}}J_{\pm m}(\xi), \ m = \frac{1}{n+2}$$
 (3.2.17)

with J as a Bessel function and it agrees asymptotically with Eq. (3.2.15). To verify this let us rewrite Eq. (3.2.1) with an additional term $\theta(x)$

$$\frac{d^2u}{dx^2} + (k^2 - \theta)u = 0 ag{3.2.18}$$

Substitution of Eq. (3.2.17) in to Eq. (3.2.18) shows that the new equation is satisfied if we define θ as

$$\theta(x) = \frac{3k'^2}{4k^2} - \frac{k''}{2k} + (m^2 - 1/4)\frac{k^2}{\xi^2}$$
(3.2.19)

The expansion of k^2 in powers of x results in the following leading term in the expansion of $\theta(x)$,

$$\theta(x) \xrightarrow[x \to 0]{} \frac{3(n+5)a^2}{2(n+4)(n+6)} - \frac{3b}{n+6}$$
(3.2.19a)

Thus $\theta \ll k^2$ in the asymptotic region and is not negligible in comparison to k^2 in a region around turning point. But quite small value of $\theta(0)$ indicates that for slowly varying potential Eq. (3.2.17) is a good approximation to actual solution of Eq. (3.2.1)

For simplicity we consider the case n = 1 corresponding to linear turning point as shown in Fig.(3.2.1). In region 1 (x > 0) Eq. (3.2.1) is used while in region

2 (x < 0) Eq. (3.2.2) is used. Putting
$$\xi_1(x) \equiv \int_0^x k dx$$
 and $\xi_2(x) \equiv \int_x^0 y dx$ so that

both ξ_1 and ξ_2 increases as x moves away from the turning point, the two independent solutions in each of the two regions become

$$u_{1}^{\pm}(x) = A_{\pm} \sqrt{\frac{\xi_{1}}{k}} J_{\pm(1/3)}(\xi_{1})$$

$$(3.2.20)$$

$$u_{2}^{\pm}(x) = B_{\pm} \sqrt{\frac{\xi_{2}}{\gamma}} I_{\pm(1/3)}(\xi_{2})$$

$$(3.2.21)$$

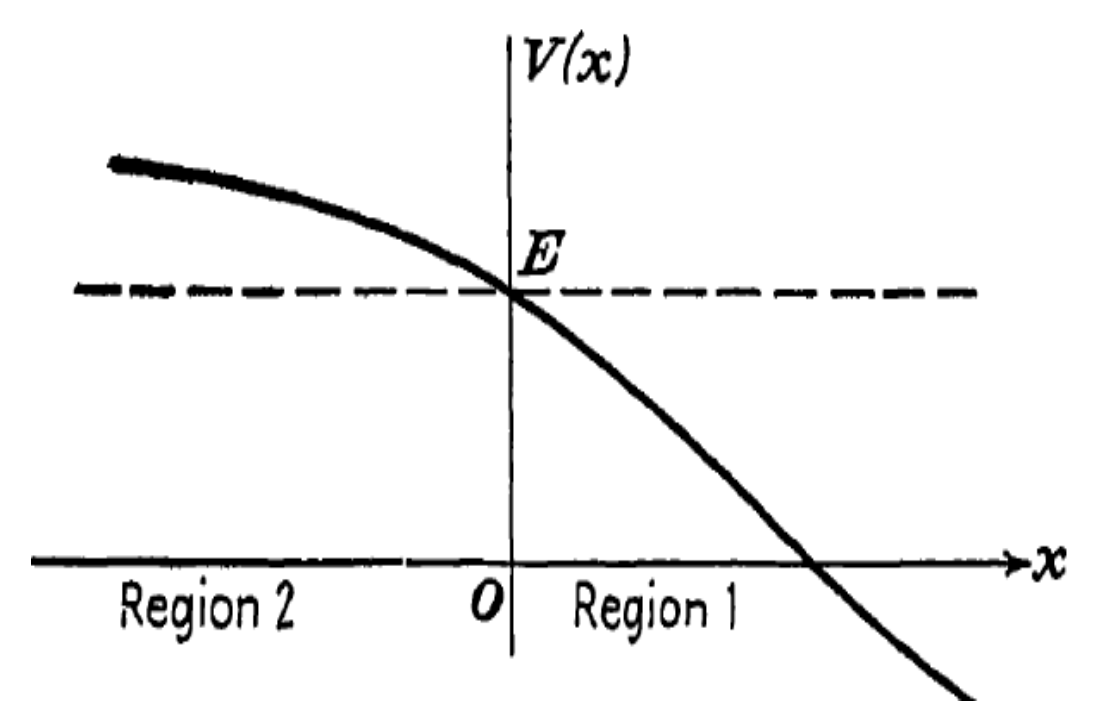


Fig. 3.2.1 A typical linear turning point is shown at the origin.

Using the leading terms of the power series expansions for these functions that is

$$J_{\pm(1/3)}(\xi_1) \xrightarrow{x \to 0} \frac{\left(\frac{1}{2}\xi_1\right)^{\pm 1/3}}{\Gamma(1\pm\frac{1}{3})}$$

(3.2.22)

$$I_{\pm(1/3)}(\xi_2) \xrightarrow{x \to 0} \frac{\left(\frac{1}{2}\xi_2\right)^{\pm 1/3}}{\Gamma(1 \pm \frac{1}{3})}$$
 (3.2.23)

and $\xi_1 \cong (2c/3)x^{3/2}$; $\xi_2 \cong (2c/3)|x|^{3/2}$ the behavior of the *u*'s near x = 0 is given as

$$u_{1}^{+} \cong A_{+} \frac{\left(\frac{2}{3}\right)^{1/2} \left(\frac{1}{3}c\right)^{1/3}}{\Gamma\left(\frac{4}{3}\right)} x,$$

$$u_{1}^{-} \cong A_{-} \frac{\left(\frac{2}{3}\right)^{1/3} \left(\frac{1}{3c}\right)^{-1/3}}{\Gamma\left(\frac{2}{3}\right)}$$
(3.2.24)

$$u_{2}^{+} \cong B_{+} \frac{\left(\frac{2}{3}\right)^{1/2} \left(\frac{1}{3}c\right)^{1/3}}{\Gamma\left(\frac{4}{3}\right)} |x|,$$

$$u_{2}^{-} \cong B_{-} \frac{\left(\frac{2}{3}\right)^{1/2} \left(\frac{1}{3c}\right)^{-1/3}}{\Gamma\left(\frac{2}{3}\right)}$$
(3.2.25)

clearly u_1^+ joins smoothly on to u_2^+ if $B_+ = -A_+$ and u_1^- joins smoothly on to u_2^- if $B_- = A_-$

These relations between the coefficients and the asymptotic expansions

$$J_{\pm(1/3)}(\xi_1) \xrightarrow{x \to \infty} \sqrt{\frac{2}{\pi \xi_1}} \cos \left(\xi_1 \mp \frac{\pi}{6} - \frac{\pi}{4} \right)$$
 (3.2.26)

$$I_{\pm(1/3)}(\xi_2) \xrightarrow{x \to \infty} \sqrt{\frac{2}{\pi \xi_2}} \left[e^{\xi_2} + e^{-\xi_2} \cdot e^{-\left(\frac{1}{2} \pm \frac{1}{3}\right)\pi i} \right]$$
(3.2.27)

can be used to obtain asymptotic forms like Eq. (3.2.15) and Eq. (3.2.16) for the two independent solutions u^+ and u^- in two regions.

$$u^{+} \xrightarrow{x \to +\infty} \sqrt{\frac{2}{\pi k}} \cos\left(\xi_{1} - \frac{5\pi}{12}\right)$$

$$\xrightarrow{x \to -\infty} -\sqrt{\frac{1}{2\pi\gamma}} \left(e^{\xi_{2}} + e^{-\xi_{2} - \frac{5\pi i}{6}}\right)$$
(3.2.28)

$$u^{-} \xrightarrow{x \to +\infty} \sqrt{\frac{2}{\pi k}} \cos\left(\xi_{1} - \frac{\pi}{12}\right)$$

$$\xrightarrow{x \to -\infty} -\sqrt{\frac{1}{2\pi \gamma}} \left(e^{\xi_{2}} + e^{-\xi_{2} - \frac{\pi}{6}}\right)$$
(3.2.29)

The asymptotic form of any linear combination of u^+ and u^- can be found from these equations which may be used to obtain convenient connection formulas between the asymptotic WKB solutions in the two regions. For instance the combination $u^+ + u^-$ which contains only the decreasing exponential, yields the first connection formula

$$\frac{1}{2\gamma^{1/2}}e^{-\xi_2} \to \frac{1}{k^{1/2}}\cos\left(\xi_1 - \frac{\pi}{4}\right) \tag{3.2.30}$$

Eqs. (3.2.1) and (3.2.2) becomes the usual radial equation if x is replaced by $V(r) + \frac{\hbar^2 l(l+1)}{2\mu r^2}$ which effectively represent a potential barrier as shown in Fig. (3.2.2)

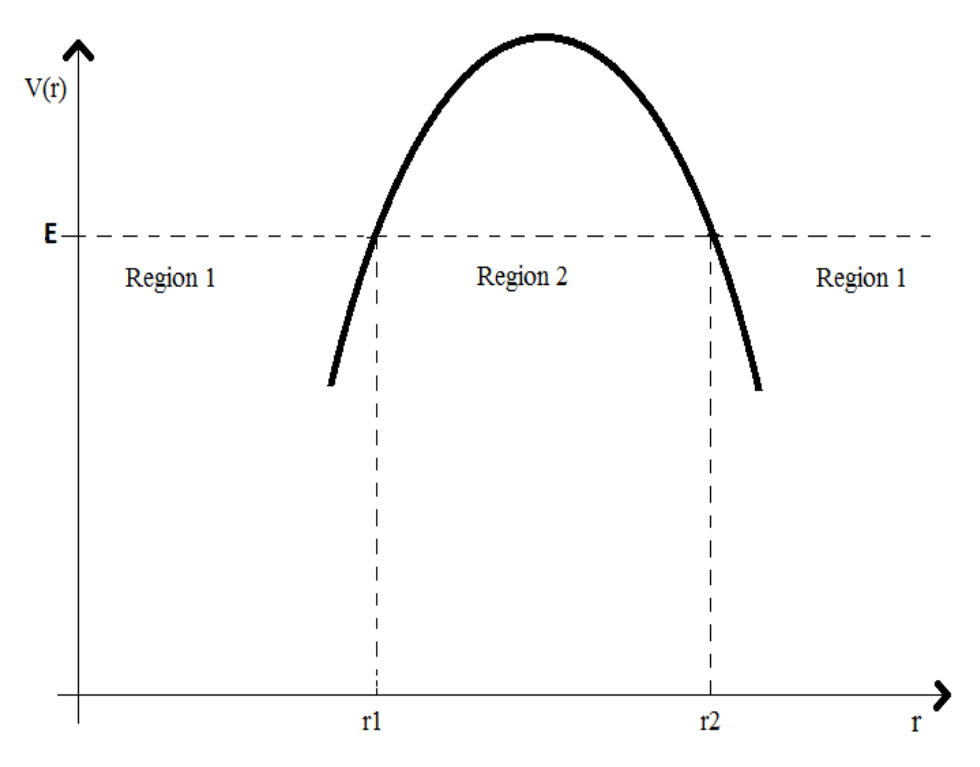


Fig.3.2.2 Single particle of energy E penetrating a barrier.

We have already seen that in region 2, the wave function is a real exponential of the form (3.2.16). If the integral $\int_{r_1}^{r_2} \gamma dr$ is appreciable larger than unity then the behavior of the solution is dominated by large ratio of the wave function at the two turning points. The ratio of the square of wave function is termed as barrier penetration factor T and is given as

$$T = \exp\left[-2\int_{r_1}^{r_2} \gamma(r)dr\right]$$
 (3.2.31)

with

$$\gamma(r) = \frac{1}{\hbar} \left\{ 2\mu \left(V(r) + \frac{\hbar^2 \ell(\ell+1)}{2\mu r^2} - E \right) \right\}^{1/2}$$
 (3.2.32)

References

- [1]. A. Diaz-Torres, D.J. Hinde, J.A. Tostevin, M. Dasgupta and L.R. Gasques, Phys. Rev. Lett. 98 (2007) 152701.
- [2]. A. Diaz-Torres, J. Phys. G, Nucl. Part. Phys. 37 (2010) 075109.
- [3]. R. Rafiei, et al., Phys. Rev. C 81 (2010) 024601.
- [4]. A. Diaz-Torres, Comput. Phys. Commun. 182 (2011) 1100.
- [5]. L.I. Schiff, Quantum Mechanics, Tata McGraw-Hill, New Delhi, 2010.

RESULTS AND DISCUSSION

4.1 Results and Discussion

In the present work we have analyzed the fusion excitation functions of reactions induced by weakly bound nuclei ^{6,7}Li and ⁹Be on massive targets having mass number greater than or equal to 152 at around barrier energies with a special emphasis on relative contribution of CF and ICF in TF for these reactions. Theoretically different models are being used for separate calculations of CF and ICF [1-11]. Here we have adopted the simplest model developed by Diaz-Torres et al [10] which is based on classical considerations. However, this model works well only in the above barrier energy region and fails completely at near and below barrier energies as will be described in detail in section 4.2. Since it is quite intuitive that at sub barrier energies fusion occurs through quantum mechanical tunneling mechanism, we have incorporated these effects in the analysis and so obtained results are discussed in section 4.3. Further another simple model based on Wong's formula in conjunction with the energy dependent Woods-Saxon potential is employed for a phenomenological description of CF and TF data and results are presented in section 4.4. In addition, a detailed description of determining optimum value of barrier radius for reactions involving deformed nuclei is given in section 4.5.

4.2 Contributions of ICF in ⁹Be+¹⁶⁹Tm, ¹⁸¹Ta and ¹⁸⁷Re Fusion Reactions

In this section we present, along with detailed discussion, the results of calculations of the fusion excitation functions for reactions induced by ⁹Be on ¹⁶⁹Tm, ¹⁸¹Ta and ¹⁸⁷Re targets in near barrier energy region using the code PLATYPUS [9-12] wherein ICF and CF events are calculated separately. Among various inputs, the centroid and width of the Gaussian function that approximates the radial probability distribution of projectile ground state wave function are important ingredients needed in the calculations. In order to determine the radial part of the ground state wave function of the projectile it is assumed that the nucleus ⁹Be may be approximated as a system consisting of two very loosely bound alpha particles. Because of the high probability of breakup of ⁹Be into ⁸Be* and a neutron it is quite justified to assume pseudo-⁸Be containing two alpha particles as projectile. The radial ground state wave function of this alpha+alpha system bound with 0.5MeV energy, under the assumption of a nodeless s-state, is obtained by solving the concerned Schrödinger equation for Woods-Saxon potential with 32.66MeV, 1.25fm and 0.62fm as depth, range and diffuseness parameters. The so obtained wave function is fitted with a Gaussian function with 2.17fm and 3.98fm as the centroid and width. Besides these, the parameters of the breakup function that is A and α are needed in the calculations and are determined by using the experimental breakup probability information at two different values of R_{min} (or energy) in the vicinity of Coulomb barrier [9]. The values of the parameters A and α for different systems are listed in table 4.2.1.

In Fig. 4.2.1 the CF and TF (CF+ICF) cross sections and in Fig. 4.2.2 the ICF cross sections are plotted as a function of incident beam energy for ${}^{9}\text{Be}{}^{+169}\text{Tm}$ system and are compared with the corresponding experimental data taken from Ref. [14]. It is clearly seen that the CF and TF data are slightly under predicted while the ICF data are slightly over predicted at above barrier energies. While at sub barrier energies cross sections for all the three fusion processes are significantly under predicted. Further it is interesting to note that theoretically

percentage contribution of ICF is found to be 35-40% at above barrier energies which is quite large in comparison to that observed experimentally (See Fig. 4.2.3). It is worth mentioning that the predicted contribution of ICF in TF at above barrier energies is in good agreement with the measurements for ⁹Be+ ¹⁸¹Ta, ¹⁸⁷Re [13-14] systems while it is significantly over predicted for ⁹Be+ ¹⁶⁹Tm system. This may be attributed to the fact that the nucleus ¹⁶⁹Tm has zero quadruple moment value while the nuclei ¹⁸¹Ta and ¹⁸⁷Re are prolate nuclei having quadruple moment values as 3.3b and 2.1b respectively. It clearly indicates that the value of quadruple moment of interacting nuclei play an important role in fusion excitation functions.

Table 4.2.1 The values of breakup function parameters A and α along with the breakup probability (P_{BU}) at two different values of R_{min} used to determine A and α for different projectile-target combinations.

System	$P_{ m BU}$	R _{min} (fm)	A	α (fm ⁻¹)
⁹ Be+ ¹⁶⁹ Tm	0.0108	15.1	2587	0.82
Ref. [14]	0.0371	13.6		
⁹ Be+ ¹⁸¹ Ta	0.0185	14.5	4116	0.85
Ref. [13]	0.0558	13.2		
⁹ Be+ ¹⁸⁷ Re	0.00406	16.3	5644	0.864
Ref. [14]	0.0315	13.8		

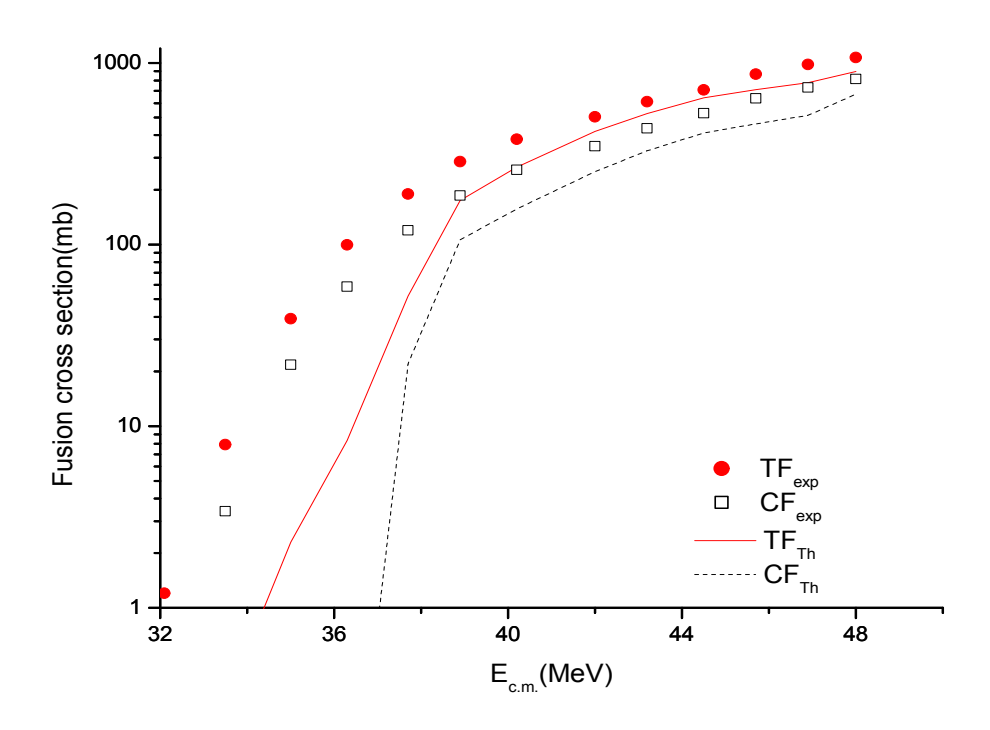


Fig.4.2.1 Fusion excitation functions for CF and TF processes, calculated through code PLATYPUS, are compared with the corresponding data taken from Ref. [14] for ${}^{9}Be + {}^{169}Tm$ system.

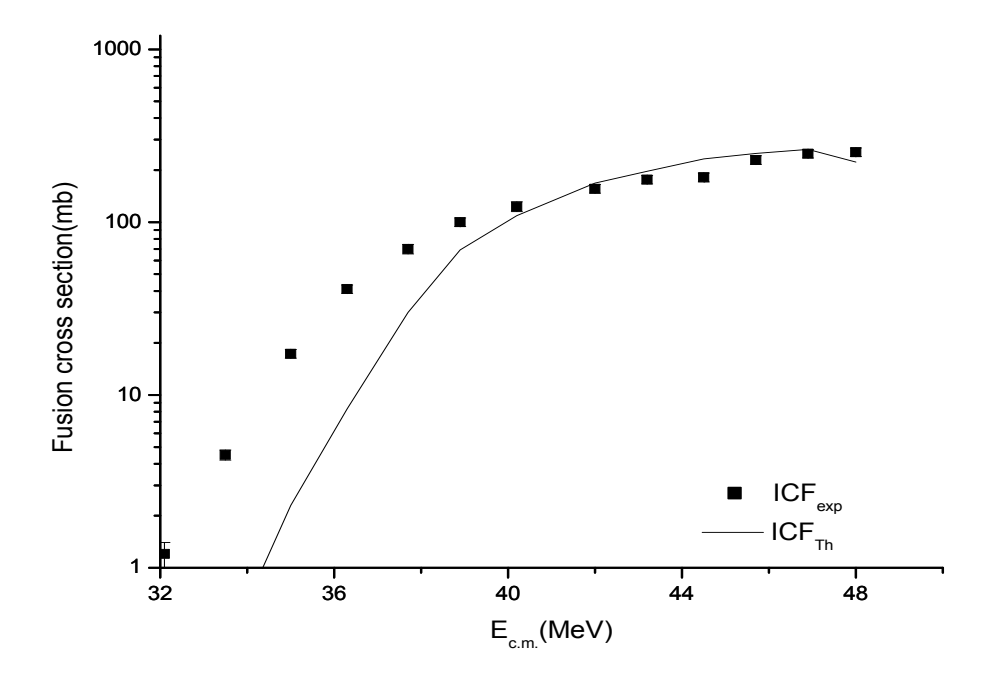


Fig.4.2.2 Fusion excitation function for ICF process, calculated through code PLATYPUS, for ${}^{9}Be+{}^{169}Tm$ system is compared with the corresponding data taken from Ref. [14]

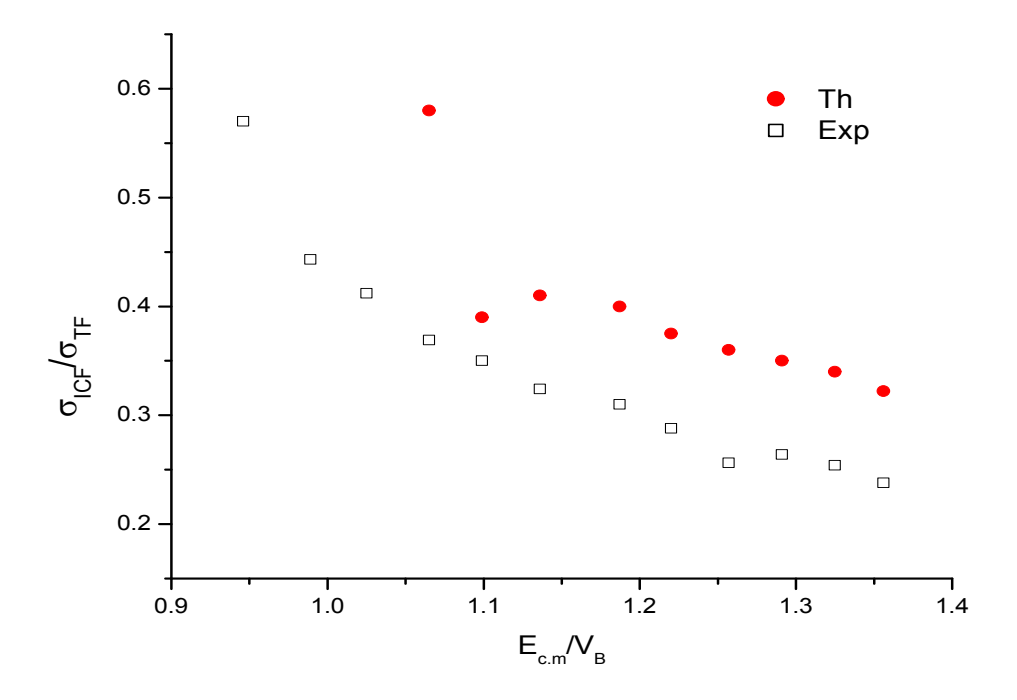


Fig.4.2.3 Ratio of ICF and TF cross sections calculated using the code PLATYPUS is plotted as a function of $E_{c.m.}/V_B$ for ${}^9Be+{}^{169}Tm$ system. [Data taken from Ref. [14]]

In Fig. 4.2.4 the CF and TF (CF+ICF) cross sections are plotted as a function of incident beam energy for ⁹Be+¹⁸¹Ta system and are compared with the corresponding experimental data taken from Ref. [13]. The experimental CF and TF cross sections are very well reproduced at energies greater than and equal to 1.14 times V_B while for energies smaller than 1.14V_B the calculations significantly under estimate the observations where V_B is the height of the barrier between interacting nuclei. In fact, at above barrier energies the quantum mechanical tunneling effects are not significant hence fusion can be described very well by the classical model resulting in a very good agreement between data and predictions. However, at around barrier energies along with the quantum mechanical tunneling various channel coupling effects play very important role in the determination of fusion cross section. Since in the classical dynamical model which is implemented in the code, these effects responsible for sub barrier fusion enhancement are not taken into account and hence the experimental data are significantly underestimated in sub barrier energy region.

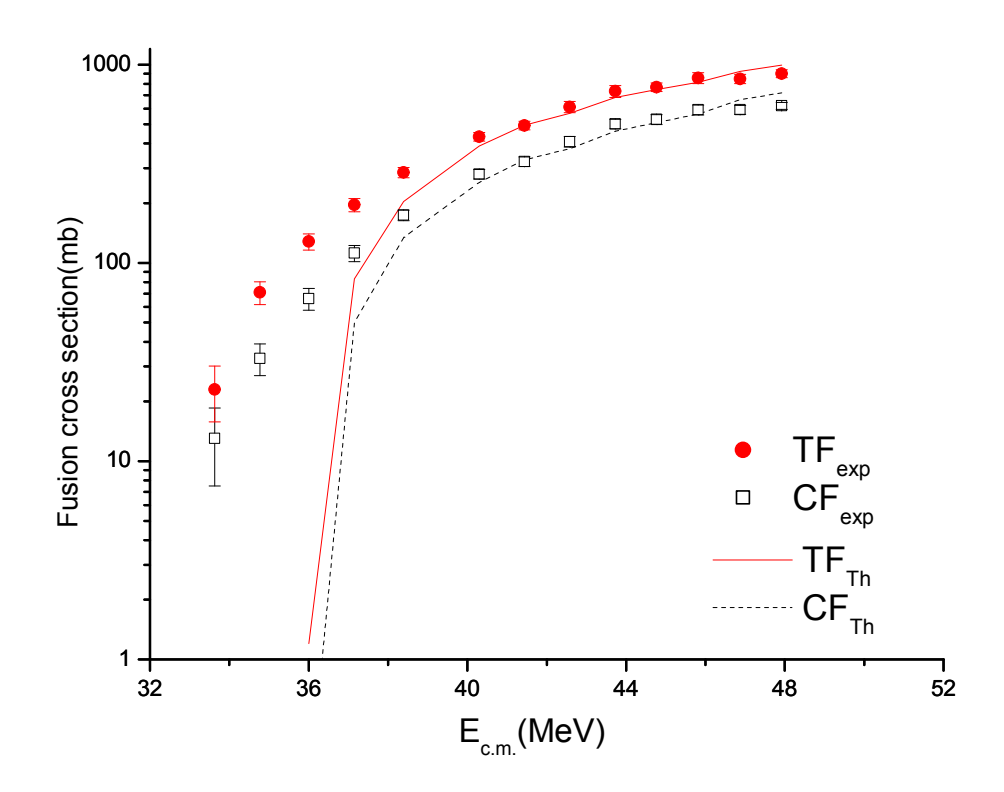


Fig.4.2.4 Fusion excitation functions for CF and TF processes, calculated using the code PLATYPUS, for ⁹Be+¹⁸¹Ta reaction are compared with the experimental data taken from Ref. [13]

Similar trend prevails for ICF originating from one alpha absorption by the target as shown in Fig. 4.2.5. In order to assess the contribution of ICF in TF more conspicuously, the variation of the ratio of σ_{ICF}/σ_{TF} with energy is compared in Fig. 4.2.6 with the corresponding experimental ratio. Both the predictions and data indicate that on an average 30-32% of TF is ICF at above barrier energies while the contribution of ICF increases significantly at near and below barrier energies.

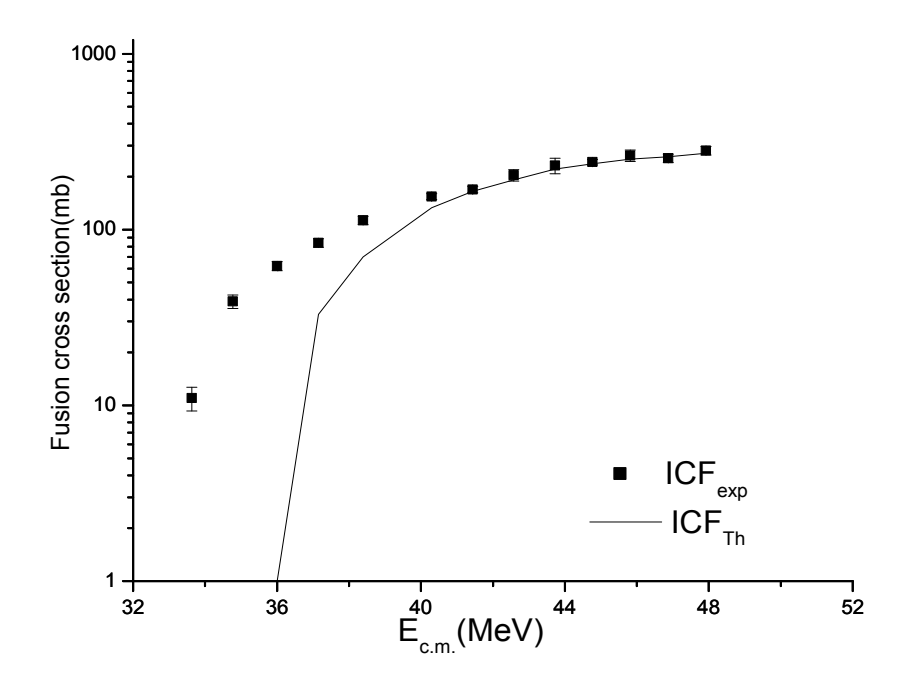


Fig.4.2.5 Fusion excitation function for ICF process, calculated using the code PLATYPUS, for ⁹Be+¹⁸¹Ta system is compared with the data taken from Ref. [13]

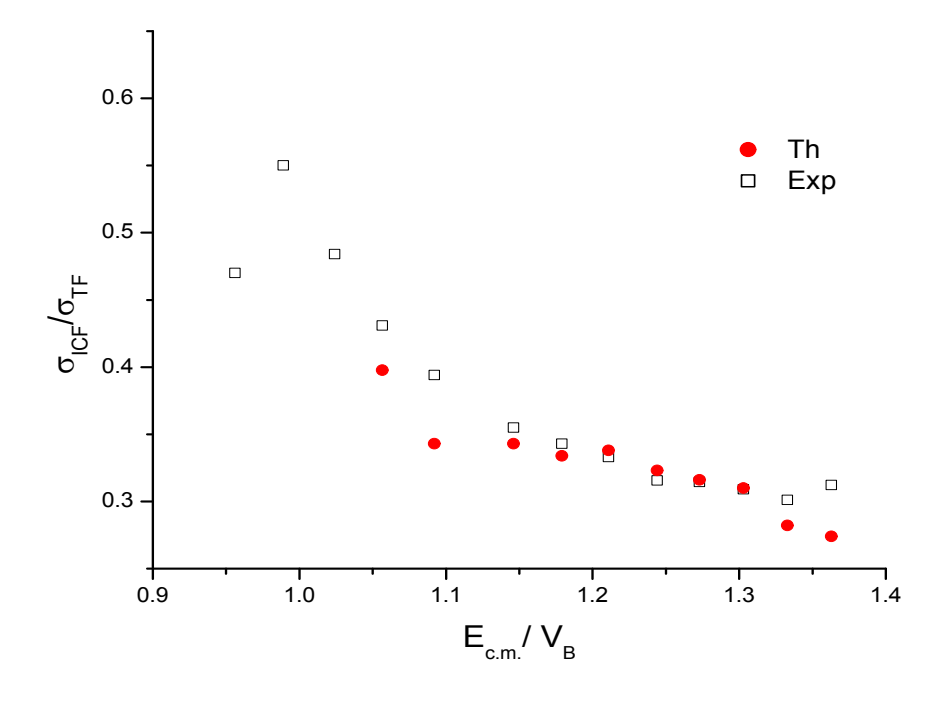


Fig.4.2.6 Ratio of ICF and TF cross sections calculated using the code PLATYPUS is plotted as a function of $E_{c.m.}/V_B$ for ${}^9Be+{}^{181}Ta$ system. [Data taken from Ref. [13]]

In Figs 4.2.7 through 4.2.9, the excitation functions for various fusion mechanisms induced by ⁹Be on ¹⁸⁷Re target at around barrier energies are compared with the corresponding data taken from Ref. [14]. The percentage contribution of ICF in TF for ⁹Be+¹⁸⁷Re system is found to be nearly 25-30% in above barrier energy region which is in agreement with the data.

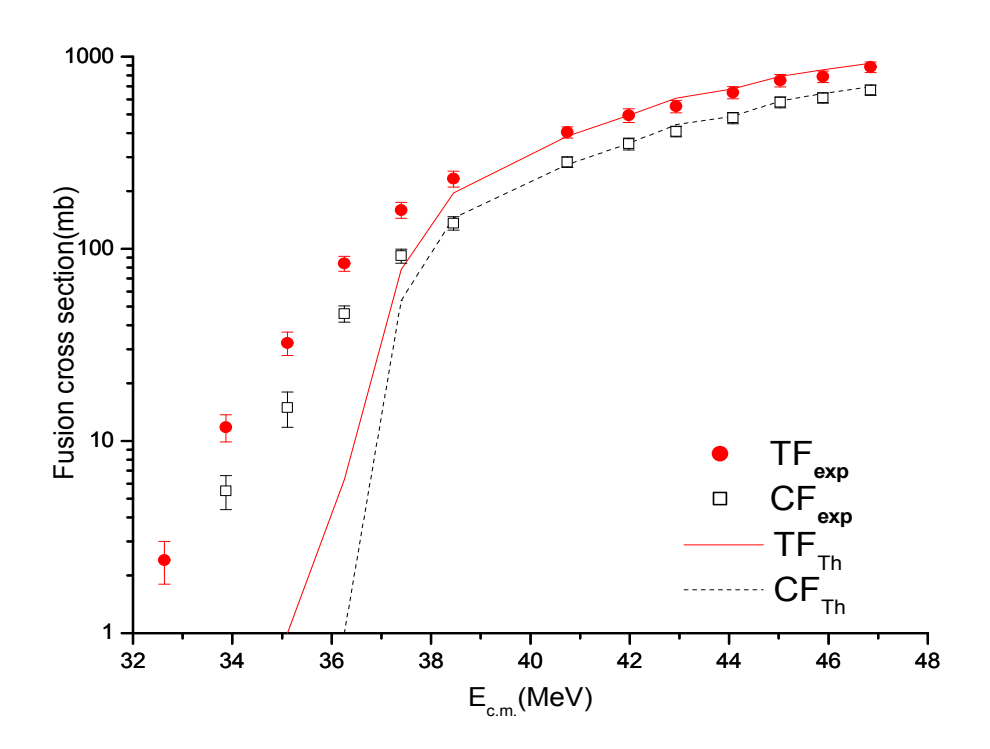


Fig.4.2.7 Fusion excitation functions for CF and TF processes, calculated using the code PLATYPUS, for ⁹Be+¹⁸⁷Re reaction are compared with the experimental data taken from Ref. [14]

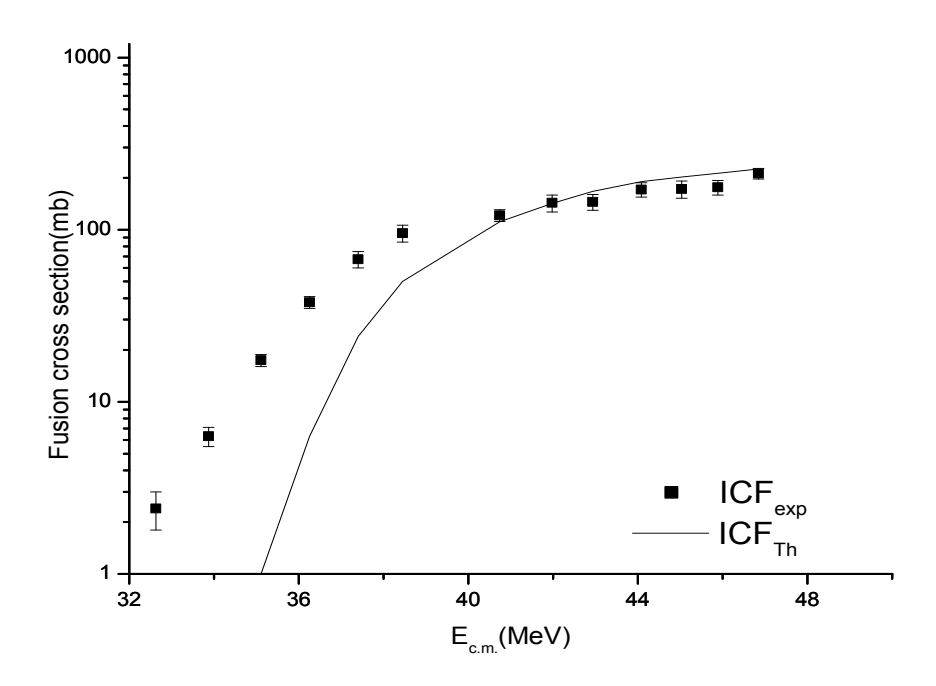


Fig.4.2.8 Fusion excitation function for ICF process, calculated using the code PLATYPUS, for ⁹Be+¹⁸⁷Re system is compared with the data taken from Ref. [14]

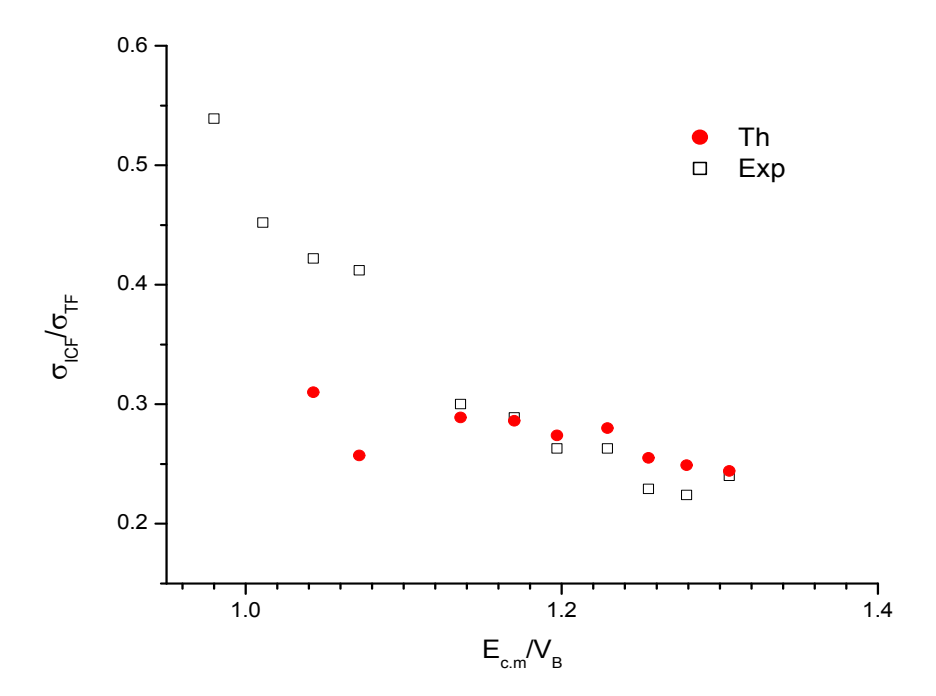


Fig.4.2.9 Ratio of ICF and TF cross sections calculated using the code PLATYPUS is plotted as a function of $E_{c.m.}/V_B$ for ${}^9Be+{}^{187}Re$ system. [Data taken from Ref. [14]]

The Tunneling Effect

4.3

We have seen in the preceding section that at energies higher than barrier energy the matching between the data and prediction is excellent whereas at energies quite close to the barrier and much smaller than the barrier the theory completely fails to explain the data. The obvious reason for this behavior is that the quantum mechanical tunneling effects play a significant role in the near and sub barrier energy region. Owing to absence of tunneling in classical picture, no fusion is expected at energies smaller than the barrier energy and hence the fusion cross section becomes zero very rapidly. Since the phenomenon of tunneling is a typical quantum effect, it cannot be introduced in a model based on classical ideas. However a correction factor arising due to the quantum mechanical tunneling may be conveniently included in the analysis. Basically, the quantum mechanical tunneling corresponds to nonzero probability of finding an object at a position where it is never observed classically. In the present case classically neither of the fragments is expected to be inside the target. But quantum mechanically there is a finite probability of finding either one or both the fragments inside the target leading to ICF and CF processes. Consequently the total flux available for classically allowed NCBU channel reduces. Thus incorporation of tunneling correction consists in multiplying the cross section of classically possible reaction channel that is NCBU, at sub barrier energies, by a tunneling factor which reduces flux available for this channel. Equivalently, some of the flux from classically allowed process has gone to classically forbidden channels. In the code it is assumed that the reaction between collision partners occurs only through CF, ICF and NCBU channels. Since at sub barrier energies CF and ICF channels are closed, all the incident flux goes to NCBU channel. If only one of the fragment is assumed to tunnel through the barrier the total flux is divided into ICF and NCBU channels. It is important to note that the fragments of ⁸Be are symmetrical and hence ICF1 and ICF2 both represent the same channel. On the other hand when both the fragments tunnel total flux is distributed among CF and NCBU channels. In fact it is assumed here that the flux to CF channel is that transferred from NCBU channel since the breakup has already occurred.

Thus the only possible mode of CF to occur is through the SCF process. When such a correction factor is taken into account in the analysis it improves to a great extent the matching between data and predictions in near and sub barrier energy region as shown in Fig.4.3.1. The tunneling factor depends on incident beam energy. It varies from unity at barrier energy to nearly zero at deep sub barrier energies. However on empirical grounds, we have incorporated tunneling effects in energy region where the value of tunneling factor is less than or equal to 0.25 because the experimental observation indicates that nearly 75% events are NCBU. As the energy decreases, the tunneling factor decreases and hence the contribution of both ICF and SCF channels reduces. At deep sub barrier energies almost all the events are NCBU. In this energy region both the fragments of the projectile have a sufficiently low energy so that they get scattered before absorption. Similarly, as a consequence of tunneling correction the experimental ICF cross section could also be reproduced very well as shown in Fig. 4.3.2.

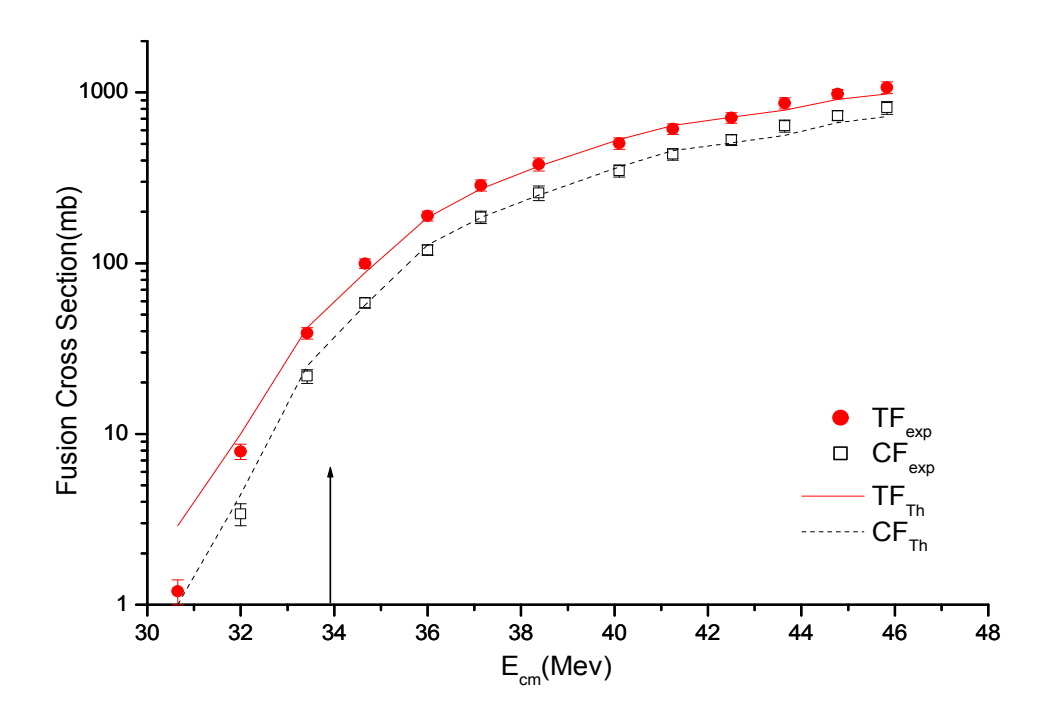


Fig.4.3.1. Fusion excitation functions for CF and TF processes, calculation through code PLATYPUS with tunneling correction, are compared with the corresponding data taken from Ref. [14] for ${}^{9}Be+{}^{169}Tm$ system.

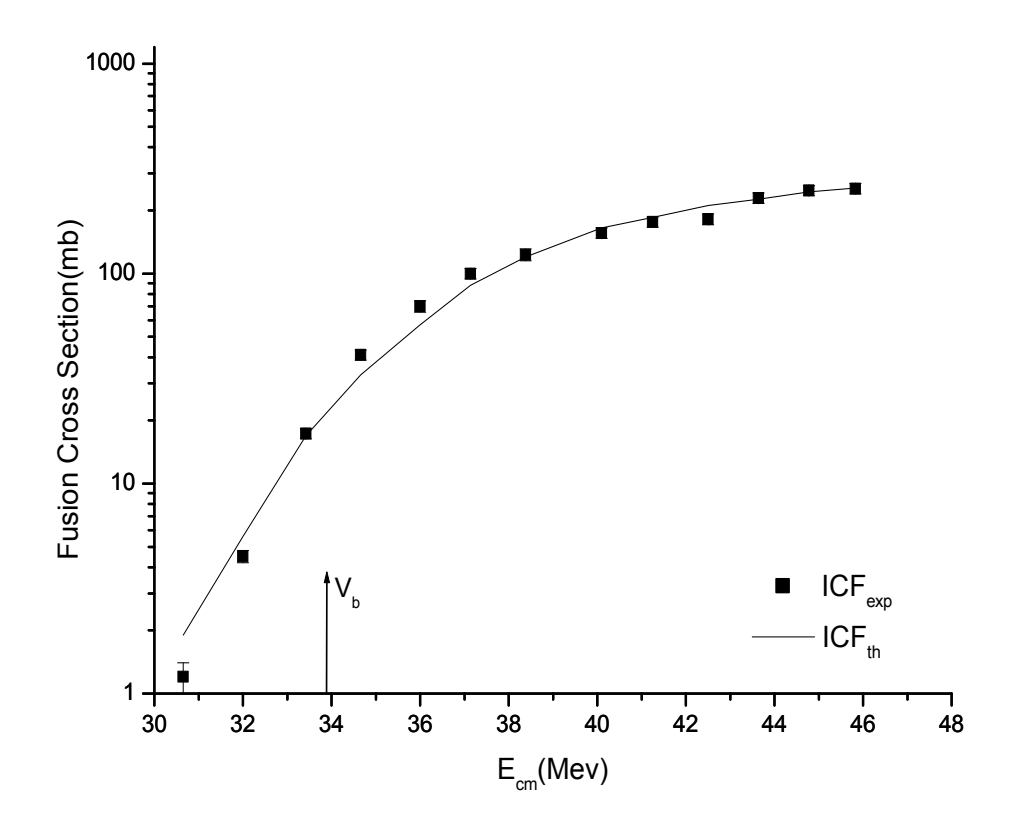


Fig.4.3.2 Fusion excitation function for ICF process, calculated through code PLATYPUS with tunneling correction is compared with the corresponding data taken from Ref. [14] for ${}^{9}Be+{}^{169}Tm$ system.

In Figs. 4.3.3 and 4.3.5 the excitation functions of complete fusion and total fusion processes are compared with corresponding data taken from Ref. [13] and [14] respectively at around barrier energies for ${}^{9}\text{Be}{}^{+181}\text{Ta}$ and ${}^{9}\text{Be}{}^{+187}\text{Re}$ systems. The ICF excitation functions for these systems along with the data taken from Ref. [13] and [14] are plotted in Fig. 4.3.4 and 4.3.6 respectively.

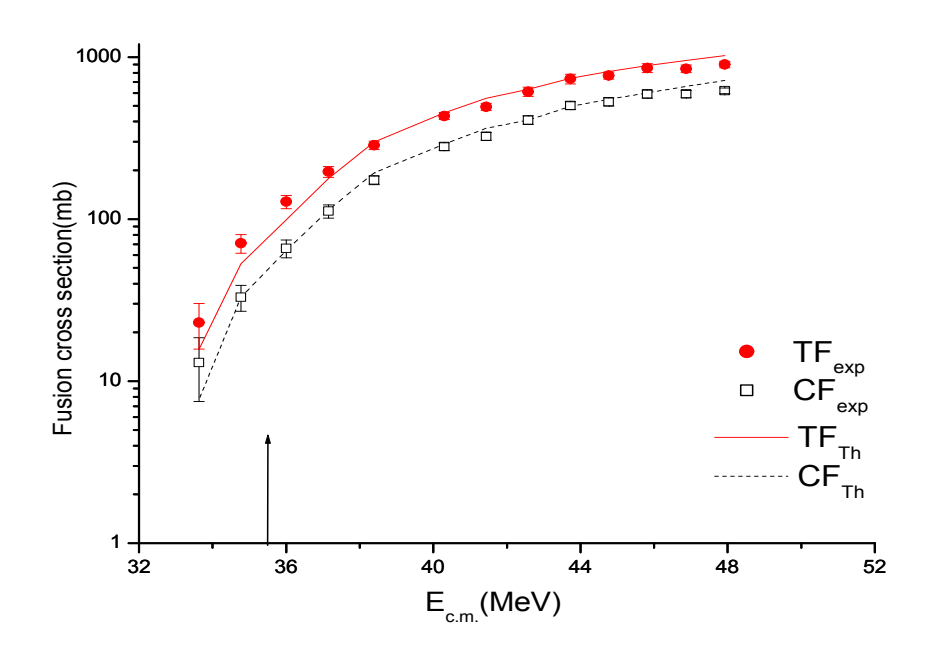


Fig.4.3.3 Fusion excitation functions for CF and TF processes, calculation through code PLATYPUS with tunneling correction, are compared with the corresponding data taken from Ref. [13] for ${}^{9}Be+{}^{181}Ta$ system.

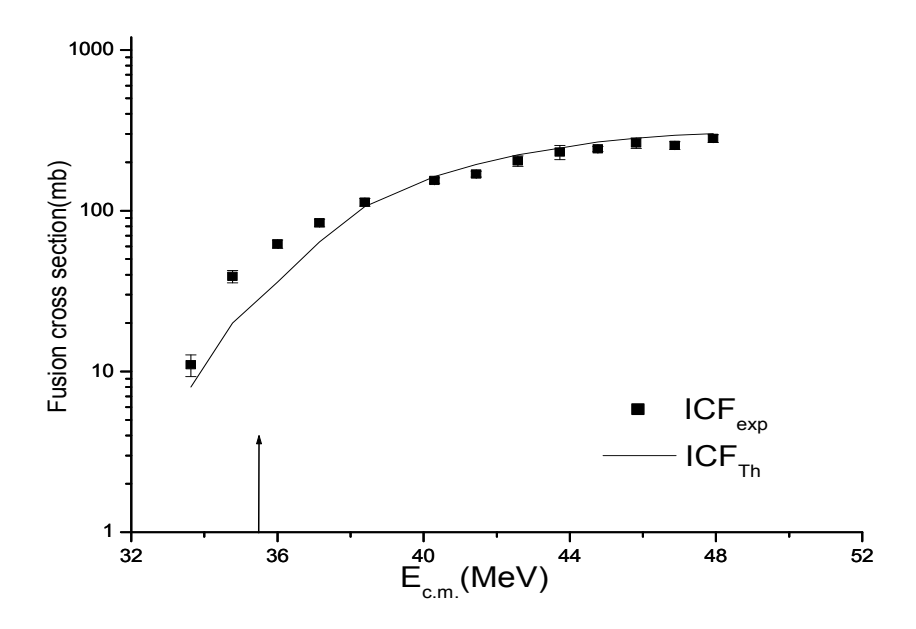


Fig.4.3.4 Fusion excitation function for ICF process, calculated through code PLATYPUS with tunneling correction is compared with the corresponding data taken from Ref. [13] for ${}^{9}Be+{}^{181}Ta$ system.

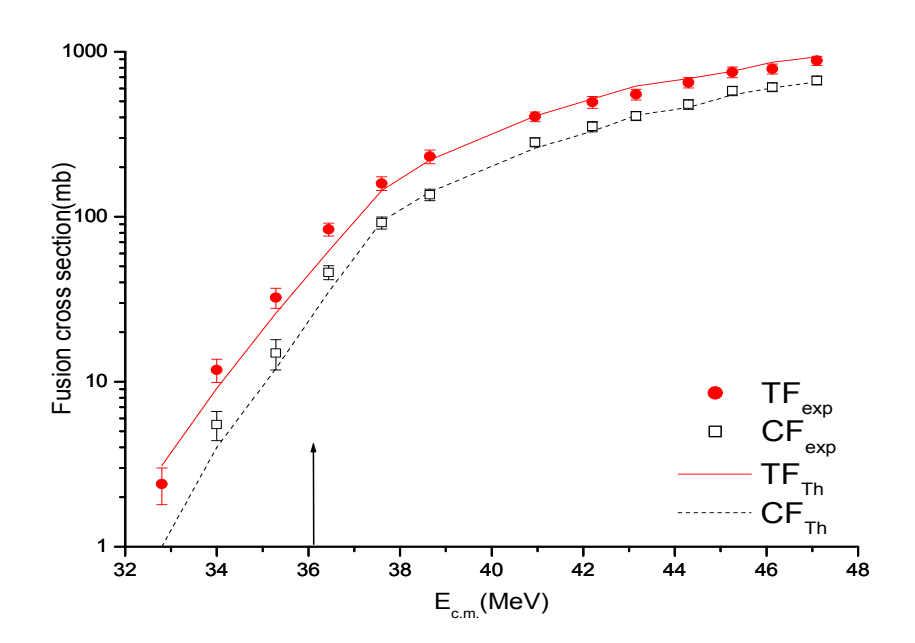


Fig.4.3.5 Fusion excitation functions for CF and TF processes, calculation through code PLATYPUS with tunneling correction, are compared with the corresponding data taken from Ref. [14] for ${}^{9}Be+{}^{187}Re$ system.

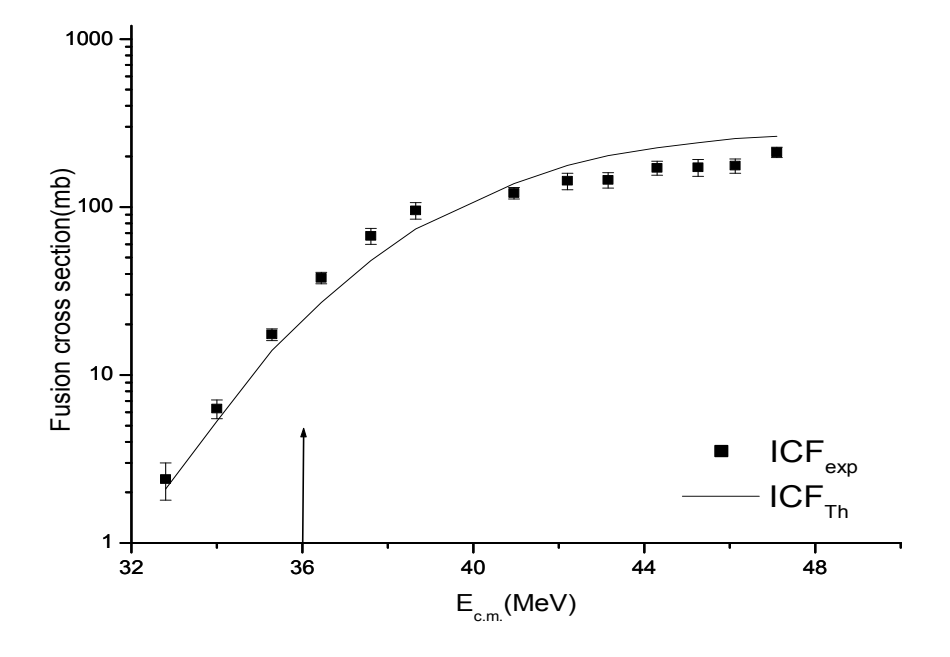


Fig.4.3.6 Fusion excitation function for ICF process, calculated through code PLATYPUS with tunneling correction is compared with the corresponding data taken from Ref. [14] for ${}^9Be+{}^{187}Re$ system.

The comparison between data and prediction made in these figures is interpreted in the same way as that for Figs. 4.3.1 and 4.3.2. However, it is very interesting to note that both CF and ICF cross sections and hence TF cross section at energies near and below the barrier is slightly over estimated for ${}^{9}\text{Be}{}^{+169}\text{Tm}$ system while these are slightly underestimated for ${}^{9}\text{Be}{}^{+181}\text{Ta}$ and ${}^{9}\text{Be}{}^{+187}\text{Re}$ systems. It may be ascribed to the fact that the tunneling reduces with the increasing mass-asymmetry of the system.

4.4 Energy Dependent Woods-Saxon

Potential and Fusion

Besides classical dynamical model, we have adopted an alternative procedure to explain the data which consists in assuming that the contribution of ICF in TF is the same as that predicted by code platypus for above barrier energy region and employing this assumption in a simplified fusion model based on Wong's formula and energy dependent Woods–Saxon potential [EDWSP] [15-16]. Although any of the fusion model may be used for this purpose, but this model is simplest one wherein various channel coupling effects are simulated through the introduction of energy dependence in the potential. Using this approach we have analyzed the ICF, CF and TF excitation functions data for ${}^{9}\text{Be}+{}^{181}\text{Ta}$ and ${}^{187}\text{Re}$ systems at around barrier energies. The so obtained fusion excitation functions for CF and TF reaction mechanisms are compared with the corresponding experimental data taken from Ref. [13] for ${}^{9}\text{Be}+{}^{181}\text{Ta}$ system are shown in Fig.4.4.1. For above barrier energy region, fusion cross sections calculated through code platypus and for below barrier energy region, calculations are performed through EDWSP model.

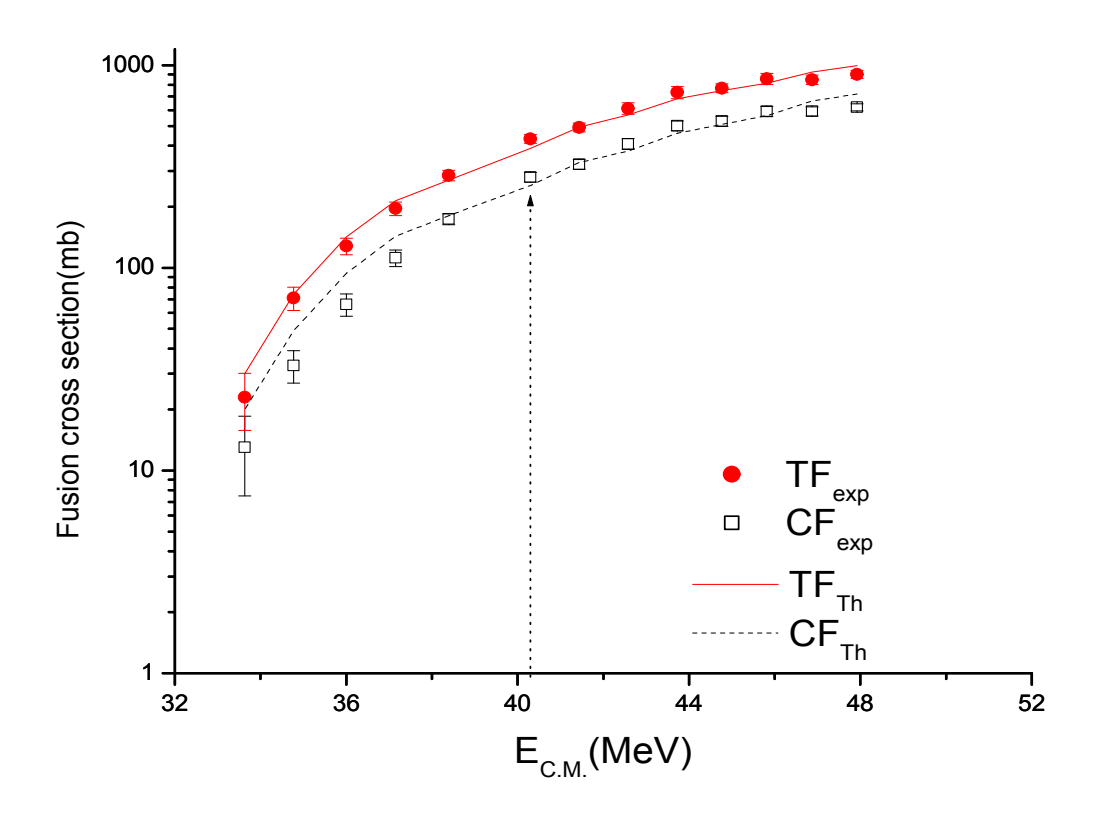


Fig.4.4.1 Fusion excitation functions for CF and TF processes for ${}^{9}Be+{}^{181}Ta$ reaction, calculated using code PLATYPUS at $E_{cm}>1.14\ V_{B}$ MeV and using Wong's formula with EDWSP for $E_{cm}<1.14\ V_{B}$, are compared with the experimental data taken from Ref. [13].

It is clearly seen that the CF data are very well explained over entire energy regime while the TF data are slightly under-predicted in the deep sub-barrier energy region. Although most of the channels coupling effects are already imitated through energy dependence in potential, the slight mismatch between TF data and prediction at deep sub-barrier energies may be ascribed to the fact that the contribution of ICF is larger than that predicted by code platypus. It may be seen more clearly in Fig.4.4.2 where ICF fusion excitation function is compared with the corresponding experimental data [13]. The matching between data and calculations could be achieved by considering 45–48% contribution of ICF in TF. However, the so obtained information about the contribution of ICF in TF is not unambiguous. Nevertheless one obtains a fairly good estimate regarding the relative importance of ICF and CF

mechanisms in below barrier energy regime. It is important to mention here that the contribution of ICF in below barrier energy is more than that for above barrier energies. For ⁹Be+ ¹⁸⁷Re system almost similar results have been found as shown in Figs. 4.4.3 and 4.4.4.

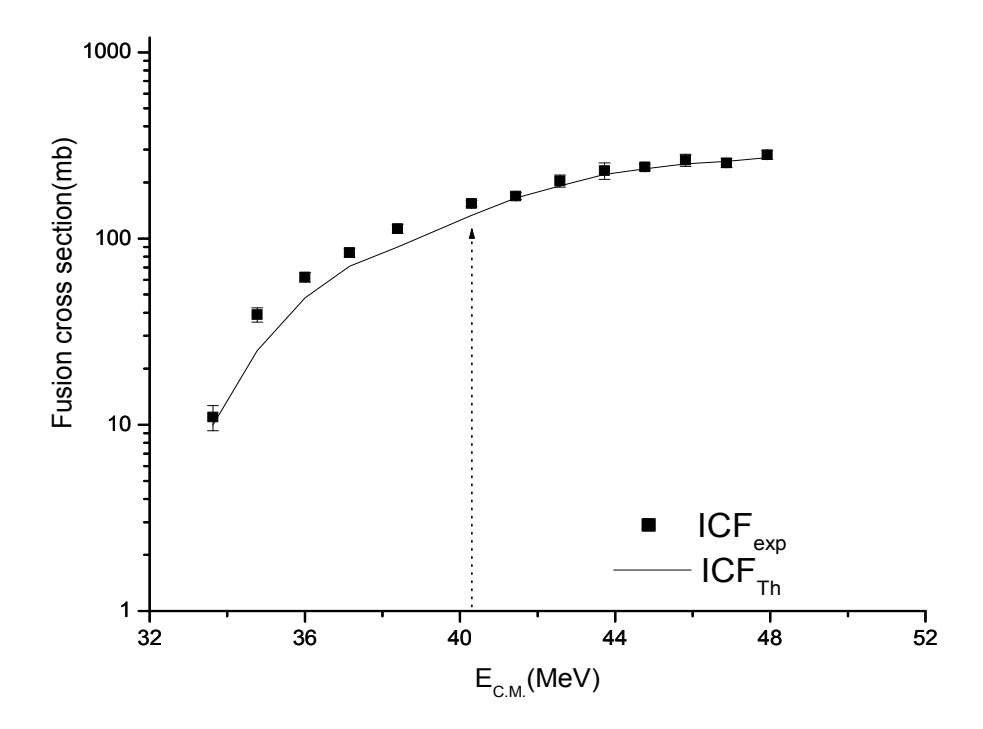


Fig.4.4.2 Fusion excitation function for ICF process for ${}^{9}Be+{}^{181}Ta$ reaction, calculated using code PLATYPUS at $E_{cm}>1.14~V_{B}~MeV$ and using Wong's formula with EDWSP for $E_{cm}<1.14~V_{B}$, is compared with the experimental data taken from Ref. [13].

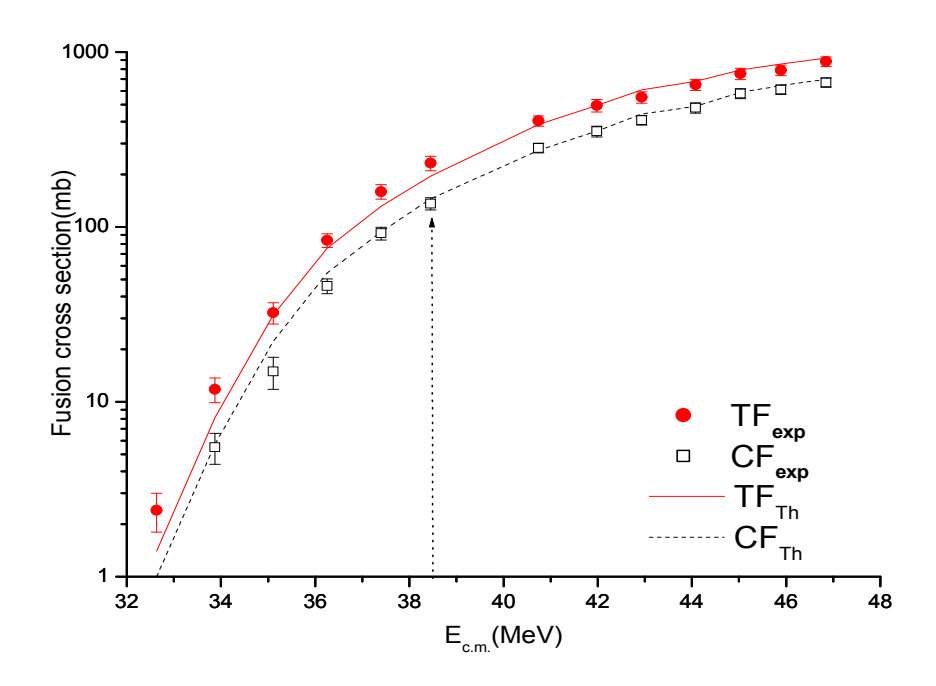


Fig.4.4.3 CF and TF cross section for ${}^{9}Be+{}^{187}Re$ calculated by code platypus (for $E/V_B \ge 1.07$) and by EDWSP model (for $E/V_B \le 1.07$) are compared with the experimental data taken from Ref. [14].

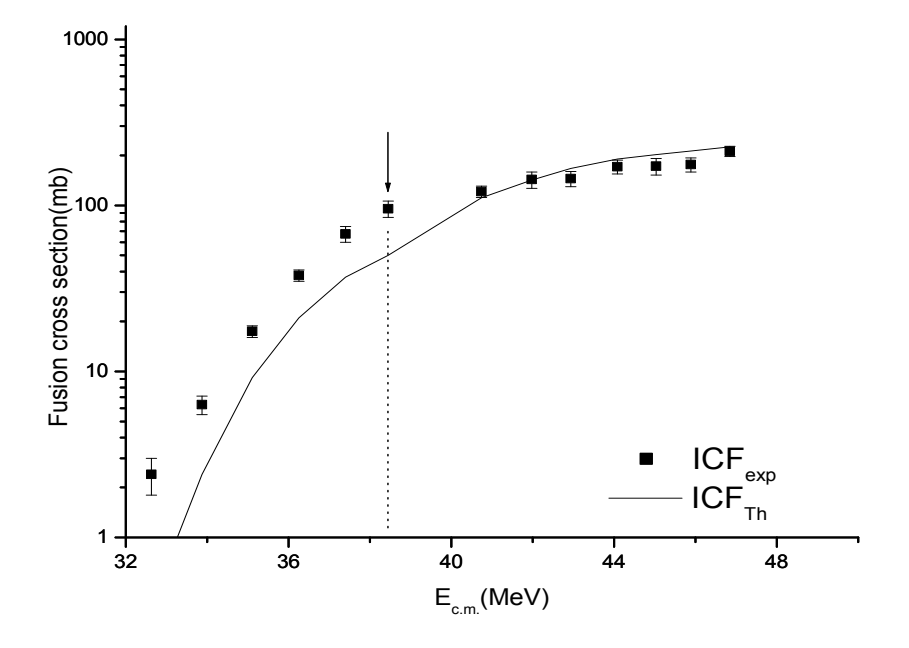


Fig.4.4.4 The ICF cross section for ${}^{9}Be + {}^{187}Re$ calculated by code platypus (for $E/V_B \ge 1.07$) and by EDWSP model (for $E/V_B \le 1.07$) are compared with the experimental data taken from Ref. [14].

Further in order to account for the proper energy dependence of the relative contribution of CF and ICF in TF we propose a selection function which represents the fact that at barrier energy, there is a strong competition between the CF and ICF processes as both are equally probable. While at energies much higher than the barrier energy, CF predominates over ICF and vice versa at very low energies. The Fig. 4.4.5 shows that the contribution of ICF varies from 20% to 35% for energies much larger than the barrier energy and increases smoothly up to approximately 55% at near barrier and slightly smaller energies. While at deep sub barrier energies, the ICF cross-section dominates. At high energies, the projectile approaches quickly to the target thus it is absorbed either directly or sequentially after the breakup by the target. Hence, at high energies, the process is predominantly the CF process. While at lower energies, each of the fragments of the projectile has sufficient time to get scattered, consequently the contribution of ICF is enhanced.

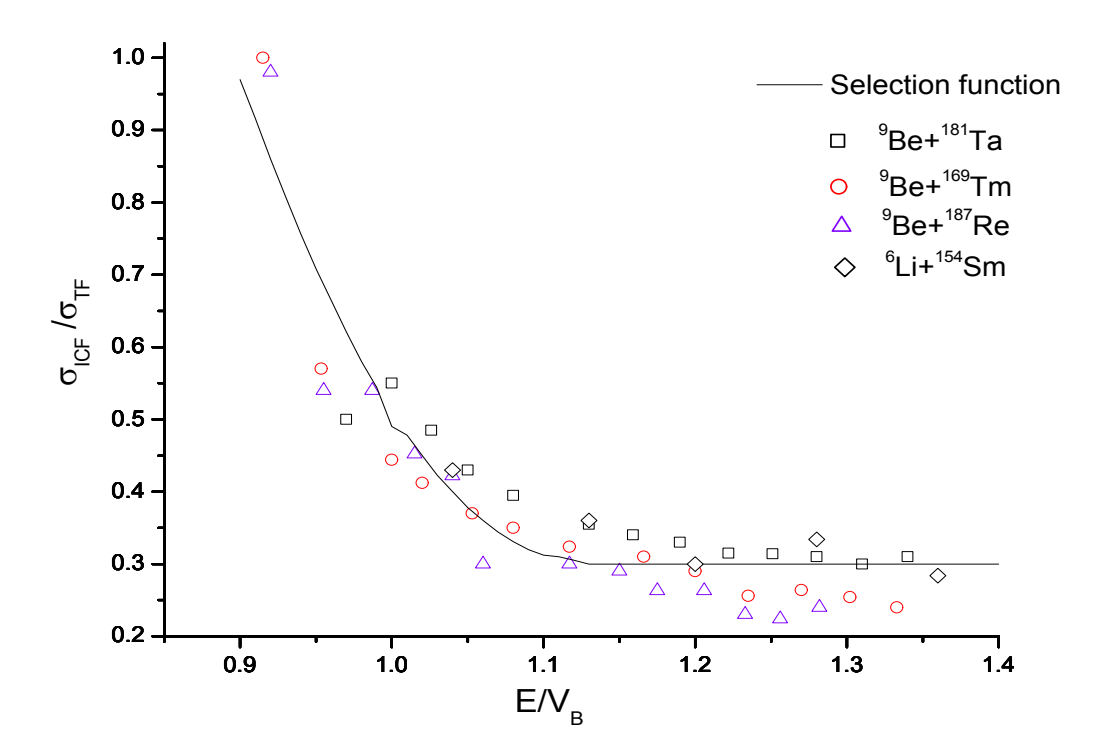


Fig.4.4.5 The ratio of ICF cross-section to TF cross-section for different projectile-target combinations is plotted as function of the ratio of projectile energy to Coulomb barrier.

By employing the selection function discussed in chapter 2 (sec. 2.2) we have calculated the excitation functions for CF, ICF and TF reactions induced by ⁹Be and ⁶Li on heavy targets for energies ranging from deep sub-barrier to above barrier region by using Wong's formula employing EDWSP and selection function for separating CF and ICF. The values of various potential and barrier parameters needed in the calculations are listed in Table 4.4.1 for different projectile-target combinations.

The range of potential depends only on the size of interacting nuclei and increases with increasing size while potential diffuseness and strength depends, besides the size, on incident energy also. Hence, a range of their values corresponding to minimum (Approx. $0.9V_{B0}$ MeV) and maximum ($1.2V_{B0}$ MeV) incident energies for a given projectile-target system is quoted in the table; the V_{B0} is barrier height corresponding to the pure Coulomb interaction. As per expectations, the diffuseness decreases with increasing beam energies and the process becomes sharper at higher energies.

Regarding barrier parameters, the barrier position is assumed to depend only on size of projectile and target. The barrier height varies with incident energy and hence simulates various channel coupling effects. This is in accordance with the fact that when coupling with collective vibrational and rotational states are taken into account, the single barrier turns into a distribution of barriers of different heights. The barrier curvature, on the other hand, is obtained by using potential strength for three different energies. Specially, the incident energy equal to average barrier height, slightly more than this and slightly less than this are used for this purpose which results in a very weak dependence of curvature on energy.

Table 4.4.1 Values of potential and barrier parameters for various projectile-target combinations. The values of energy dependent quantities are given for an energy range $\sim\!0.9V_{B0}$ to $1.2V_{B0}$ MeV. Here V_{B0} denotes the average height of the Coulomb barrier.

P-T System	R_{θ}	а	V_0	R_B	ħω	V_B
	(fm)	(fm)	(MeV)	(fm)	(MeV)	(MeV)
⁹ Be+ ¹⁶⁹ Tm	9.02	0.69-0.63	50.52-46.13	11.03	4.40	33.74-34.20
⁹ Be+ ¹⁸¹ Ta	9.18	0.69-0.63	50.7-46.3	10.99	4.9	34.57-35.78
⁹ Be+ ¹⁸⁷ Re	9.26	0.69-0.63	50.82-46.40	11.07	4.99	35.56-36.54
⁹ Be+ ²⁰⁹ Bi	9.53	0.64-0.63	47.46-46.71	11.54	4.45	39.47-39.58
⁶ Li+ ¹⁵² Sm	8.38	0.69-0.63	44.3-40.43	10.27	5.4	23.4-24.17
⁶ Li+ ¹⁵⁴ Sm	8.42	0.63	0.66-0.63	10.34	6.25	23.74-24.07

The introduction of energy dependence in the potential results in the sub-barrier fusion enhancement as shown in Fig. 4.4.6 for ⁹Be + ¹⁶⁹Tm fusion reaction. Since it is well-established, both experimentally as well as theoretically, that coupling to various channels leads to significant increase in fusion cross-section at energies lower than the barrier energy, the enhancement shown in Fig. 4.4.6 is a clear manifestation of the channel coupling effects.

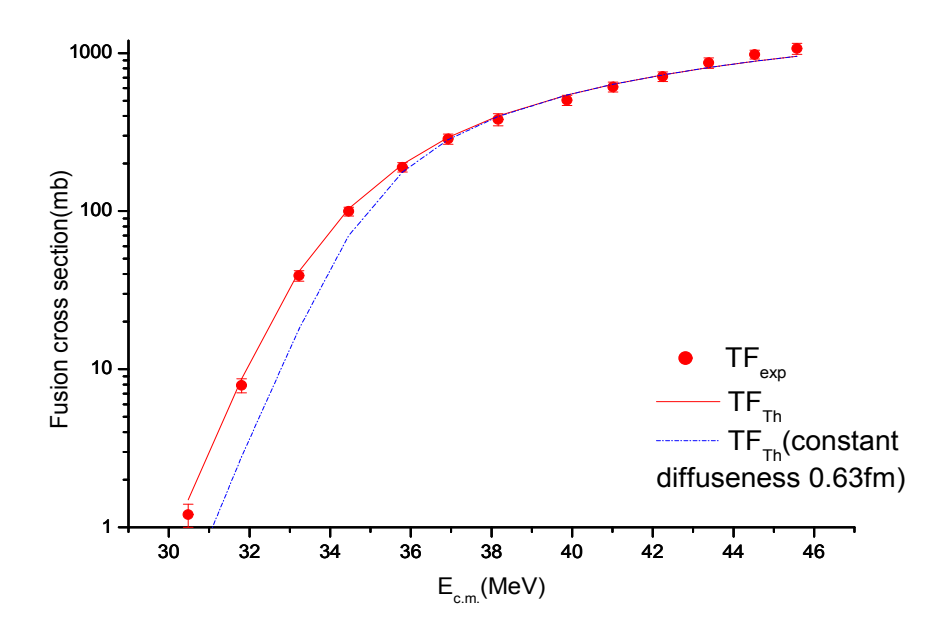


Fig.4.4.6 Total fusion excitation functions for ${}^{9}Be + {}^{169}Tm$ reaction corresponding to constant (dashed line) and energy dependent (solid line) diffuseness parameters are compared with the corresponding experimental data taken from Ref. [14].

In Fig. 4.4.7, TF, CF and ICF excitation functions for ${}^{9}\text{Be}{}^{+169}\text{Tm}$ fusion reaction have been compared with the corresponding data taken from Ref. [14]. The almost perfect matching between data and results of calculations indicates that the method proposed to separate CF and ICF from TF works very well for target with zero quadruple moment, as the nucleus ${}^{169}\text{Tm}$ has zero quadruple moment in its ground state. However, it is worthwhile to mention that at energies well above the barrier, the CF and TF both are under predicted though to a small extent. The large measured TF cross-sections at high energies in comparison to the theoretical values may be ascribed to the

fact that the contribution of the processes other than ICF leading to the formation of same residual nuclei cannot be separated out in measurements. Further at energies much larger than the barrier, the CF cross sections tend to be same as TF cross-sections which indicate that the contribution of ICF becomes negligible. Since at higher energies, the fusion no longer occurs through the quantum mechanical tunneling, hence the probability of fusing whole projectile is quite large and process is predominantly the CF process. In addition, the disagreement between the results of calculations and the measurements at very high energies is due to the fact that at these energies theoretically it is assumed that still 30% of events are ICF events which is no longer valid at these energies.

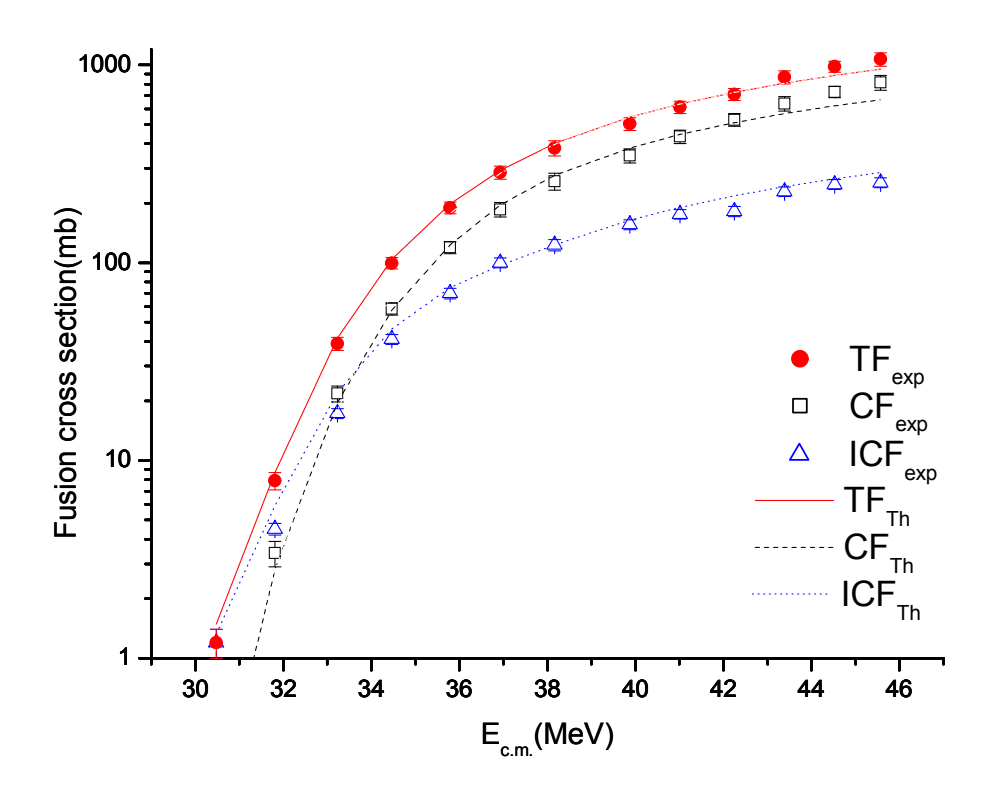


Fig.4.4.7 Fusion excitation functions for ICF, CF and TF processes for ${}^{9}Be + {}^{169}Tm$ reaction compared with the corresponding experimental data taken from Ref. [14].

In order to check the validity of the technique to separate ICF from TF for processes involving target with nonzero quadruple moment, we have compared the experimental and predicted CF, ICF and TF cross-sections in Fig. 4.4.8 for ⁹Be+¹⁸¹Ta system and in Fig. 4.4.9 for ⁹Be+¹⁸⁷Re at near barrier energies. The experimental data shown in Fig. 4.4.8 are taken from Ref. [13] and those in Fig. 4.4.9 are taken from Ref. [14]. Besides larger charge (*Z*) and mass number (A) of ¹⁸¹Ta and ¹⁸⁷Re with respect to ¹⁶⁹Tm the former two are nuclei having ground state quadruple moment value approximately 3.3b and 2.1b respectively. As mentioned earlier, for such nuclei slightly smaller value (1.42 fm) of radius parameter r₀ is taken in evaluation of barrier radius R_B which takes into account the effects of nonzero quadruple moment of target. Once again a reasonably good agreement between the data and predictions is found. The slight mismatch at higher energies may be interpreted in the same manner as earlier.

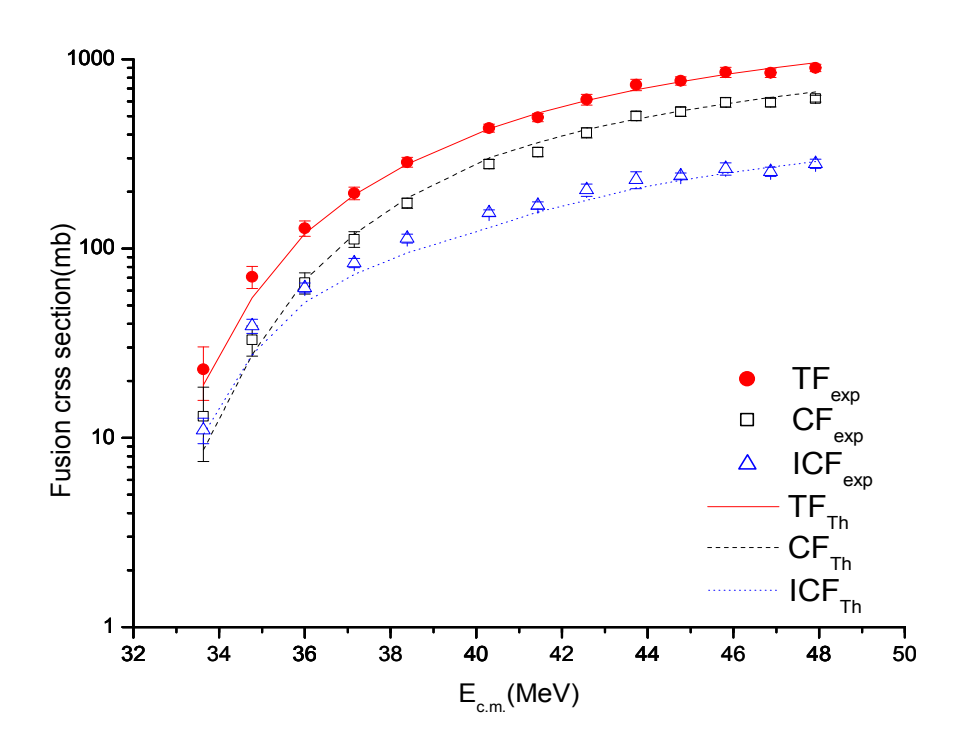


Fig.4.4.8 Similar to Fig.4.4.7 but for ${}^{9}Be+{}^{181}Ta$ reaction. Experimental data are taken from Ref. [13].

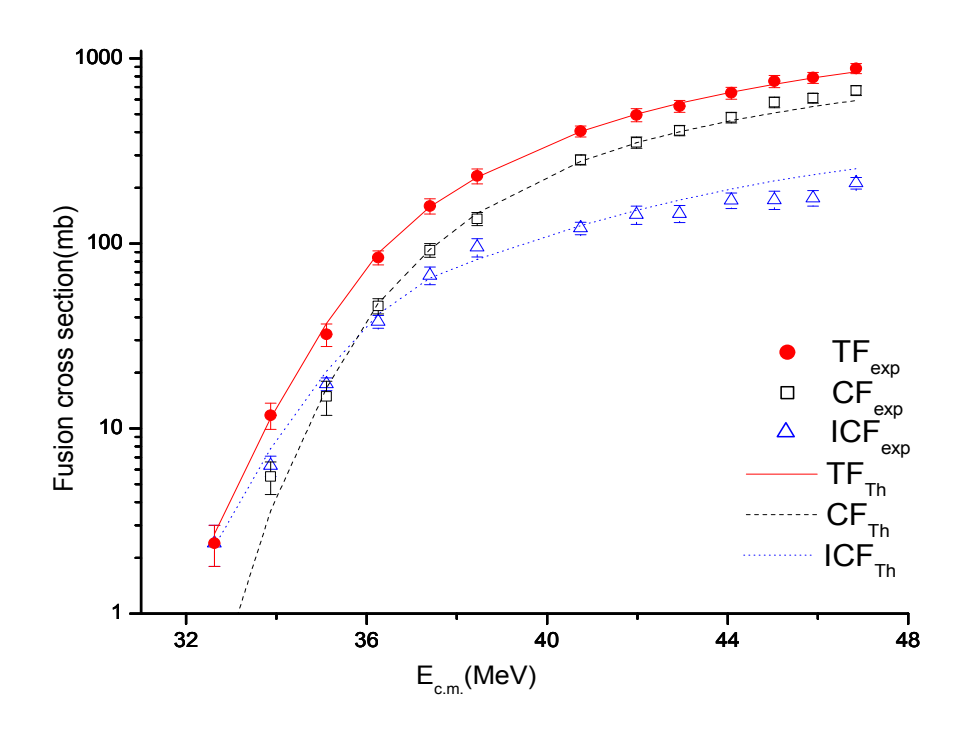


Fig.4.4.9. Similar to Fig.4.4.7 but for ${}^{9}Be+{}^{187}Re$ reaction. Experimental data are taken from Ref. [14].

In case of ${}^9\mathrm{Be}$ + ${}^{209}\mathrm{Bi}$ system because of the availability of CF data only, in Fig. 4.4.10 we depict the comparison of calculated CF excitation function with the measured one. Since target ${}^{209}\mathrm{Bi}$ has quadruple moment value around -0.5b in its ground state, the value 1.44 fm of r_0 is used in the determination of R_B to nullify the quadruple moment effects. The CF cross-sections extracted from the TF cross-section employing the selection function proposed in chapter 2 are found to be in good agreement with the measured one. In Fig. 4.4.10, the calculated excitation functions for TF and ICF are also given. The relative contribution of ICF in TF is found to vary from 37% to 34% for incident energies 42.15 MeV to 57.5 MeV.

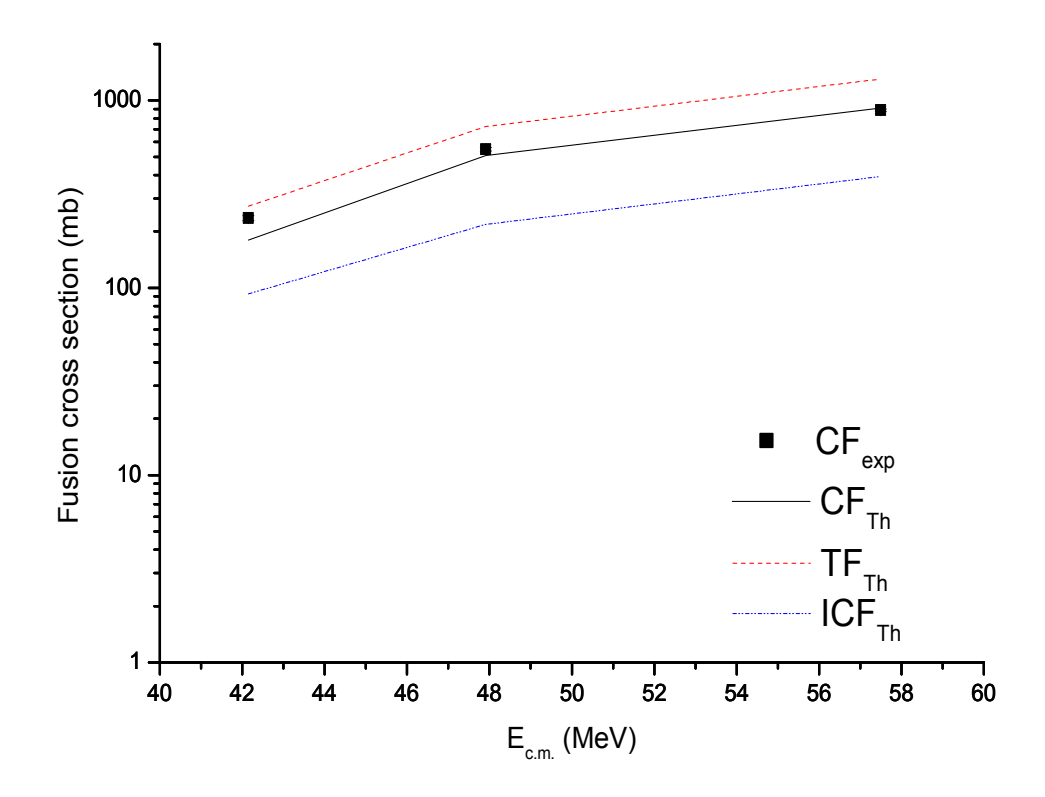


Fig.4.4.10. Complete fusion excitation function for ${}^{9}Be + {}^{209}Bi$ reaction compared with the experimental data taken from Ref. [17]. The calculated TF and ICF excitation functions are also shown.

For ⁶Li+ ^{152,154}Sm systems similar results are found as shown in Figs. 4.4.11 and 4.4.12.

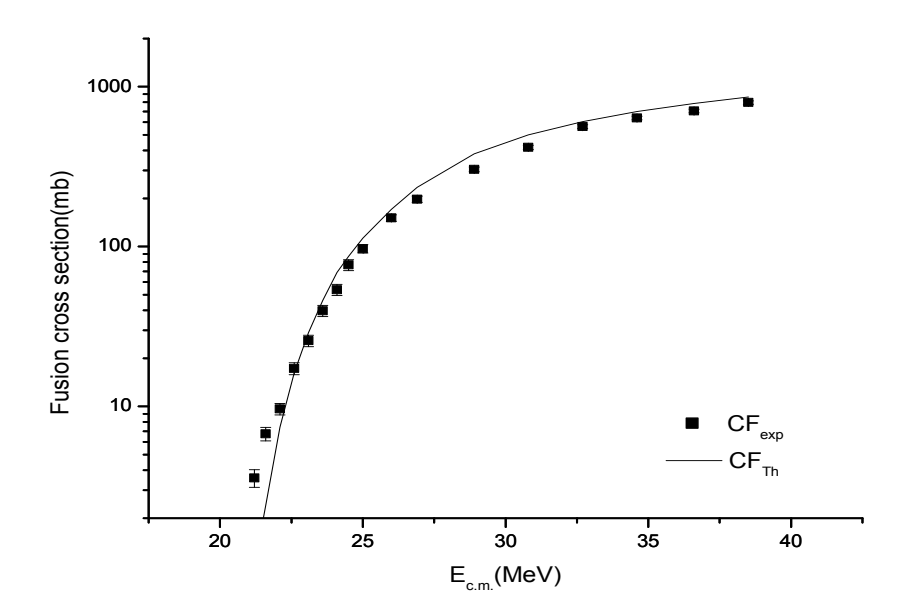


Fig.4.4.11 Fusion excitation functions for CF process for 6 Li+ 152 Sm reaction are compared with the experimental data taken from Ref. [18]

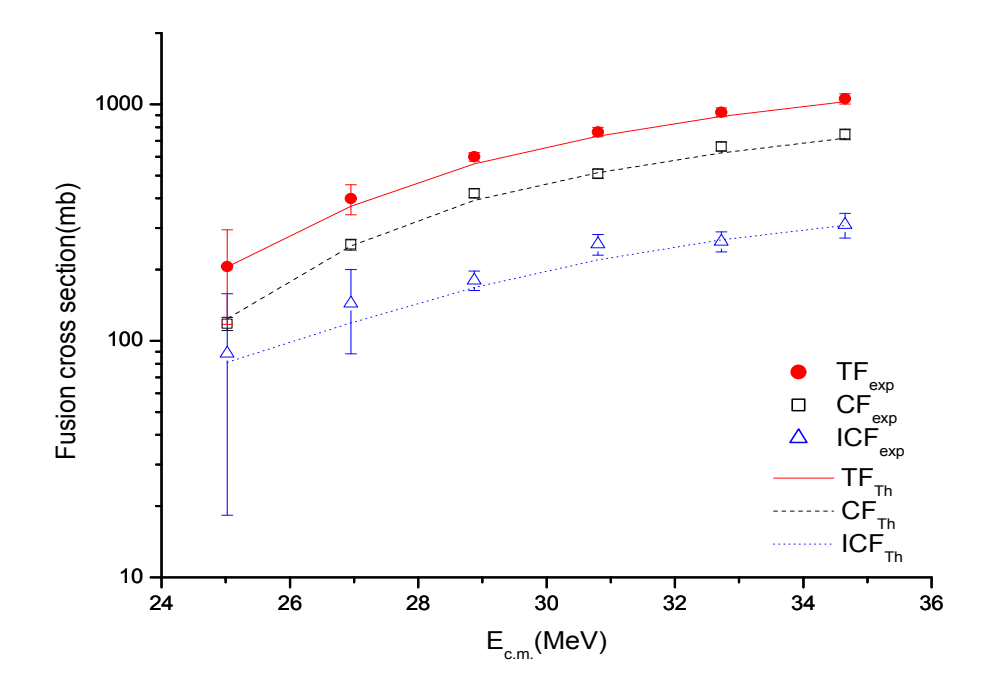


Fig.4.4.12 Fusion excitation functions for CF, TF and ICF processes for ⁶Li+¹⁵⁴Sm reaction are compared with the experimental data taken from Ref. [19]

4.5 Optimum Barrier Radius for Deformed

Targets

In this section we propose a simple systematic to determine barrier radius R_B for fusion reactions involving stable weakly bound nuclei and different deformed and massive targets. Since the fusion cross section is highly sensitive to barrier radius, a very small change in its value may results appreciable change in fusion cross section. It is obvious that barrier radius must depend on the deformation of target nucleus only because the quadruple moments of the projectiles ⁶Li, ⁷Li and ⁹Be are negligibly small in comparison to that of target. Phenomenologically, we have found that the parameter r₀ used to determine barrier radius varies from 1.38 to 1.39fm for reactions involving targets having quadruple moment smaller than 0.5b, from 1.40 to 1.41fm for reactions involving targets with quadruple moment 0.5 to 1.5b and 1.42 to 1.44 fm for reactions invovling targets with quadruple moment greater than 1.5b. Using the so decided values of barrier radii we have calculated the fusion excitation functions for CF processes for 7Li+209Bi, 6Li+159Tb and ⁷Li+¹⁵²Sm systems at around barrier energies and have compared with the corresponding experimental data as shown in Figs. 4.5.1, 4.5.2 and 4.5.3 respectively. The matching between the data and predictions, as can be seen clearly from these figures, is very promising which is turn indicates that the proposed phenomenology is quite convincing.

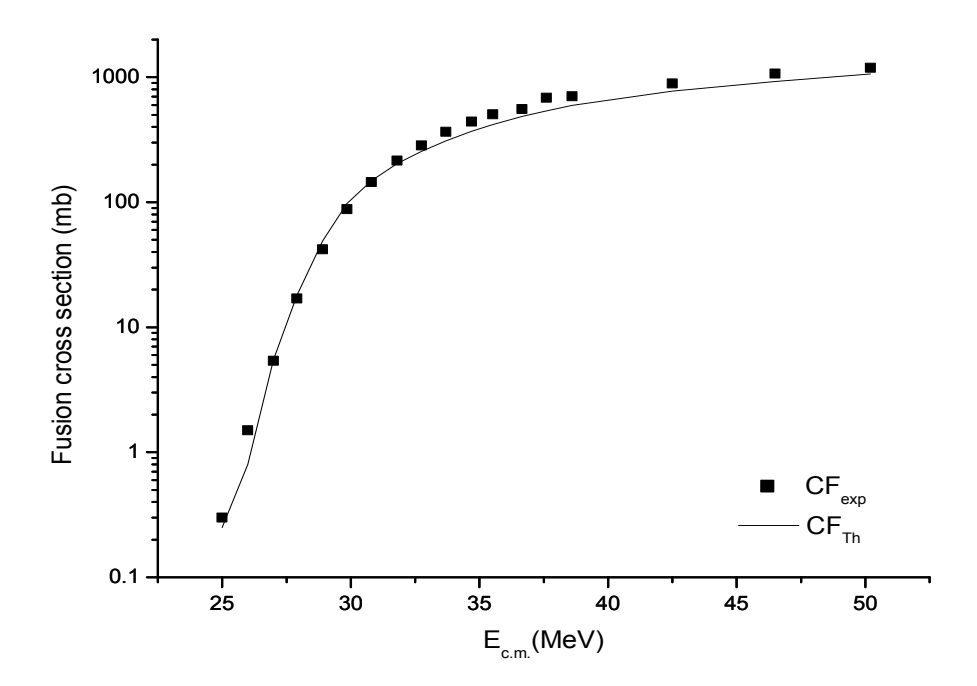


Fig.4.5.1 Fusion excitation functions for CF process for 7 **Li**+ 209 **Bi** (Q.M.=-0.4b) reaction is compared with the experimental data taken from Ref. [20-21]

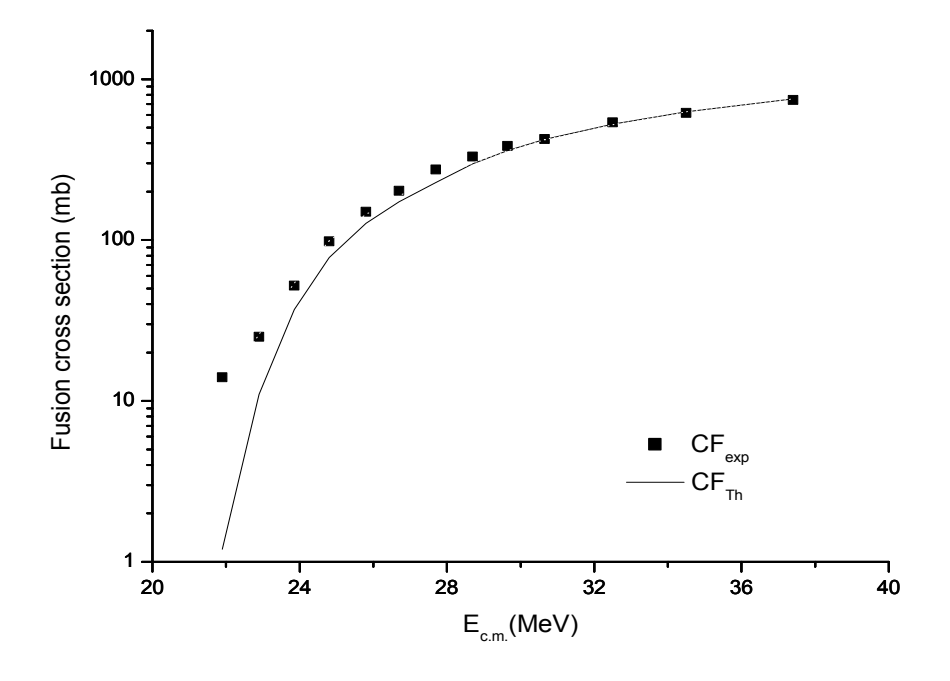


Fig.4.5.2 Fusion excitation function for CF process for 6 **Li**+ 159 **Tb** (Q.M.= 1.4b) reaction is compared with the experimental data taken from Ref. [22]

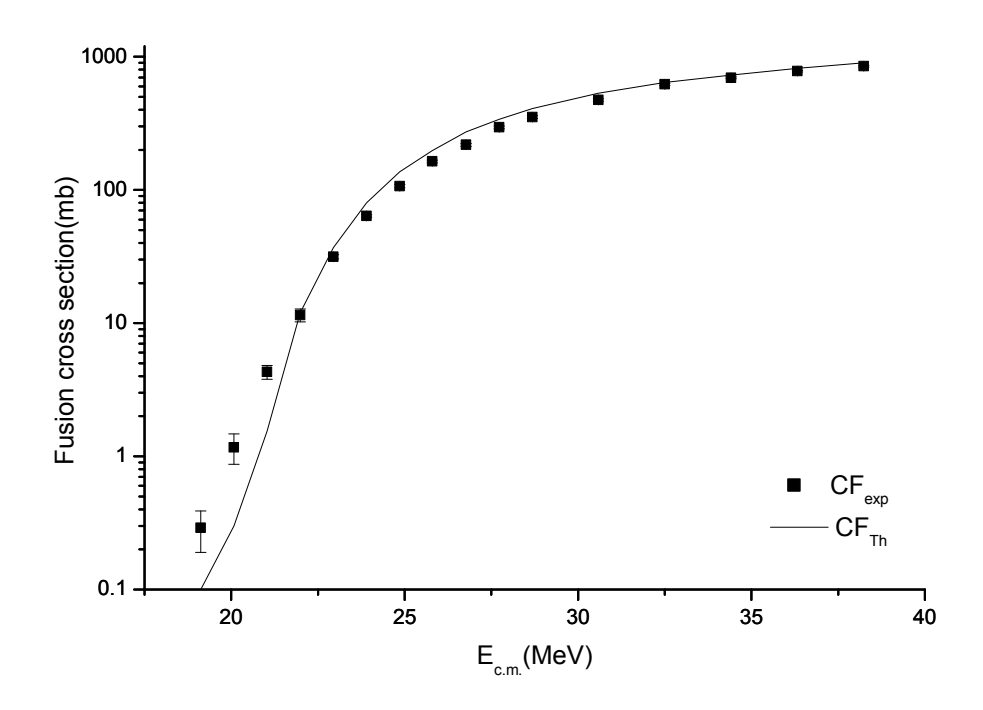


Fig.4.5.3 Fusion excitation function for CF process for 7 Li+ 152 Sm (Q.M.=-1.7b) reaction is compared with the experimental data taken from Ref. [23]

References

- [1]. K. Hagino, A. Vitturi, C.H. Dasso and S.M. Lenzi, Phys. Rev. C 61 (2000) 037602.
- [2]. A. Diaz-Torres and I.J. Thompson, Phys. Rev. C 65 (2002) 024606.
- [3]. A. Diaz-Torres, I.J. Thompson and C. Beck, Phys. Rev. C 68 (2003) 044607.
- [4]. J.A. Tostevin, F.M. Nunes and I.J. Thompson, Phys. Rev. C 63 (2001) 024617.
- [5]. C. Beck, N. Keeley and A. Diaz-Torres, Phys. Rev. C 75 (2007) 054605, and references therein.
- [6]. K. Hagino, M. Dasgupta and D.J. Hinde, Nucl. Phys. A 738 (2004) 475.
- [7]. K. Yabana, M. Ito, M. Kobayashi, M. Ueda and T. Nakatsukasa, Nucl. Phys. A 738 (2004) 303.
- [8]. N. Keeley and R.S. Mackintosh, Phys. Rev. C 90 (2014) 044602.
- [9]. R. Rafiei et al., Phys. Rev. C 81 (2010) 024601.
- [10]. A. Diaz-Torres et al., Phys. Rev. Lett. 98 (2007) 152701.
- [11]. A. Diaz-Torres, J. Phys. G, Nucl. Part. Phys. 37 (2010) 075109.
- [12]. A. Diaz-Torres, Comput. Phys. Commun. 182 (2011) 1100.
- [13]. N.T. Zhang et al., Phys. Rev. C 90 (2014) 024621.
- [14]. Y.D. Fang et al., Phys. Rev. C 91 (2015) 014608.
- [15]. Manjeet Singh, Sukhvinder S. Duhan and Rajesh Kharab, Mod. Phys. Lett. A 26 (2011) 2129; Nucl. Phys. A 897 (2013) 198.
- [16]. Sukhvinder S. Duhan, Manjeet Singh, Rajesh Kharab and H.C. Sharma, Mod. Phys. Lett. A 26 (2011) 1017.
- [17]. M. Dasgupta, D. J. Hinde, S. L. Sheehy and B. Bouriquet, Phys. Rev. C 81 (2010) 024608.
- [18]. P. K. Rath et al., Nucl. Phys. A 874 (2012) 14.
- [19]. C. L. Guo et al., Phys. Rev. C 92 (2015) 014615.
- [20]. M. Dasgupta et al., Phys. Rev. C 70 (2004) 024606.
- [21]. M. Dasgupta, et al., Phys. Rev. C 66 (2002) 041602(R).
- [22]. M. K. Pradhan et al., Phys. Rev. C 83 (2011) 064606.
- [23]. P.K. Rath et al. Phys. Rev. C 88 (2013) 044617.

CONCLUSIONS

5.1 Conclusions

This chapter is devoted to important conclusions, drawn on the basis of comparison between predictions and corresponding data, of the present study. We have analyzed the fusion excitation function data of reactions induced by stable weakly bound projectiles on different targets in near barrier energy region within the framework of Classical Dynamical Model and Wong's formula with energy dependent Woods-Saxon potential. Owing to very low binding energies of ^{6,7}Li and ⁹Be their breakup significantly affects the fusion process induced by impinging these projectiles on various targets [1-13]. One of the important consequence of breakup occurring before fusion is to initiate a new incomplete fusion (ICF) reaction channel beside the usual complete fusion (CF) process. Thus there arises an immediate need to develop new theoretical models capable of calculating separately CF and ICF cross sections. One such simple model frequently referred to as classical dynamical model was developed by Diaz-Torres [14-17]. According to this model, the projectile-target relative motion is treated classically and its time evolution is described by the classical equations of motion for mutual Coulomb and nuclear forces between projectile and target. Separate calculations of CF and ICF cross sections are made possible by introducing a stochastically sampled breakup function [14, 17]. Here we have used the code PLATYPUS, wherein the classical dynamical model is employed, to study the separate contribution of ICF and CF in total fusion (TF) for reaction induced by ⁹Be on ¹⁸¹Ta target in near barrier energy region. It is found that this model work very well only at above barrier energies and fails completely at energies well below the Coulomb barrier where the fusion occurs through quantum mechanical tunneling [18]. Thus, we have introduced the tunneling correction in this model at below barrier energies and analyzed the CF and ICF cross section data of fusion reactions induced by ⁹Be on ¹⁶⁹Tm and ¹⁸⁷Re targets at around barrier energies. A significant improvement between the data and prediction is found as a result of tunneling correction particularly at below barrier energies [19]. The basic strategy used to incorporate the tunneling correction is to multiply the no captured breakup (NCBU) cross section at below barrier

energies by a tunneling factor based on WKB approximation [20]. Basically, the quantum mechanical tunneling corresponds to non-zero probability of finding an object at a position where it is never observed classically. Thus incorporation of tunneling correction results in sub barrier fusion which is a classically forbidden channel and improves matching between predictions and data at energies smaller than the barrier energy. Besides the tunneling effects, the channel coupling effects also play major role in the sub barrier fusion process. Therefore we have also used another simple model based on Wong's formula in conjugation with energy dependent Woods-Saxon potential [21-23]. In this model the channel coupling effects are simulated through the energy dependence in the potential. However only TF cross section is calculated through this model and the separate contribution of CF and ICF in TF is obtained by assuming that the relative contribution of these processes in TF is same as that predicted by code platypus at above barrier energies and have found that these are not consistent in this energy region [18]. Rather the contribution of ICF is found to be larger than that predicted by code platypus in TF for below barrier energies. In order to remove this discrepancy a simple energy dependent selection function is proposed to extract relative contribution of CF and ICF from TF process [24]. It is found that the contribution of ICF decreases with increasing incident energy. However, it never becomes zero, a minimum of approximately 25% contribution of ICF remains in TF even at energies much larger than the barrier energy. Further for heavier target, the contribution of ICF is found to be enhanced in comparison to lighter ones. Further since the barrier radius parameter is quite sensitive to the quadruple moment of interacting nuclei, it is quite tempting to obtain its optimum value for a given projectile-target combination. In present study we have found that the parameter r₀ used to determine barrier radius varies from 1.38 to 1.39fm for reactions involving targets having quadruple moment smaller than 0.b, from 1.40 to 1.41fm for reactions involving targets with quadruple moment 0.5 to 1.5b and 1.42 to 1.44fm for reactions invovling targets with quadruple moment greater than 1.5b.

Finally in terms of future prospective the work may be extended to address the following issues.

- For complete understanding of the dynamics of complete fusion and incomplete fusion more experiments are required to be carried out and more sophisticated models are needed to be developed.
- 2. The role of nuclear size, shape and structure in the process of CF and ICF is still not so clear.
- A fully quantum mechanical model taking tunneling and other channel coupling effects into account is required for better physical insight and unambiguous understanding of fusion reactions involving weakly bound nuclei.
- 4. In order to differentiate between direct transfer and ICF processes more measurements and calculations concerning breakup, transfer and ICF processes are yet to be carried out.

References

- [1]. C.S. Palshetkar, et al., Phys. Rev. C 89 (2014) 024607.
- [2]. S.P. Hu, et al., Phys. Rev. C 91 (2015) 044619.
- [3]. M.K. Pradhan, et al., Phys. Rev. C 83 (2011) 064606.
- [4]. P.R.S. Gomes, et al., Phys. Rev. C 73 (2006) 064606.
- [5]. Y.D. Fang, et al., Phys. Rev. C 91 (2015) 014608.
- [6]. N.T. Zhang, et al., Phys. Rev. C 90 (2014) 024621.
- [7]. Y.D. Fang, et al., Phys. Rev. C 87 (2013) 024604.
- [8]. M. Dasgupta, D.J. Hinde, S.L. Sheehy, B. Bouriquet, Phys. Rev. C 81 (2010) 024608.
- [9]. M. Dasgupta, et al., Phys. Rev. Lett. 82 (1999) 1395.
- [10]. Y.W. Wu, et al., Phys. Rev. C 68 (2003) 044605.
- [11]. M. Dasgupta, et al., Phys. Rev. C 70 (2004) 024606.
- [12]. A. Mukherjee, et al., Phys. Lett. B 636 (2006) 91.
- [13]. P.K. Rath, et al., Phys. Rev. C 79 (2009) 051601.
- [14]. A. Diaz-Torres, D.J. Hinde, J.A. Tostevin, M. Dasgupta, L.R. Gasques, Phys. Rev. Lett. 98 (2007) 152701.
- [15]. A. Diaz-Torres, J. Phys. G, Nucl. Part. Phys. 37 (2010) 075109.
- [16]. A. Diaz-Torres, Comput. Phys. Commun. 182 (2011) 1100–1104.
- [17]. R. Rafiei, et al., Phys. Rev. C 81 (2010) 024601.
- [18]. Rajesh Kharab, Rajiv Chahal and Rajiv Kumar, Nucl. Phys. A 946 (2016) 1.
- [19]. Rajesh Kharab, Rajiv Chahal and Rajiv Kumar, Nucl. Phys. A 960 (2017) 11.
- [20]. L.I. Schiff, Quantum Mechanics, Tata McGraw-Hill, New Delhi, 2010.
- [21]. C.Y. Wong, Phys. Rev. Lett. 31 (1973) 766.
- [22]. Manjeet Singh, Sukhvinder S. Duhan and Rajesh Kharab, Mod. Phys. Lett. A 26 (2011) 2129.
- [23]. Sukhvinder S. Duhan, Manjeet Singh, Rajesh Kharab and H.C. Sharma, Mod. Phys. Lett. A 26 (2011) 1017.
- [24]. Rajesh Kharab, Rajiv Chahal and Rajiv Kumar, Mod. Phys. Lett. A 31 (2016) 1650201.